save the blue heart of europe

Measuring of sediment transport and morphodynamics at the Vjosa river / Albania

Measuring of sediment transport and morphodynamics at the Vjosa river / Albania

May 2019

Author:

University of Natural Resources and Life Sciences

Department for Water -Atmosphere-Environment Institute of Hydraulic Engineering and River Research

Project leader:
Priv.-Doz. Dipl.-Ing. Dr. Christoph Hauer

control:
PD Dr. Christoph Hauer

Approval:
06.05.2019

Revisions nb:	Bemerkungen	date

date: 06.05.2019		Revisions nb: 0
	Internal Nb: 004	Pages: 85

Commissionedby:
Riverwatch - Society for the Protection
of Rivers, Neustiftgasse 36,
1070 Vienna, Austria

Contact person: DI Ulrich Eichelmann

EuroNatur - Stiftung Europäisches Naturerbe
Westendstraße 3
78315 Radolfzell, Germany

Contact person: Dipl.-Geogr. Theresa Schiller

With contributions of:
EcoAlbania – Center for Protection of
Natural Ecosystems in Albania
Rr. Kavajes, P.Qendra Globe, Sh.1. Ap.34,
1023 Tirana, Albania

Contact person: PhD Candidate Olsi Nika

Funded by:
MAVA Fondation pour la Nature
Rue Mauverney, 28
1196 Gland, Switzerland

Imprint:
This study is commissioned within the
"Save the Blue Heart of Europe" campaign
(www.balkanrivers.net) organized
by Riverwatch – Society for the Protection
of Rivers (www.riverwatch.eu/en/) and
EuroNatur – European Nature Heritage
Foundation (www.euronatur.org).

Operated by:
Institute of Hydraulic Engineering
and River Research,Department
Water – Atmosphere – Environment,
University of Natural Resources and
Life Sciences,
Muthgasse 107, 1190 Vienna, Austria

Polytechnic University of Tirana, Albania
Dëshmorët e Kombit,
Sheshi Nënë Tereza Nr. 4, Tiranë,
Albania
(Dr.Klodian Skrame)

Project team IWA:
Dipl.-Ing. Hannes Aigner
Dipl.-Ing. Martin Fuhrmann
Dipl.-Ing. Martin Hinterleitner
Dipl.-Ing. Patrick Holzapfel
Dipl.-Ing. Rolf Rindler
Dipl.-Ing. Sebastian Pessenlehner
Dipl.-Ing Daniel Pucher
Dipl.-Ing. Dr. Marcel Liedermann
Priv.-Doz. Dipl.-Ing. Dr. Christoph Hauer

Suggestion for citation: Hauer, C.,Aigner, H., Fuhrmann, M., Holzapfel, P., Rindler, R.,Pessenlehner, S., Pucher, D., Skrame, K.,Liedermann, M. 2019. Measuring of sediment transport and morphodynamics at the Vjosa River / Albania, 85 pp.

List of Abreviations

UAV – unmanned aerial vehicle
DTM – digital terrain model
RPV – remotely piloted vehicle
UVS – unmanned vehicle systems
RPA – remotely piloted aircraft
ROA – remotely operated aircraft
UAS – unmanned aircraft systems
GCS – ground control station
LiDAR – light detection and ranging
NASA – national aeronautics and space administration
FAA – federal aviation administration
UA – unmanned aircraft
GSD – ground sample distance
DSM – digital surface model
GPS – global positioning system
INS – inertial navigation system
VTOL – vertical take-off and landing
DGPS – differential global positioning system
GCP – ground control point
CPU – central processing unit
GPU – graphics processing unit
RAM – random access memory
IDW – inverse distance weighting
DEM – digital elevation model
RMS – root mean square
GSD – grain size distribution
LZA – Linienzahlanalyse (pebble count samples)
BfG – Bundesamt für Gewässerkunde (federal institute for hydrology)
ASTM D4822 – 88 – standard guide for selection of methods of particle size analysis of fluvial sediments
ADCP – acoustic Doppler current profiler
DVWK – Deutscher Verband für Wasserwirtschaft und Kulturbau
BMLFUW – Bundesministerium für Land- und Forstwirtschaft, Umwelt und Wasserwirtschaft
DIN – deutsche Institut für Normung
USACE – United States Army Corps of Engineers
Qbf – bankfull discharge

d50 – The d50 is the diameter of the particle that 50% of a sample's mass is smaller/larger than
HN – hydrodynamic-numerical
SMS – surface water-modelling system
HMID – hydro-morphological index of diversity
CV – coefficient of variation
ETRS – European Terrestrial Reference System
HPP – hydro power plant
USSD – unstructured supplementary service data
ICOLD – international commission on large dams

00 Table of content

01 Introduction

01.01 Balkan rivers

River channel morphology in the Balkans strongly depends on geology and tectonical dynamics (e.g. Schumm, 1969; Whipple et al., 1999). The river systems of the Balkans are dominated by two mountain ranges. The first one, the Dinaric Mountains (Outer- and Inner Dinaric Mountains), is a 600 km long mountain range running along the Adriatic Sea from Slovenia to Northern Albania (Bognar et al., 2012). The `Inner Dinarides´ contain lower mountain heigths compared to the near coastal ´Outer Dinarides´ (max. 1700 – 1800 a.sl.), with a constant lowering towards the Pannonian Plate. Due to high precipitation ranges (up to 5000 mm annually) and the resulting runoff, especially in the central part, the Dinaric mountains contain several important river systems. From North to South, Kupa River, Una River, Sana River, Vrbas River, Bosna River and Drina River are discharging into the Save River and further on into the Black Sea. Only four major rivers lead into the Adriatic Sea, namely Krka River, Cetina River, Neretva River and the Moraca River., For all rivers of the Dinarden, gorges and canyons are dominant in most of the draining systems, for example the world-famous Tara-river canyons (compare to urović, & Petrović, 2007). In addition to fluvial incision, valleys in higher altitudes were shaped by glaciers during the last ice ages with longitudinal extents into the valleys of 10 – 15 km.

The second mountain range is the so-called "Prokletije", part of the Southern Dinarden, running from Eastern Montenegro to Northern Albania. High mountain altitudes accompanied with glacier shaped valleys (Ropojani River, Grbaja River, Valobona River; compare to Hughes et al., 2011) give this particularmountain range alpine characteristics which are very spceialfor the Balkan region. In the "Prokletije" the age of rock decreases from West (limestone, dolomite) to the East (partially Flysch), providing different conditions for channel formation and sediment production in the draining river systems. In summer, the rivers of the "Prokletije" partially contain very low flow, and may fall dry, especially in large alluvial fans. However, springs originating in the karst-mountains may contain high discharge quantities, providing enough water for irrigation (e.g. Valbona valley). Due to the high diversity in geology and mountain characteristics, river channel patterns are frequently not following ´traditional´ concepts of headwater-to-mouth morphology.

The rivers in the Balkans either drain large catchments with long runs to the mouth (e.g. Vjosa River), or arerather short when discharging out of the Karst mountains close to the coast (e.g. 7 km Jadro River, Croatia). Moreover, meandering channel patterns may be found at high altitudes in alluvial basins (e.g. around Tomislavgrad N43°43´00´´/E17°13´42´´) and incised, straight patterns close to mouth. Delta formation of rivers is common for the mouth into the Adriatic Sea but also into lakes, like the alluvial fan close to the city of Podgorica (N42°26´18´´/E19°15´50´´). Thus, the rivers inthe Balkans exhibitquitea high diversity of catchment types as well as asthe longitudinal profile views. The studied Vjosa River contains almost all channel types found in Balkan rivers: incision and formation

of gorges in the upper parts, braiding / anabranching channel patterns in areas of valley widening, and sinuous / meandering characteristics close to the mouth.

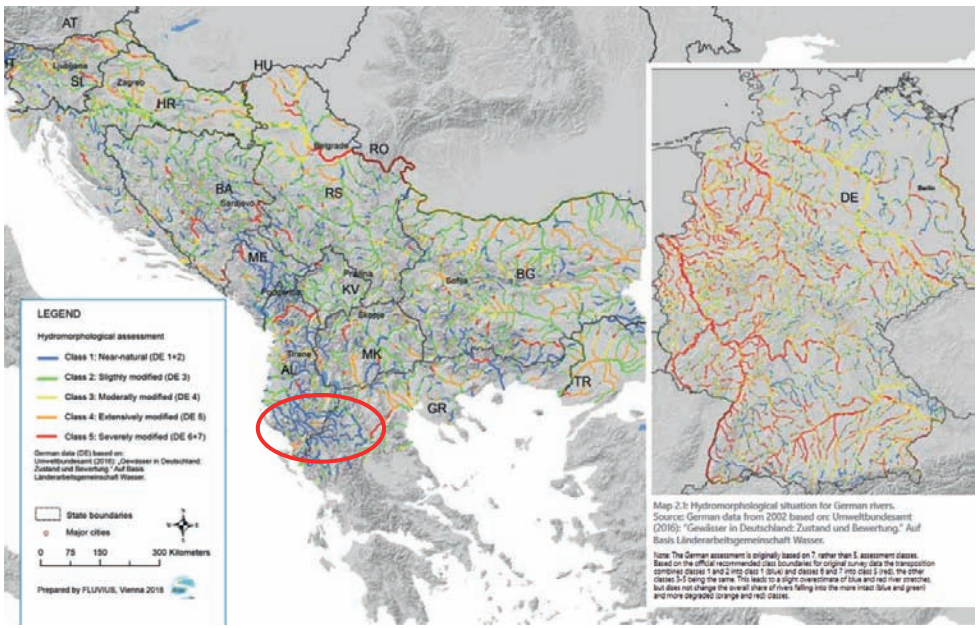

Map 2.1: Hydromorphological situation for German rivers.
Source: German data from 2002 based on: Umweltbundesamt (2016): "Gewässer in Deutschland: Zustand und Bewertung." Auf Basis Länderarbeitsgemeinschaft Wasser.

Note: The German assessment is originally based on 7, rather than 5, assessment classes. Based on the official recommended class boundaries for original survey data the transposition combines classes 1 and 2 into class 1 (blue) and classes 6 and 7 into class 5 (red), the other classes 3-5 being the same. This leads to a slight overestimate of blue and red river stretches, but does not change the overall share of rivers falling into the more intact (blue and green) and more degraded (orange and red) classes.

(b)

Figure 1(a): Hydromorphological status of Balkan rivers compared to rivers in Germany (rivers with catchment size > 500 km2); catchment of the Vjosa highlighted in red circle (data source: EuroNatur & Riverwatch (2018)), (b) Map of the Vjosa-Aoos catchment. Indicated are major mountain ranges in the Albanian part (dottet line) and the position of major cities: Mif (Mifoli), Sel (Selenica), Poc (Poçem), Tep(Tepelena), Per (Permet), Car (Çarshova), Gji (Gjirokastro) (data source: Schiemer et al., 2018).

01.02 The Vjosa river (www.balkanrivers.net)

The Vjosa River in Albania is one of Europe's last living wild rivers. Except for the first 10 kilometers belowits springs, its entire course of about 260 kilometers it is untamed, free-flowing and characterized by beautiful canyons, braided river sections, islands, oxbows and meandering stretches. In some areas the riverbed expands over more than 2 km in width. However, what makes this river really outstanding internationally is the fact that almost all its tributaries are free-flowing and intact as well, creating a living rivers network that is without par in Europe.The main source of the Vjosa River is on Greek territory near the village of Vouvoussa (the ancient name of Vjosa). On its first 80 kilometres the river flows through Greece and is named Aoos. In Albania it turns into Vjosa. The meandering lower part opens up into a valley with extensive wetlands, providing habitats for spawning fish, migratory birds and others. Finally, it drains into the AdriaticSea just north of the Narta lagoon – one of the biggest and ecologically richest lagoons of Albanian and, as such, designated as Managed Nature Reserve. The Vjosa is draining a total area of 6,700 km^2 in Albania and Greece and discharges an average of 204 m^3/s into the Adriatic Sea.

Its unique value is a result of the widely undisturbed and well-preserved fluvial dynamics throughout its course, from the headwaters in Greece (Aoos) to the delta in southern Albania (Vjosa). The ecological functions and specific biodiversity of river-floodplain ecosystems are highly dependent on their intact geomorphic dynamics (Schiemer et al., 2018). The highly undisturbed river dynamics and the river-floodplain ecosystems along the Vjosa are in an excellent state of preservation. All iverine habitats typical for the Vjosa have become very rare in Europe and are thus listed in the Annex 1 of European Union Habitats Directive, stressing the importance for their conservation at an European scale. They harbour viable communities of species that have largely or completely disappeared from other European rivers systems. Due to their specific demands and dependence on a functioning and uninterrupted river ecosystem, most of these species have almost entirely gone extinct in Central Europe.

01.03 Aims of study

The aims of the presented study are (i) **measurements** of **bed load transport** and (ii) suspended sediment load transport at the Vjosa at Pocem Bridge. Moreover, (iii) **grain size sampling** in the area of Kalivac accombined with (iv) preperation **high-resolution Digital Terrain** Data based on UAV survey providings novel and fundamental data for the environmental assessment of the highly dynamic section at Kalivac; (v) application of h**ydrodynamic-numcerical modelling (1D and 2D),** targeted at achieving important boundary conditions for the hydromorpho logical assessment as well as opportunities to evaluate how dam constuctions will affect the impounded sections as well as dynamics of sediment transport in terms of high flows. Finally, (vi) repeated survey of characteristic cross sections to underline the dynamics in habitat turn-over of this specific Balkan river. The

measurements and the study itself were carried out in close cooperation with the Polytechnic University of Tirana, particularly in regards tomeasurements themselves, and even more so in regards to the evaluation of the samples (e.g. grain distribution curves) and maintenance / reading of the continuous measuring instruments at the Pocem bridge.

All these data serve to evaluate the dam projects for the areas of Kalivac and Pocem, concerning (vii) how long it will take until **the reservoirs are filled up to 80%** and (viii) if the applied hydropower concepts are feasible for a river system like the Vjosa and (ix) what can be expected concerning coastal erosion if the sediments transported by the Vjosa are trapped in one or more reservoirs.

02 UAV survey and DTM creation

This first part of the study is dealing with the application of UAV based survey to derive a state-of-science Digital Terrain Model (DTM) of a morphological high diverse section in the area of Kalivac. These data are not only suitable for the assessment of the current status in hydromorphology, they are also important data for high quality hydrodynamic-numerical modelling, which can be applied for both habitat assessment of instream biota as well as analyzing semi-aquatic habitats (e.g. connectivity) or floodplain dynamics (e.g. inundation areas and durations).

02.01 Definition UAV

"UAVs are to be understood as uninhabited and reusable motorized aerial vehicles." states van Blyenburgh, 1999. These vehicles are remotely controlled, semi-autonomous, autonomous, or have a combination of these capabilities. Comparing UAV to manned aircraft, it is obvious that the main difference between the two systems is that on the UAV no pilot is physically present in the aircraft. This does not necessarily imply that an UAV flies by itself autonomously. In many cases, the crew (operator, backup-pilot etc.) responsible for a UAV is larger than that of a conventional aircraft (Everaerts, 2008).

The term UAV is commonly used in the Computer Science, Robotics and Artificial Intelligence, as well as the Photogrammetry and Remote Sensing communities. Additionally, synonyms like Remotely Piloted Vehicle (RPV), Remotely Operated Aircraft (ROA) or Remotely Piloted Aircraft (RPA) and Unmanned Vehicle Systems (UVS) can also infrequently be found in the literature. RPV is a term to describe a robotic aircraft flown by a pilot using a ground control station. The first use of this term may be addressed to the United States (U.S.) Department of Defense during the 1970's and 1980's. The terms ROA and RPA have been used by National Aeronautics and Space Administration (NASA) and Federal Aviation Administration (FAA) in the U.S. in place of UAV. Furthermore, the term Unmanned Aircraft System (UAS) is also being used (Colomina, et al., 2008). The FAA has adopted the generic class UAS, which was originally introduced by the U.S. Navy. Common understanding is that the terminology UAS stands for the whole system, including the Unmanned Aircraft (UA) and the Ground Control Station (GCS)(Eisenbeiß, 2009).

02.02 UAV photogrammetry

The new terminology UAV photogrammetry (Eisenbeiss, 2008c) describes a photogrammetric measurement platform, which operates remotely controlled, semi-autonomously, or autonomously, without a pilot sitting in the vehicle. The platform is equipped with a photogrammetric measurement system, including, but not limited to a small or medium size still-video or video camera, thermal or infrared camera systems, airborne LiDAR system, or a combination thereof. Current standard UAVs allow the registration and tracking of the position and

orientation of the implemented sensors in a local or global coordinate system. Hence, UAV photogrammetry can be understood as a new photogrammetric measurement tool. UAV photogrammetry opens various new applications in the close range domain, combining aerial and terrestrial photogrammetry, but also introduces new (near-) real time application and low-cost alternatives to the classical manned aerial photogrammtry (see Table 1). A detailed study on real-time data collection using airborne sensors including UAVs can be found in Kerle, et al., 2008 (Eisenbeiß, 2009).

Table 1: Features of Aerial, close range and UAV photogrammetry.

	Aerial	Close Range	UAV
Planning	(semi-)automatic	manual	automatic-manual
Data acquisition / Flight	assisted/manual	autonom/assisted/manual	autonom/assisted/manual
Size of the area	km^2	mm^2 - m^2	m^2 - km^2
Image resolution /GSD	cm-m	mm - dm	mm - m
Distance to the object	100m- 10km	cm - ~300m	m - km
Orientation	normal case, recently also oblique	normal/oblique	normal/oblique
Absolut accuracy of the initial orientation values	cm - dm	mm-m	cm - 10m
Image block size/ number of scans	10 - 1000	1 - 500	1 - 1000
Special applications (examples) and features	large scale areas (Mapping, Forestry, Glaciology, 3D-City modeling)	small-scale areas and objects (archaeological documentation, 3D modeling of buildings)	small- and large-scale areas (archaeological documentation, monitoring of hazards, 3D modeling of buildings and objects)
		architectural and industrial photogrammetry	applications in inaccessible areas and dangerous objects
	aerial view	terrestrial view	aerial view
			real-time applications (monitoring)

02.03 Advantages of UAV's

Major advantages of UAVs compared to manned aircraft systems are that UAVs can be used in high risk situations without endangering a human life and inaccessible areas, at low altitude and at flight profiles close to the objects where manned systems cannot be flown. These regions are for example natural disaster sites, e.g. mountainous and volcanic areas, flood plains, earthquake and desert areas and scenes of accidents. In areas where access is difficult and where no manned aircraft is available or even no flight permission is given, UAVs are sometimes the only practical alternative. Furthermore, in cloudy and drizzly weather conditions, the data acquisition with UAVs is still possible, when the distance to the object permits flying below the clouds. Such weather conditions do not allow the data acquisition with large format cameras integrated into manned aircrafts due to required larger flight altitude above ground. In addition, one fundamental advantage of using UAVs is that they are not burdened with the physiological limitations and economic expenses of human pilots.

Moreover, supplementary advantages are the real-time capability and the ability for fast data acquisition, while transmitting the image, video and orientation data in real time to the ground control station.

Most of the (non-)commercially available UAV systems on the market focus

on low cost systems, and thus a major advantage of using UAVs is also the cost factor, as UAVs are less expensive and have lower operating costs than manned aircrafts have. But, sometimes as mentioned in the previous section - depending on the application - the cost can be similar to manned systems. As for small-scale applications the expenses for manned aircrafts are not maintainable, projects are quite often not feasible or terrestrial systems have to be used as alternative systems, recognizing not all project requirements are met. Thus, UAVs can be seen as supplement or replacement to terrestrial photogrammetry in a certain area of applications.

In the case of combination of terrestrial and UAV photogrammetry, it is even possible to use the same camera system and having the same distance to the object, which simplifies the combined data processing.

In addition to these advantages, the UAV-images can be also used for the high resolution texture mapping on existing DSMs and 3D-models, as well as for image rectification. The rectified images and derivates, like image mosaics, maps and drawings, can be used for image interpretation. The implementation of GPS/INS systems as well as the stabilization and navigation units allow precise flights, guaranteeing, on the one hand, sufficient image coverage and overlap and on the other hand, enabling the user to estimate the expected product accuracy preflight.

Looking at rotary wing UAVs, the platform allows vertical take-off and landing, vanishing the need for an available runway. Furthermore, the use of VTOL (Vertical take-off and landing) systems permits the image acquisition on a hovering point, while the camera is turning in vertical and horizontal direction (Eisenbeiß, 2009).

02.04 Limitations of UAV's

UAVs, especially low-cost UAVs, limit the sensor payload in weight and dimension, so that often low weight sensors like small or medium format amateur cameras are selected. Therefore, in comparison to large format cameras, UAVs have to acquire a higher number of images in order to obtain the same image coverage and comparable image resolution.

Moreover, low-cost sensors are normally less stable than high-end sensors, which results in a reduced image quality. In addition, these payload limitations require the use of low weight navigation units, which implies less accurate results for the orientation of the sensors. Furthermore, low-cost UAVs are normally equipped with less powerful engines, limiting the reachable altitude. Existing commercial software packages applied for photogrammetric data processing are rarely set up to support UAV images, as through no standardized workflows and sensor models are being implemented.

In addition to these drawbacks, UAVs do not benefit from the sensing and intelligent features of human beings. Thus, UAVs cannot react like human beings in unexpected situations, e.g. unexpected appearance of an obstacle. In general, there are no sufficient regulations for UAVs given by the civil and security authorities (Colomina, et al., 2008). Low-cost UAVs are not equipped with air traffic

communication equipment and collision avoidance systems, like manned aircrafts. Therefore, due to the lack of communication with the air traffic authorities, UAVs are restricted to the flight in line-of-sight and to operate with a back-up pilot. The flight range of the UAV is also, in addition to the line-of-sight regulation, dependent on the skill of the pilot to detect and follow the orientation of the UAV-system. To take full advantage of the impressive flying capabilities of UAVs, like the fully automated operating rotary wing UAVs, there needs to be a well-trained pilot, due to security issues. The pilot should be able to interact with the system at any time and maneuvers (Eisenbeiß, 2009).

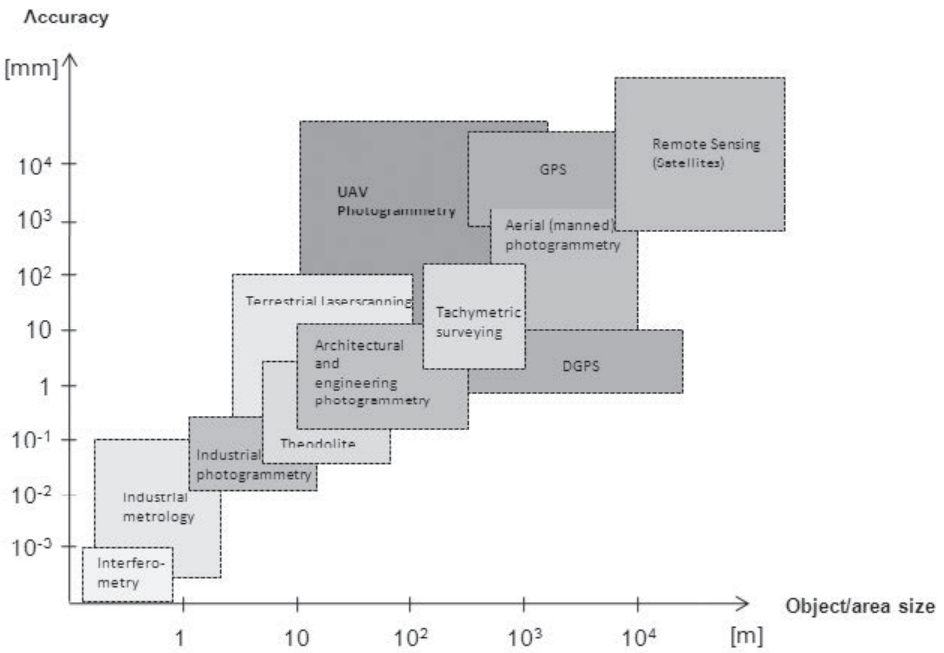

Figure 2: The accuracy of measurement methods in relation to the object/area size; modified from Fig. 1.4 (in Luhmann et al., 2006, p. 4 byEisenbeiß, 2009).

02.05 DTM creation

In this chapter the various steps of the workflow to achieve a high-quality DTM are presented. There are mainly six steps required for the final result. In Figure 3, the flight plan as well as camera positions and effective overlap of the images in the studied area are presented. Moreover, Figure 4 shows the sites of the requested ground control points (GCPs) which determine both the planimetric as well as the heigt in a local coordinate system.

Overview workflow:

1. **Observing** the area of interest
2. **Distributing** the GCP homogenous
3. Develop **a flight** plan(executed flight plan inFigure 3)
4. **Terrestrial surveying** of the GCP (Figure 4 and Figure 6)
5. **Flight operation** (Figure 5andTable 2)
6. **Post processing**

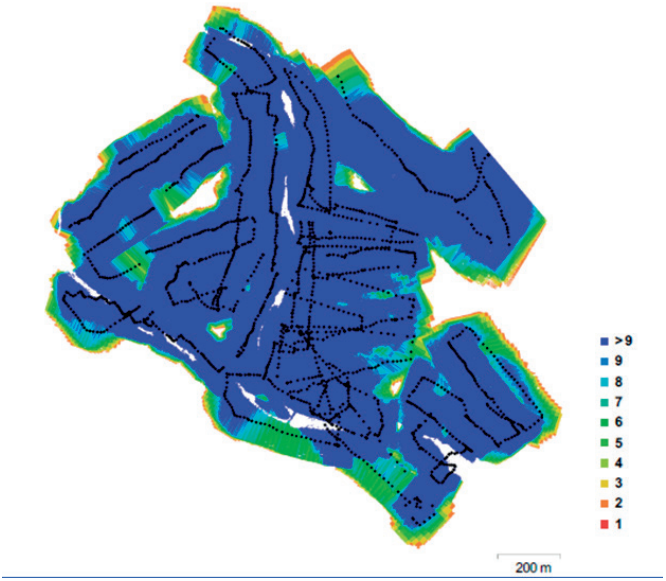

Figure 3: Flight plan, camera positions and effective overlap of the images in the study area.

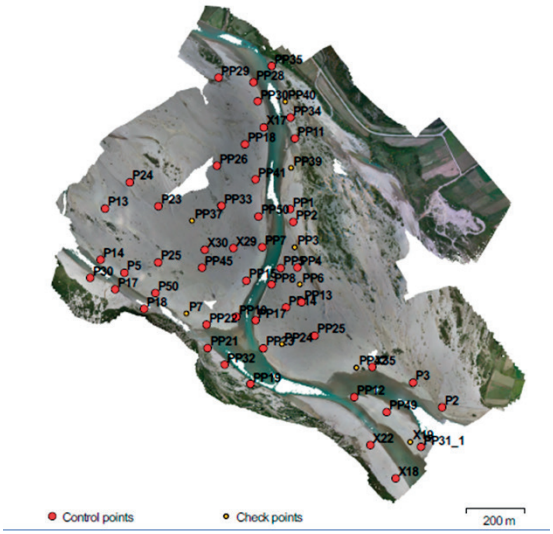

Figure 4: GCP locations.

Figure 5: KR6I5 Hexacopter with 24MP camera.

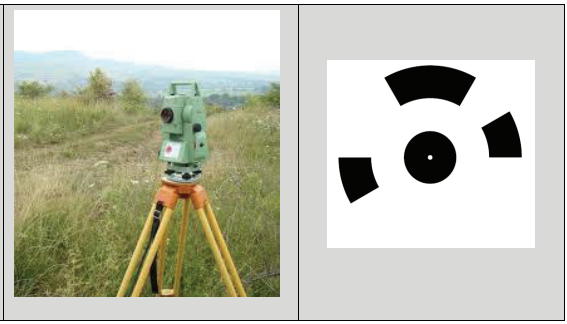

Figure 6: Leica TCR-407 electro-optical total station(left) and 12-bit-circular target (GCP)(right).

Table 2: Camera settings.

Camera Model	Resolution	Focal Length	Pixel Size	Precalibrated
Sony ILCE-6000	6000 x 4000	16 mm	4 x 4 µm	No

02.05.01 Ground control points (GCP)

The ground control points (GCP) were obtained by using terrestrial surveying. The type of the tachymeter device used to collect the data was a Leica TCR-407 (Figure 6). The coordinates of 59 GCP were collected and located on well-defined features with good and homogeneous distribution over the study area. These were measured in a local coordinate system. From all collected points, only 50 were used as GCPs and the remaining 9 points were used as Check Points as show in Table 3 and Table 4.

Table 3: Control points RMSE.

Count	X error (cm)	Y error (cm)	Z error (cm)	XY error (cm)	Total (cm)	Image (pix)
50	3.62	4.04	2.51	5.42	5.97	0.48

Table 4: Check points RMSE.

Count	X error (cm)	Y error (cm)	Z error (cm)	XY error (cm)	Total (cm)	Image (pix)
9	4.58	4.84	2.07	6.67	6.98	0.42

02.05.02 Workflow of the post precessing using AGISOFT PHOTOSCAN PROFESSIONAL

02.05.02.01 Import and Align Photos

- **Manually remove** images that are obvious 'outliers' (e.g., images that have been taken before take-off or after landing).
- **Estimate image quality:** Disable all images that have an image quality below 0.7-0.85. Estimate Image Quality feature provides only the information about the sharpest border detected on the image and should be used to find only images which are obviously blurred.
- **Align photos** (quality HIGH, pair preselection: GENERIC (REFERENCE using camera GPS), key point limit: 40,000, tie point limit: 4,000, adaptive camera model fitting: YES). These are empiric values, which show the best ratio between processing results and processing time.

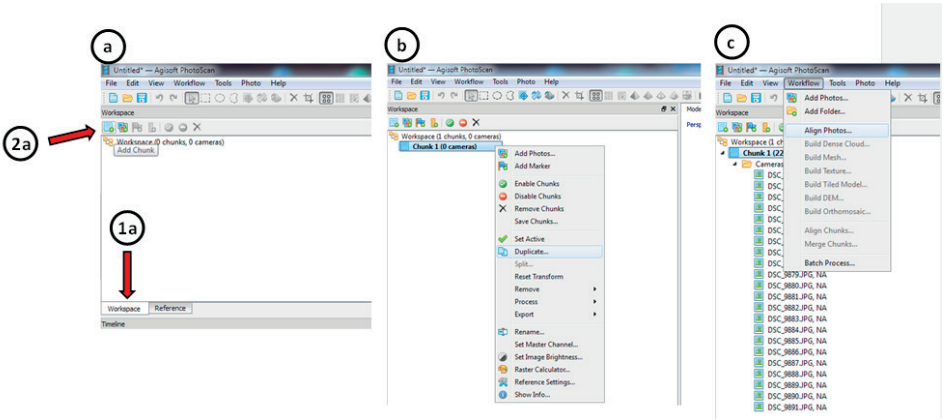

Figure 7: Workflow add chunk, add photos, align photos using AGISOFT Photoscan Professional.

As a result of the photo alignement the tie point cloud is constructed (Figure 8).

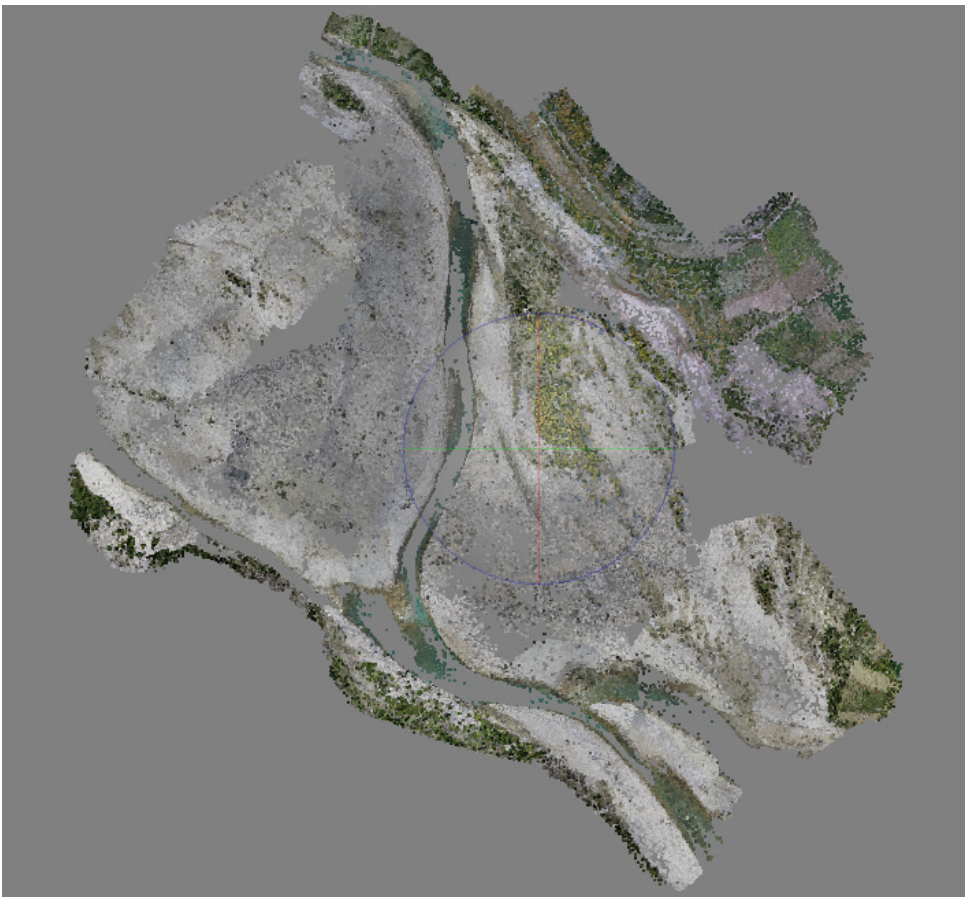

Figure 8: Tie point cloud of the study area 389,513 of 806,891 points (ortho view).

02.05.02.02 GCP and dense point cloud and DTM creation

- Import list of ground control points (Figure 9). In case of problems with the automated GCP detection (12-bit-circular targets), the GCP has to be detected and numbered manually on the images. (Three days work duration in this case).

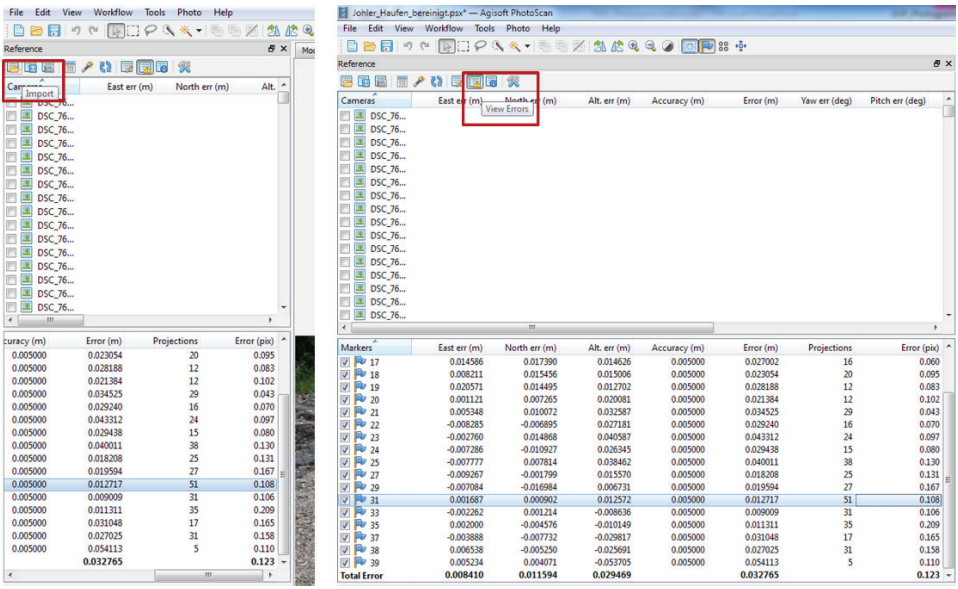

Figure 9: Importing the coordinates of the GCP.

Assuming that you have a sufficient number (depending on the study area size) of high accuracy ground control points, uncheck all images in the reference pane and also uncheck a few GCPs (20 to 30%) in order to use them as check points instead of control points. This will give you a better measure of the 'real accuracy' of your dataset.

- **Clean sparse point cloud** (=tie point cloud)(EDIT > GRADUAL SELECTION). Remove all points with high reprojection error (choose a value below 1, suggestion to use 0.5-0.8) and high reconstruction uncertainty (try to find the 'natural threshold' by moving the slider).
- **Optimize camera alignment**
- **Build dense cloud (Figure 10):** Choose HIGH or *MEDIUM* quality, but it depends on what you want to do with the data and on your hardware including CPU, GPU and RAM.

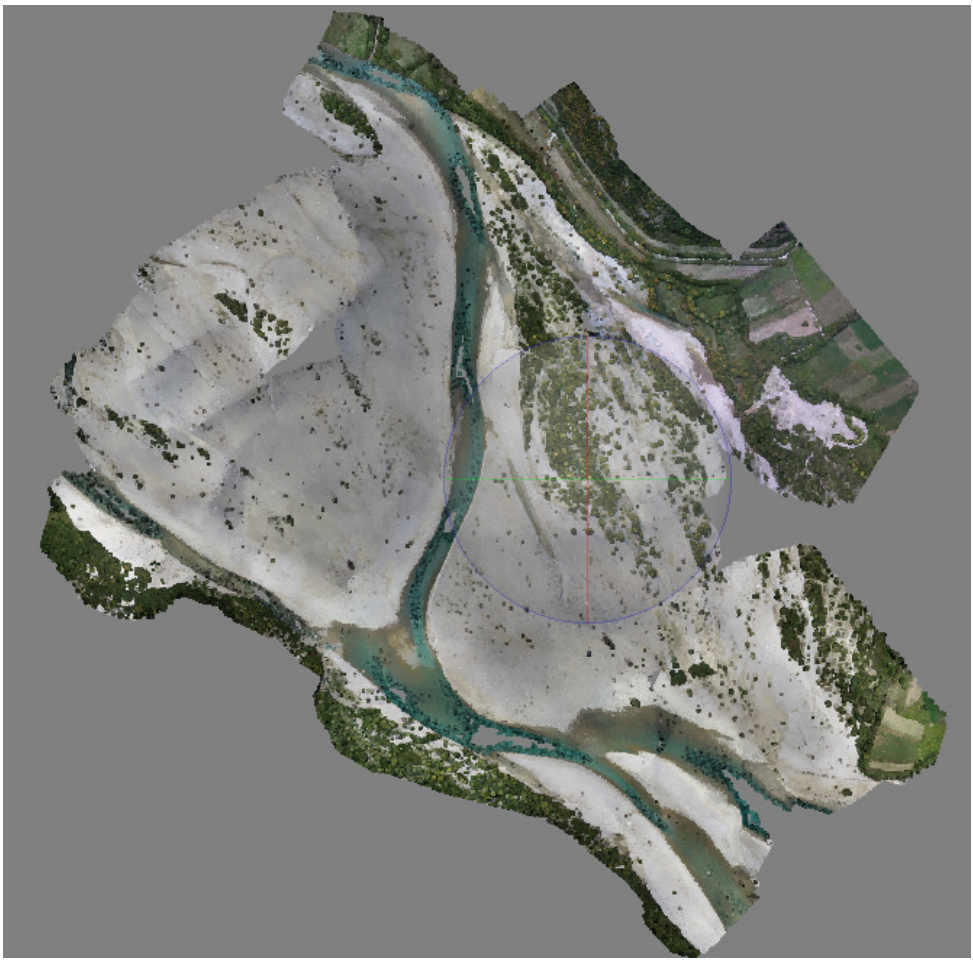

Figure 10: Dense point cloud including 192032208 points (ortho view).

- **Build DEM (from dense cloud).** Agisoft uses IDW Interpolation on the specified resolution without up sampling; usually less noise around sharp structures (Figure 11).

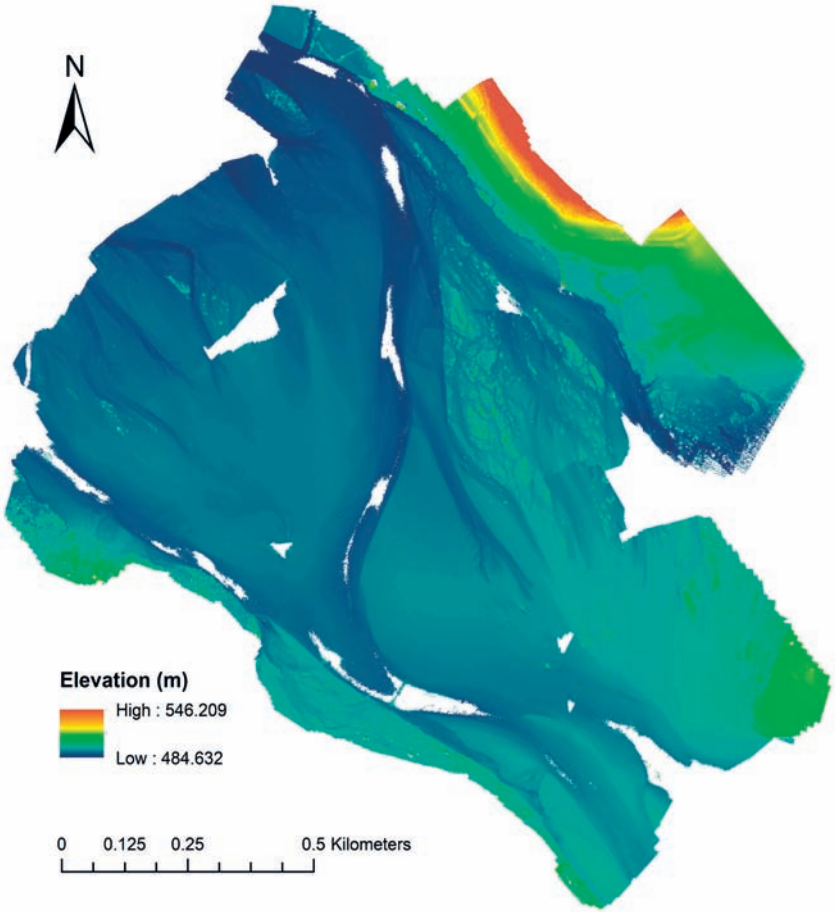

Figure 11: DEM based on the dense point cloud (10 x 10 cm resolution).

Finally, Figure 12 shows an overall summary about the post processing operations, used specifications and the calculating durations using a Intel i7-6700 with 16 GB RAM.

Processing Parameters

General	
Cameras	1919
Aligned cameras	1919
Markers	59
Coordinate system	Local Coordinates (m)
Point Cloud	
Points	389,513 of 806,891
RMS reprojection error	0.28917 (0.838275 pix)
Max reprojection error	1.99837 (40.2003 pix)
Mean key point size	2.86438 pix
Effective overlap	10.5379
Alignment parameters	
Accuracy	High
Pair preselection	Generic
Key point limit	40,000
Tie point limit	4,000
Constrain features by mask	No
Adaptive camera model fitting	Yes
Matching time	14 hours 13 minutes
Alignment time	40 minutes 28 seconds
Optimization parameters	
Parameters	f, b1, b2, cx, cy, k1-k4, p1, p2
Optimization time	47 seconds
Dense Point Cloud	
Points	192,032,208
Reconstruction parameters	
Quality	Medium
Depth filtering	Aggressive
Depth maps generation time	1 days 8 hours
Dense cloud generation time	3 hours 50 minutes
DEM	
Size	25,892 x 26,704
Coordinate system	Local Coordinates (m)
Reconstruction parameters	
Source data	Dense cloud
Interpolation	Disabled
Processing time	35 minutes 6 seconds
Orthomosaic	
Size	16,403 x 17,152
Coordinate system	Local Coordinates (m)
Channels	3, uint8
Blending mode	Mosaic
Reconstruction parameters	
Surface	DEM
Enable color correction	Yes
Processing time	5 hours 17 minutes
Software	
Version	1.2.6 build 2834
Platform	Windows 64 bit

Figure 12: Summary of the post processing operations and calculating durations.

03 Grain size analyses of surface material

The grain size distribution (GSD) of the surface layer is known to be very heterogeneous – this is especially the case for Natural Rivers such as the Vjosa. Optical inspection of the surface layer in the inundation area at Queserat show numerous patches and areas with a succession of different GSD. The formation of these patches is based on the flow respectively flood history of the river, respectively the morphological changes associated with it. The transition between those patches seem to be mostly gradual in flow direction and relatively sudden orthogonal to the flow.

Due to two main reasons, the classical sieving approach to determine the surface GSD was not feasible. Firstly, the wide span of grain sizes would require very bulky samples for coarser patches. Secondly, the very spacious sample area makes the transportation of these samples very difficult and unreasonably laborious (Bunte and Abt 2001). Therefore, an alternative method (which was originally developed to counter the described problems) was used, namely the pebble counts method along defined transects.

There, a predefined number of particles (usually at least 150) is collected along linear transects which should be placed parallel to the direction of to the former flow path. The location of the transects should by representative for the surrounding area. Starting from one end of a transect, all particles bigger than approximately 1 cm are collected. The collected particles are then fractioned by grain size using a simple metal frame (Figure 13). For representative results, it is advised to collect a minimum of 150 particles with at least 30 particles in the middle fraction.

As the mass of the particles is not measured, this analysis only provides particle size distribution of surface layer at first. The application of the empirically derived formula (1), developed by Fehr (1987), converts the particle size distribution into mass fractions of a volume sample.

$$\Delta p_i = \frac{\Delta q_i * d_{mi}^{0.8}}{\sum q_i * d_{mi}^{0.8}} \qquad (1)$$

Whereas: Δp_i is the fraction mass [kg]; Δq_i number of particles in fraction i; d_{mi} the characteristic or mean grain size of fraction i in [mm]; n the number of stones per fraction

Figure 13: Metal frame for the fractional determination of the collected particles.

The biased sampling (smaller particles are usually under-sampled) leads to an underestimation of fine material. The empiric formula (2) is used to (partially) correct this error (Fehr, 1987).

$$p_{IC} = 0.25 + 0.75 * \sum \Delta p_i \quad (2)$$

Whereas: p_{ic} corrected probability per fraction i; Δp_i mass of fraction i divided by total sample mass

The missing fraction smaller 10 mm could be further corrected by the implementation of a Fuller function (Fehr, 1987). This correction would somehow lead to ambiguous results for coarser samples. In favour of the comparability of the different pebble count samples, the Fuller-correction therefore disregarded.

During the monitoring campaign in the area of Queserat, 10 pebble count per transect samples of the surface layer have been taken. Most of the sample locations where in relatively close proximity to the main river channel as displayed in Figure 14. Samples 3 and 4 were taken close to a secondary river channel which has fallen dry during the low flow period.

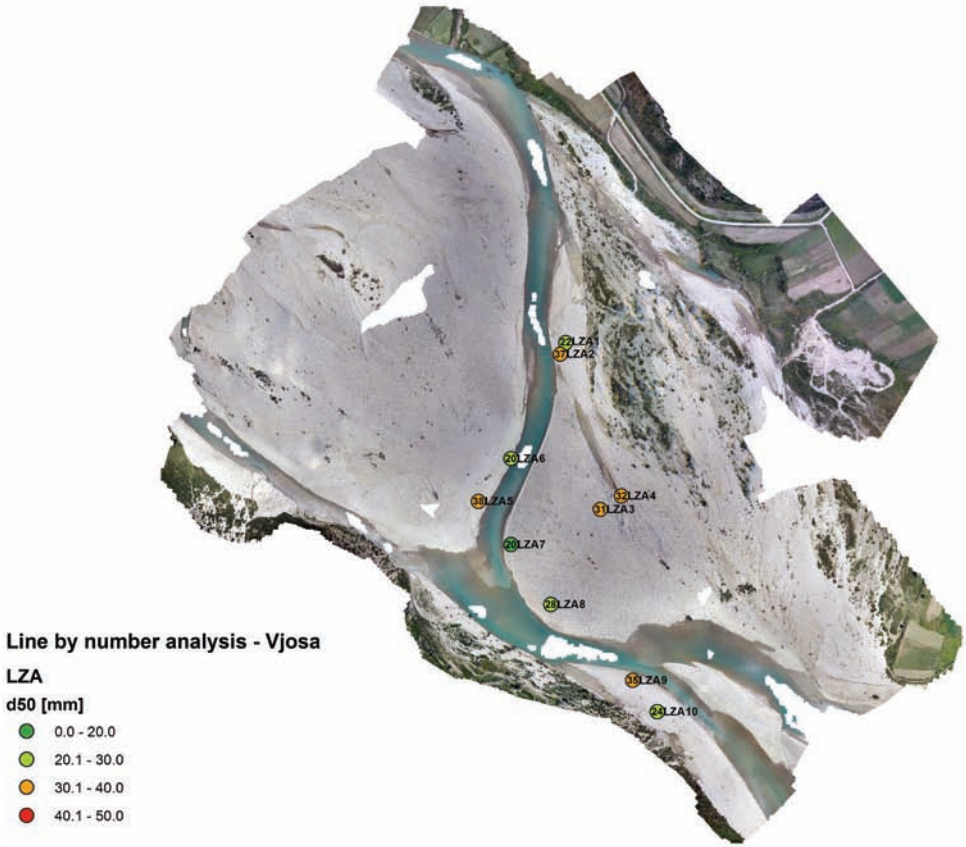

Figure 14: Location of the pebble count per transect samples of the surface layer, Vjosa/Queserat.

The results of the grain size analyses of the surface material are listed in Table 5. The characteristic grain size is 35,4mm on average with 24,6mm for the finest and 48,1mm for the coarsest sample. The grain size distribution of the pebble count samples differ mainly in grain size but less in the distribution characteristic itself (Figure 15a). A comparison between bedload material (bigger than 4mm in size) gathered during the monitoring campaign in Pocem and the pebble count samples is displayed in Figure 15b. Due to the different sampling technique (and therefore missing fraction of surface material <10mm), the samples are not completely comparable. Nevertheless, the results indicate, that the bedload material collected in Pocem is relatively similar to the surface material at the inundation area in Pocem. Transported bedload material consists of grain particles which usually have been eroded and deposited beforehand. Unsurprisingly, the collected bed load material in Pocem reflects the variability of subsurface material found upstream.

Table 5: Characteristic grain sizes and distribution parameters for 10 pebble count per transect samples of the surface layer, (Vjosa/Queserat).

	d_m (mm)	U	Cc	d_{10} (mm)	d_{20} (mm)	d_{30} (mm)	d_{40} (mm)	d_{50} (mm)	d_{60} (mm)	d_{70} (mm)	d_{80} (mm)	d_{90} (mm)	d_{16} (mm)	d_{84} (mm)
LZA1	24.6	1.9	0.97	13.3	16.0	17.8	19.9	22.2	24.8	27.7	30.9	38.3	14.9	32.7
LZA2	43.3	2.4	0.93	18.0	22.8	26.8	31.4	36.7	42.8	50.3	59.5	77.7	20.8	63.6
LZA3	38.8	2.0	0.94	17.9	21.5	24.5	27.4	30.7	35.8	42.8	53.9	70.8	20.0	59.6
LZA4	42.4	1.9	0.91	19.6	23.5	26.1	29.0	32.4	38.3	45.3	56.1	75.6	22.4	61.1
LZA5	48.1	2.6	0.78	18.9	23.6	26.8	30.5	38.3	48.6	57.8	69.6	85.6	22.1	75.6
LZA6	24.6	2.2	0.94	10.5	12.8	15.1	17.5	20.1	23.2	28.5	35.2	44.0	12.0	38.5
LZA7	24.7	2.0	0.87	11.3	13.0	14.9	17.1	19.7	22.6	26.4	30.7	42.6	12.3	33.7
LZA8	37.6	2.1	0.91	15.4	18.3	21.4	24.6	28.2	32.4	41.7	54.5	74.0	17.3	60.8
LZA9	43.0	2.5	0.86	17.7	22.1	25.7	29.6	35.2	43.6	51.7	60.8	78.0	20.2	65.5
LZA10	27.0	1.7	0.91	15.5	17.6	19.6	21.7	24.2	27.0	30.2	34.7	41.4	16.9	37.3
Composite LZA	35.4	2.2	1.0	14.5	17.9	21.1	24.3	27.7	31.6	38.8	49.0	65.1	16.8	54.7

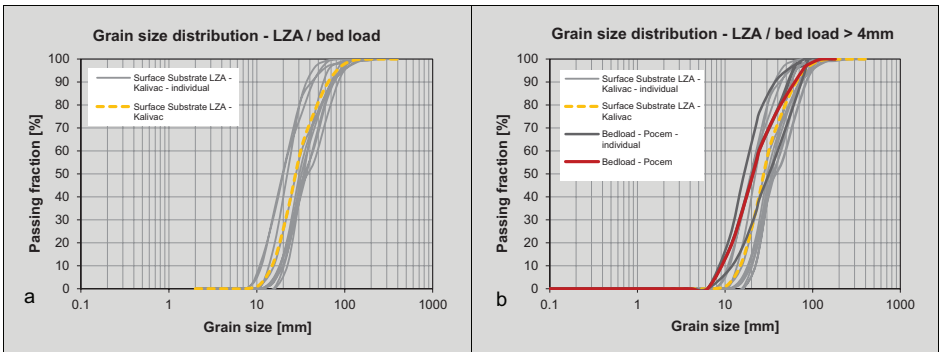

Figure 15: (a) Grain size distribution of the surface substrate (Vjosa/Queserat); (b) Grain size distribution of the surface substrate (Vjosa/Queserat) compared to grain size distribution of bedload samples limited to particles bigger then 4mm (Vjosa/Pocem).

Figure 16 is an approximation of surface layer GSD based on a combination between the pebble count samples and the information gathered by drone based digital elevation model (especially the local standard deviation). It should be noted that vegetation cover has a strongly negative influence in the result of the analyses (e.g the area on the left bank or the area in the north east). Furthermore, some changes in the local standard distribution of the digital elevation model are due to actual changes in the elevation and not due to changes in the GSD. The relative high flight height of the drone (needed to cover the area) somehow amplifies this effect. However, this error is difficult to distinguish as changes in elevation and GSD often appear hand in hand.

With this preface in mind, Figure 16 still shows some interesting qualitative details about the surface GSD in the area. Clearly visible is the secondary channel around LZA 3 and 4. During a visual observation on site, both channel banks showed a relatively course bank substrate which is adequately reflected in the GSD approximation. The approximated surface GSD of the local area around the other LZA seems to be a good estimation of the natural distribution on site. Patches with relative fine surface material (triangle LZ 6-7-3) very much converge with visual observations on site.

Changes in the surface GSD are typically gradual in flow direction (e.g gravel bar east of LZA8). In contrast, more sudden GSD changes appear orthogonal from the flow direction – typical for bank areas around present (and former) flow channels.

The surface GSD in the monitored area appears to be very complex and heterogeneous. In general, the surface GSD of a river can be interpreted as a memory of its flow history – this is especially the case for areas which inundated only occasionally. Morphologically very active rivers like the Vjosa therefore regularly overprinted parts of this flow memory through a reconfiguration of the surface GSD during flood events.

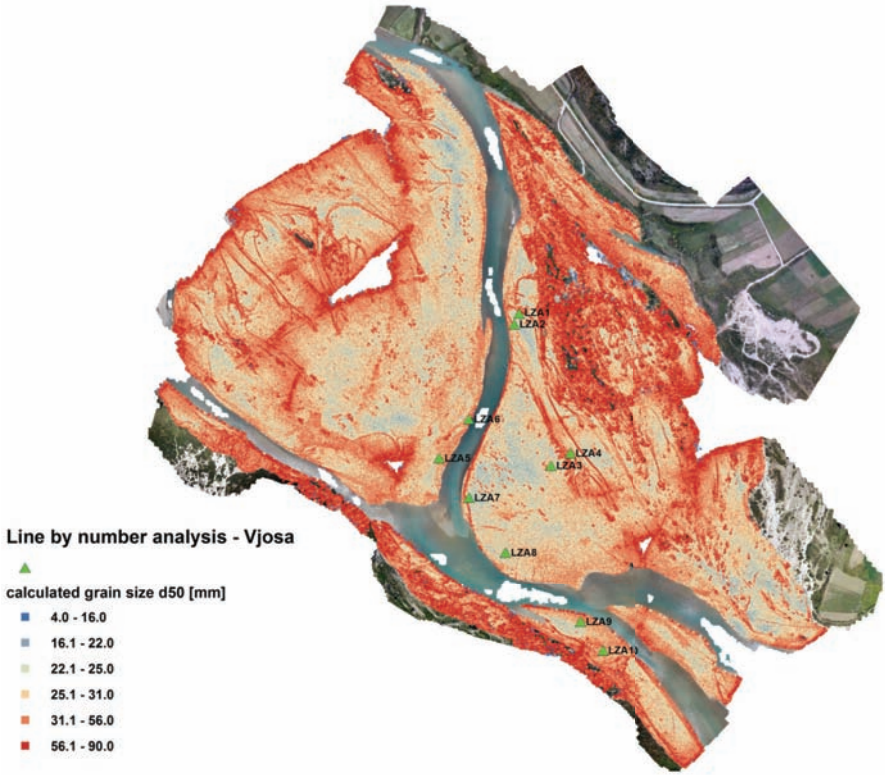

Figure 16: Approximation of the surface layer grain size distribution (note errors due to vegetation cover and potentially insufficient correction of elevation changes).

04 Sediment transport monitoring

This chapter is dedicated to the central aims of the presented study. Both, (i) bed load and (ii) suspended sediment transport monitoring are presented from the methodological aspects as well as the derived results which are used for discussion about the deposition rates of the planed reservoris in the Vjosa.

04.01 Methods Bed load measurment

Basket samplers are among the most frequently used methods for direct bedload transport measurement in gravel-bed rivers (Liedermann et al., 2018). The sampling of bedload at the riverbed by suitable containers (basket, box) in a given measuring time is a method used for decades. An overview of measuring devices of this kind has been published amongst others by Hubell (1964), Van Rijn (1986) and Habersack (1997).

As the Vjosa River can reach high flow velocities and turbulences at discharge peaks, a suitable measuring device to deal with these conditions was necessary. Therefore, an adapted version of the BfG basket sampler (Figure 17) was chosen as anapproved and tested, standardized mobile measuring device for gravel bed rivers. The device is based on the device used by the Federal Institute of Hydrology in Koblenz, Germany and is characterized by a more massive construction with heavier loads to obtain higher stability during the sampling process (Liedermann et al., 2012). The sampler is characterised by a mesh size of 1 mm, an orifice size of 160 × 80 mm and a device weight of approximately 200 kg.

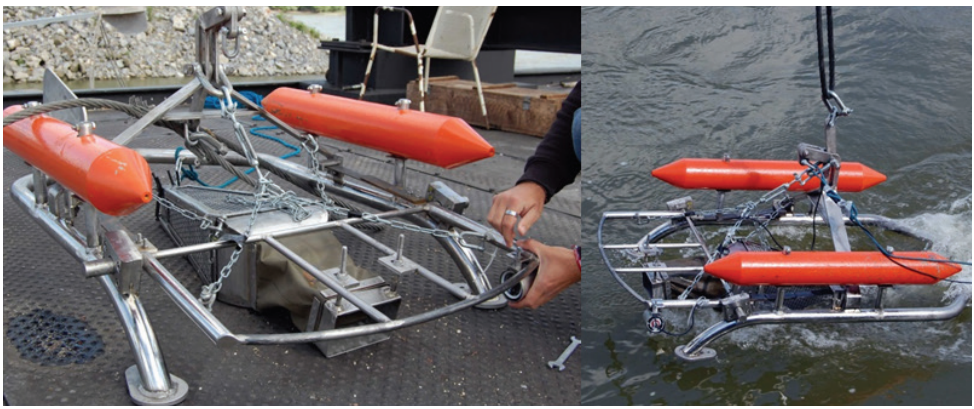

Figure 17: Adapted BfG basket sampler.

The adapted BfG sampler uses shape-induced pressure differences to compensate for backpressure. The net with the appropriate mesh size generates a certain

backpressure depending on flow velocity, so that the entry velocity approximates the flow velocity and results in a neutral catching behaviour.To ensure that no additional material except the transported bedload enters the sampler basket, the device uses a time-shifted touchdown and take-off of the inlet opening, operated by a separate hanger assembly and hardened steel springs representing another substantial advantage of the chosen sampler (Liedermann et al., 2018).

Measurement and data processing

Due to the high spatial-temporal variability of bed load transport (Habersack, 1997), the BfG collector is lowered for three times at every vertical (Figure 18a). After each measurement, the captured sample is collected from the basket and labelled in separate containers (Figure 18b). A regular measurement lasts for five minutes; deployment time is shortened depending on the transported load in order to avoid overfilling the sampler basket (Liedermann et al., 2018).

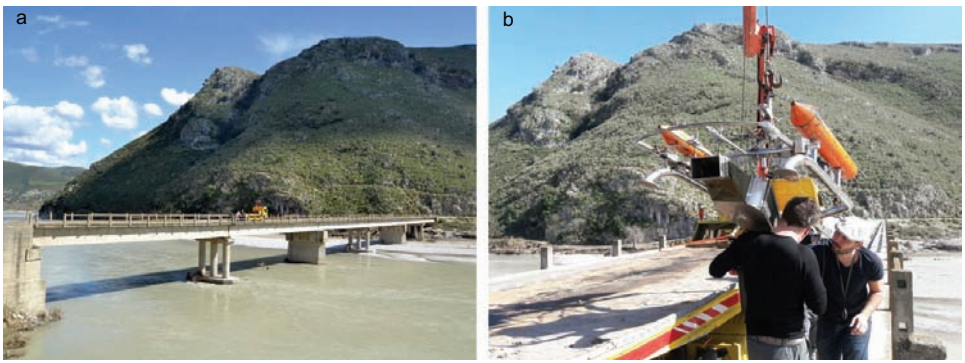

Figure 18: (a) Bed load measurement at the bridge cross-section in Pocem; (b)Emptying of the BfG basket sampler.

To calculate sediment transport, the collected samples must first be dried, weighed and sieved. An empirically developed equalisation function provides correction coefficients for sampling amounts between 2.5 and 6 kg in order to compensate for the increased backflow effect and calculate the undisturbed load. Correction values can be applied up to a maximum of 6 kg. For samples exceeding this weight, time was adapted in order to apply an adjustment factor (Dröge et al., 1992). Transport over the cross-section is calculated by integrating the medium loads for each location (Table 6). Finally, bedload transport within the entire cross-section is determined graphically (Liedermann et al., 2018).

Laboratory analysis of bed load samples

There were 86 sediment samples obtained from the sampling stations at the bridge in Poçem (Figure 19). 20 sediment samples were collected during 15-16 March 2018, and 66 sediment samples were collected during 27-28 March 2018.

In order to dermine the particle size distribution of the captured samples, the ASTM D4822 – 88 standard was applied. Most of the captured samples were air-dried at room temperature as shown on Figure 19a, only in some cases (Figure 19b) the samples were dried in the oven at 105°C for 12 h. Once dry, the samples were cooled and weighed. The samples were continued with the sieve analysis, a procedure commonly used in engineering to dermine the particle size distribution of the granular material.

A series of sieves, of square-mesh woven-wirecloth, conforming to the ASTM standard were chosen. The full set of sieves includes the following series:

(125 mm)	(8 mm)
(90 mm)	(4 mm)
(63-mm)	(2 mm)
(56-mm)	(1 mm)
(31,5-mm)	(500 μm)
(22,4 mm)	(250 μm)
(16-mm)	(125 μm)
(11,2 mm)	(75-μm)

Figure 19: (a) Sediment sample No. LR7-B1 of 27 March 2018 drying at room temperatures; (b) Sediment sample No. L19-B1/B2 of 16 March 2018 prepared for the oven drying process.

The mechanical sieving operation was conducted by means of a lateral and vertical motion of the sieve, accompanied by a jarring action inorder to keep the sample moving continuously over the surfaceof the sieve. The percentages of the sample retained and passed through the sieves were calculated using the following formulas

$$\% \, retained = \frac{w_r}{w_t} x \, 100\% \tag{3}$$

$$\frac{\sum w_r}{w_t} x \, 100\% \; < 2\% \tag{4}$$

where w_r denote the weight retained in each siever and w_t is the total weight of the sample.

At the end of weighing, the sum of the masses retained on the entire sieves used equal closely the original mass of the quantity sieved. In order to have a full spectrum of the grain size distribution the material passing the No. 200 (75-μm) sieve was weighed together.

The results of the grain size analysis obtained are shown on Figures 20, 21, 22 and 23.

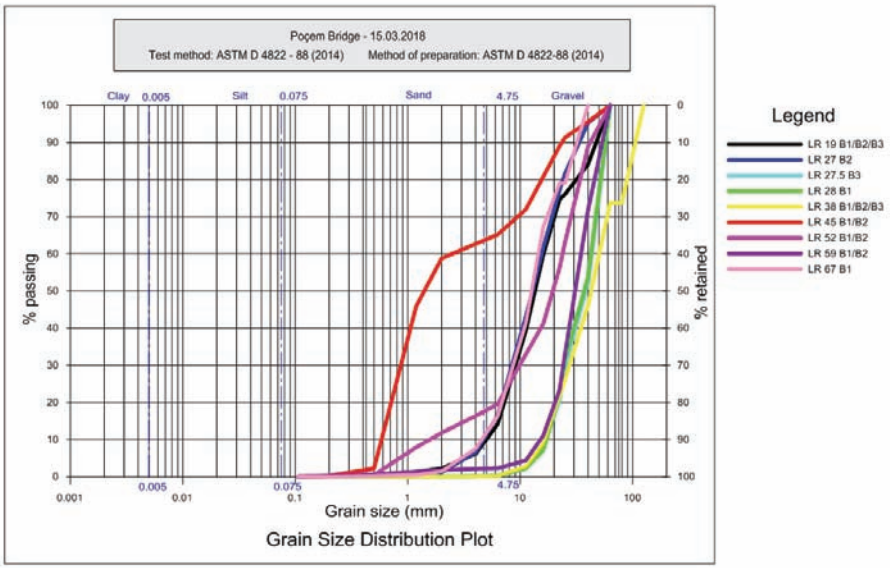

Figure 20: Thegrain distribution curves of the samples of 15 March 2018.

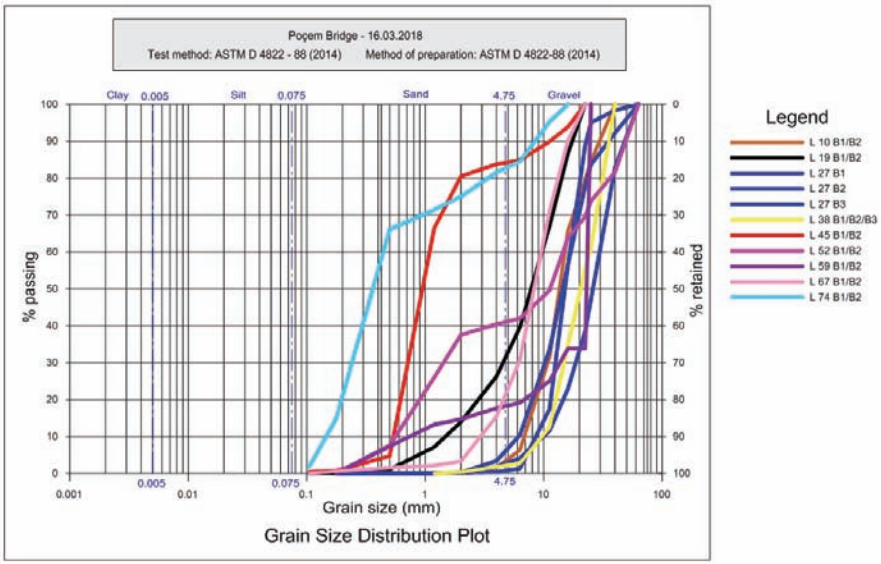

Figure 21: Thegrain distribution curves of the samples of 16 March 2018.

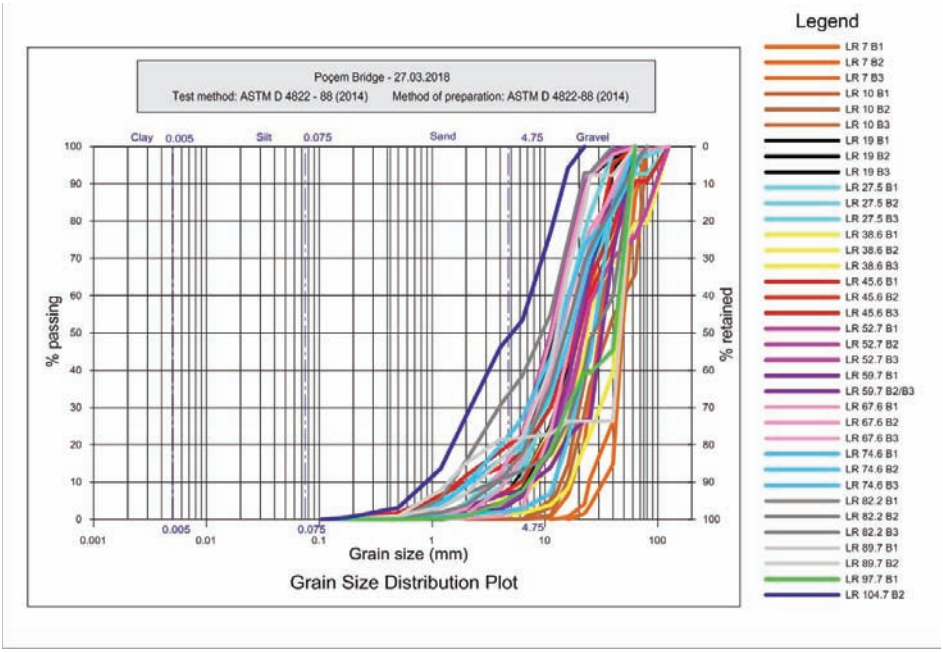

Figure 22: Thegrain distribution curves of thesamples of 27 March 2018.

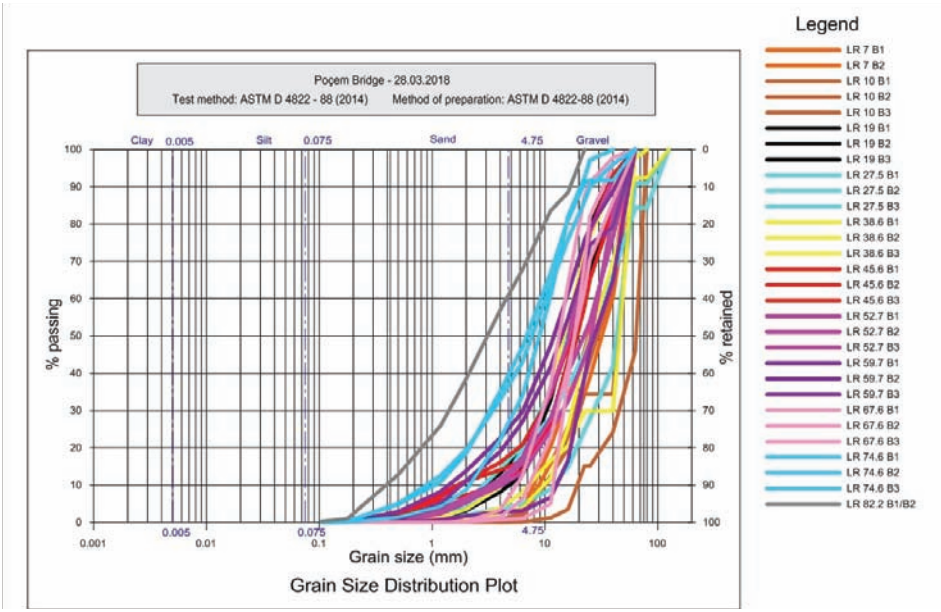

Figure 23: Thegrain distribution curves of the samples of 28 March 2018.

Table 6: Calculation bed load – 27.03.2018.

						samples < 2500g	samples > 6000g			samples 2500 - 6000g				
Station	Distance from right bank	Duration	Weight	per width of basket	mean at one vertical	per 1 m width	Conversion factor	Concersion duration	Concersion weight	Factor 100 %	Corrected weight	per width of basket	mean at one vertical	per 1 m width
	[m]	[s]	[g]	[g/s*b]	[g/s*b]	[g/s*m]	[%]	[s]	[g]		[g]	[g/s*b]	[g/s*b]	[g/s*m]
I	7.0	300	4771	16						1.36	6489	22	10	67
		300	1613	5								5		
		300	1281	4								4		
II	10.0	300	18319	61			32.75	98	6000	1.50	9000	92	67	430
		180	9591	53			62.56	113	6000	1.50	9000	80		
		180	4082	23						1.25	5103	28		
III	19.0	180	16115	90			37	67	6000	1.50		0	5	34
		120	8203	68			73	88	6000	1.50		0		
		120	1916	16								16		
IV	27.5	180	15685	87			38	69	6000	1.50		0	0	0
		120	11980	100			50	60	6000	1.50		0		
		120	3146	26						1.05		0		
V	38.6	180	14846	82			40	73	6000	1.50		0	0	0
		120	3333	28						1.09		0		
		120	9593	80			63	75	6000	1.50		0		
VI	45.6	180	1167	6								6	2	14
		300	8254	28			73	218	6000	1.50		0		
		300	13557	45			44	133	6000	1.50		0		
VII	52.7	180	9825	55			61	110	6000	1.50		0	4	26
		180	7851	44			76	138	6000	1.50		0		
		180	2184	12								12		
VIII	59.7	180	15990	89			38	68	6000	1.50		0	0.65	4
		300	387	1								1		
IX	67.6	180	10236	57			59	106	6000	1.50		0	0	0
		180	21925	122			27	49	6000	1.50		0		
		120	4869	41						1.38		0		
X	74.6	180	2811	16						1.02		0	3	21
		180	1721	10								10		
		180	6582	37			91	164	6000	1.50		0		
XI	82.2	180	527	3								3	2	11
		300	681	2								2		
		300	8607	29			70	209	6000	1.50		0		
XII	89.7	300	1594	5	3	19								
		300	205	0.68										
XIII	97.7	330	326	0.99	0.49	3								
		300	0	0										
XIV	104.7	300	0	0	0.32	2								
		300	191	0.64										
XV	111.7	300	0	0	0	0								
XVI	118.7	300	0	0	0	0								
XVIII	138.7	300	0	0	0	0								

04.02 ADCP – discharge and Flow velocity

An "Acoustic Doppler Current Profiler" (ADCP) uses the Doppler effect to measure velocities in flowing waters. The signals emitted by the ultrasound transducer are reflected by particles in the water body and the bottom of the water. From the frequency shift between the emitted and the reflected beam, the flow rate can be determined. The ADCP divides the water column into depth cells (also referred to by some software and references as bins) and reports a velocity for each depth cell. After repeated measurements by pulling the ADCP device across the river or performing a section per section measurement (Figure 24) a flow velocity distribution as well as a discharge for the cross section is available (Mueller et al., 2009).

Figure 24: ADCP measurement boat at the bridge profile in Pocem (left) and live view results of the performed measurement (right).

04.03 Method Suspended Load Measurement

To quantify suspended sediment loads in rivers, the distribution of the suspended sediment concentration in the cross section (spatial variability) as well as the temporal variability related to different discharge levels has to beconsidered (Wass and Leeks, 1999). To address these requirements, different methods to measure the spatial and temporal variability of the suspended sediment transport are normally used.

04.03.01 Multi-point sampling

When using the multi-point sampling method, the flow cross-section is subdivided into several verticals, ateach of which samples are taken at different depths. The number of verticals and the number of measurement points per vertical depend on the width and depth of the water body (DVWK, 1986). In general, five to ten verticals are sufficient to determine the horizontal distribution of suspended sediments (Edwards and Glysson, 1999). By measuring the local velocities simultaneously in the respective sampling points, the calculation of the velocity-weighted average suspended matter concentration in the profile can be determined. According to DVWK (1986), the multi-point method is considered to be the most accurate sampling method for measuring suspended sediment transport, restrictions are given due to the high time consumption, necessary for applying this method (BMLFUW, 2017). A schematic illustration of a multi-point suspended sediment sampling strategy is depicted in Figure 25.

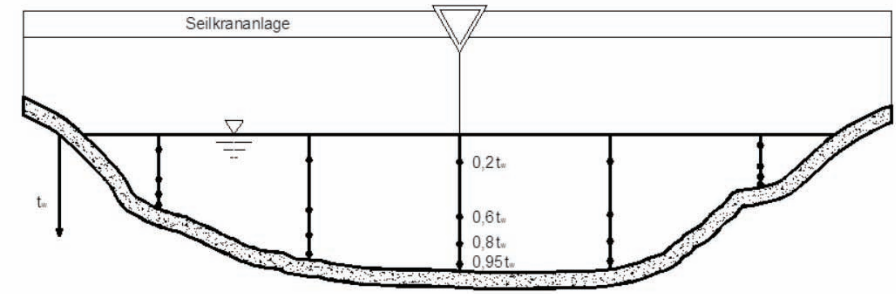

Figure 25: Scheme of a multi-point suspended sediment sampling (BMLFUW, 2017).

04.03.02 Depth integration method

When using the integration method – which was chosen for the current project -, the flow area is also divided into several verticals. At each vertical, the sampling device is lowered and respectively uplifted with constant speed from the water level to the riverbed. When using sampling devices with valve control, the sample can be opened either during the lowering or during the lifting process. This method provides the average velocity-weighted suspended sediment concentration between the surface and riverbed at every vertical. The prerequisite for this is that the inflow into the measuring device is mainly isokinetic. The advantage of the integration method compared to the multi-point method lies in the faster operationtime (DVWK, 1986). However, this method is less accurate with increasing flow rate compared to the multi-point method (BMLFUW, 2017). A schematic illustration of a depths integrated suspended sediment sampling scheme is depicted inFigure 26.

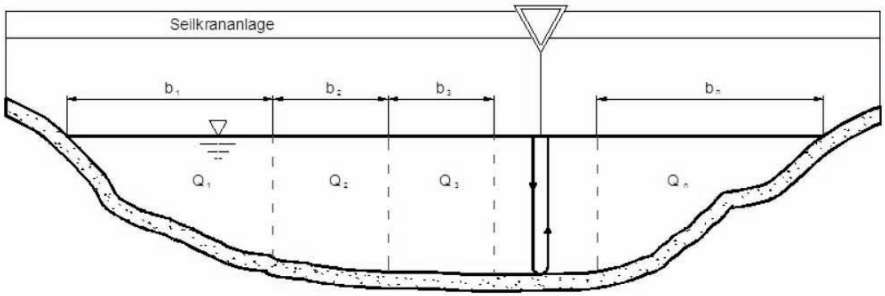

Figure 26: Scheme of a depth integrated suspended sediment sampling (BMLFUW, 2017).

The samples at the Vjosa were taken by using a US - P61A Suspended Sediment Sampler (Figure 27). TheUS - P61 collector weights approximately 50 kg, is streamline shaped and equipped with "tail fins" ensuring a stable positioning within the stream so that the inlet opening points in the direction of flow. The inlet closure is released by sending a current pulse to the rotary valve. Inside the collector a 1-liter plastic bottle is placed, which ideally should not be completely filled to ensure sample representativeness. Samples are taken isokinetically, which means that the inflow velocity into the collector is equal to the flow velocity of the surrounding water. This ensures that the concentration of suspended solids in the sample bottle is equal to the concentration of suspended solids in the water (FISP, 2007).

Figure 27: US-P61A Suspended Sediment Sampler.

Laboratory

The samples are analysed in a specially equipped laboratory by filtration for their content - the volume-related mass of the undissolved substances contained in the water, which are filtered off under certain conditions and then weighed after a specified drying process.They are based on the volume of the water sample and expressed in mg/l(DIN 38 409 Part 2, 1987).

The analysis is carried out with a filter unit and a vacuum pump, using a membrane filter with a pore size of 0.45 μm. These filters must be dried in a drying oven at 105 +/- 2 ° C for two hours prior to use and then cooled to room temperature in a desiccator for 30 - 60 minutes. The following weight determination is carried out with an analytical balance to 1 mg. The filter is then placed in the vacuum filter unit and the entire volume of the sample, which was previously determined, is filtered. The used filters are dried, cooled and weighed as described above.Figure 28 shows the filtration unit and the vacuum pump as well as new and used filters (BMLFUW, 2017).

Figure 28: Filter unit with pump in the background (left); used filters (above) new filters (below) (right).

The evaluation of the content of filterable substances is carried out according to DIN 38 409 part 2 by means of the following equations 1 and 2:

$$\beta_A = \frac{m_T}{V_P} \cdot f \qquad (5)$$

$$m_T = m_b - m_a \qquad (6)$$

when

βA	filterable substances [mg/l]
mT	dry matter [g]
ma	mass of filter [g]
mb	mass of filter and filterable substances [g]
VP	volume of the sample [l]
f	factor: f = 1.000 mg/g

When using theintegration method with flow measurements, the calculation of the sediment load is based on the product ofmean velocity in the vertical (vm) and suspended sediment concentration of the integration sample (cs). By using the known water depth (h(tv)) in the measures verticals and the distances (b) between the vertical lots, the suspended sediment load can be calculated according to Table 7 (BMLFUW, 2017).

Table 7: Calculation suspended load - 15.03.2018 - integration method.

Station	Water depth	C_s	V_m	$C_s * V_m$	S-rate	Distance from 0	S-transport	Q_{part}
	h(tv)				$f_{Cs}=(C_s*V_m)*h$	b	$m_{s(i)}=[(f_{Cs(i+1)}+f_{Cs(i)})/2]*(b_{(i+1)}-b_{(i)})$	
		[g/m³]	[m/s]	[g/m²*s]	[g/m*s]	[m]	[g/s]	m³/s
						6.2	3422.48	9.38
10	6.50	182.5	1.52	277.04	1801.31	10	14110.06	80.08
19	4.58	172.0	1.69	291.20	1334.26	19	11262.92	62.24
27	3.97	191.8	1.94	372.79	1481.47	27	13950.82	78.87
38	3.20	160.5	2.05	329.39	1055.04	38	7822.63	44.07
45	3.07	195.9	1.96	384.49	1179.99	45	6872.25	37.01
52	2.52	170.7	1.82	310.91	783.50	52	4180.32	22.39
59	1.60	200.0	1.29	257.60	410.87	59	2338.11	12.54
67	1.38	153.5	0.82	125.56	173.66	67	1319.78	4.30
						82.2		

Suspended load [kg/s]:	**65279.37**
Suspended load [g/s]:	**65.28**
Discharge [m³/s]:	**350.87**
Concentration [mg/l]:	**186.05**

05 Results

In Table 8an overview of the performed measurements at the Vjosa River is depicted, showing the date of the measurements, water levels, discharges, transported bedload and transported suspended sediment loads.

Table 8: Overview of the performed measurements.

Date	Water level (cm)	Discharge (m^3s^{-1})	Bed load (kgs^{-1})	Suspended load (kgs^{-1})
15.03.2018	148	350	1	65
16.03.2018	136	302	1	47
27.03.2018	246	870	29	1045
28.03.2018	211	627	25	497

05.01 ADCP – discharge and Flow velocity

The rivers' width ranges from 80 m at a discharge of 302 m3s-1 (Figure 29b) to 155 m at a discharge of 870 m3s-1 (Figure 29c). Mean flow velocities range from 1.30 ms-1 at a discharge of 302 m3s-1 (Figure 29b) to 2.30 ms-1 at a discharge of 870 m3s-1 (Figure 29c). High flow velocities concentrate near the right river bank for all discharge measurements. This is also the deepest part of the cross section and is characterized as an outer bank with a steep rock shore. Furthermore, low flow velocities respectively backwaters behind the bridge piers are clearly visible.

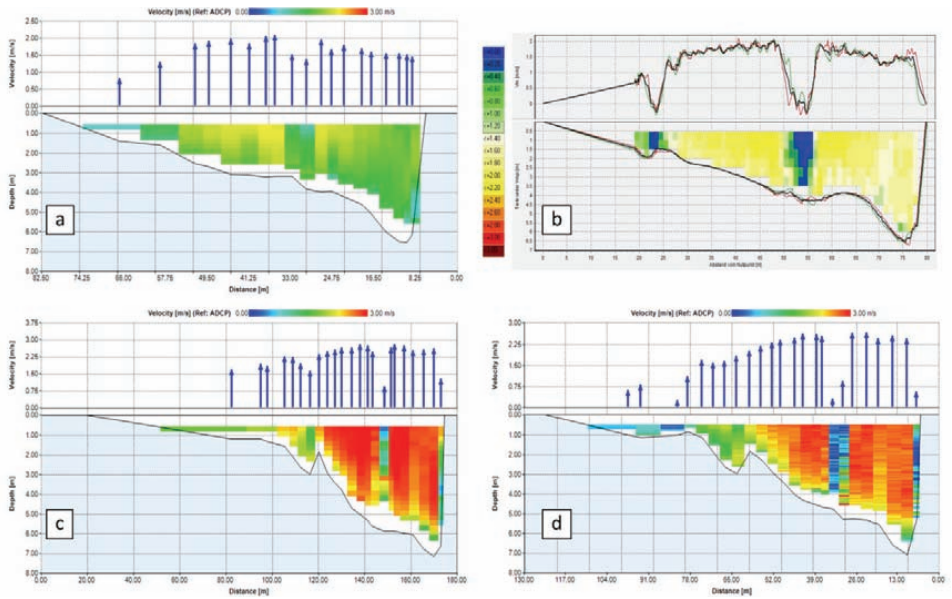

Figure 29: Result graphs of the performed ADCP measurements; (a) 15.03.2018 at 350 m3s-1, (b) 16.03.2018 at 302 m3s-1, (c) 27.03.2018 at 870 m3s-1 and (d) 28.03.2018 at 627 m3s-1.

05.02 Hydrograph / gauging station

As it is crucial for the calculation of sediment loads a gauging station was installed at the right riverbank of the measured cross-section in Pocem (Figure 30; right). The used device for tracking the water level was an OTT Orpheus Mini. By relating the discharge values of the ADCP measurements to the water level values a rating curve was determined (Figure 30; left) and furthermore a discharge hydrograph as the basis for the calculation of sediment yields can be derived.

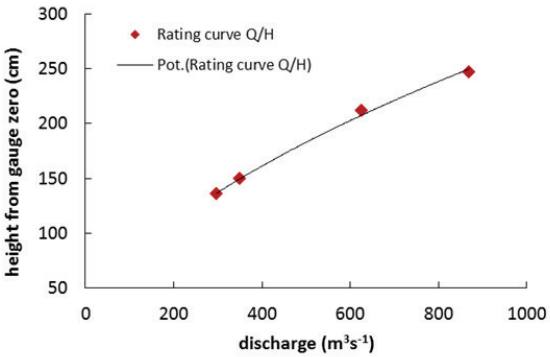

Figure 30: Rating curve discharge/water level (left) at the installed gauging station (right).

Unfortunately, the gauging station fell victim to vandalism or theft. Therefore, no current data of the project period regarding water levels at the cross section in Pocem is available for further data processing. Alternatively, a discharge hydrograph of the nearby gauging station was used as a basis to calculate bed load and suspended load yields. The provided hydrograph consists of daily averaged discharge values from 1958 to 1990 and is depicted inFigure 31. The discharge in this period ranges from a minimum of 15 m3s-1 to a maximum of 3.140 m3s-1, the mean discharge is calculated with 148 m3s-1.

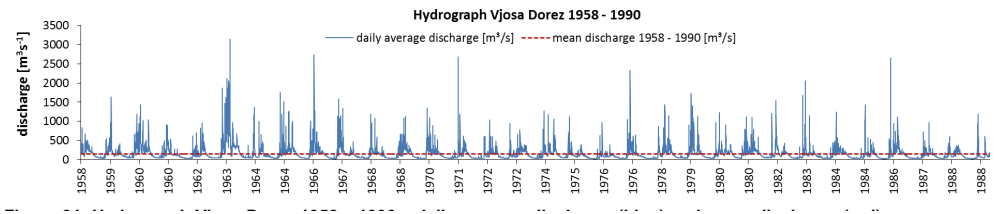

Figure 31: Hydrograph Vjosa Dorez 1958 – 1990 – daily average discharge (blue) and mean discharge (red).

Figure 32 shows the monthly average for each year of the period (grey) as well as for the whole period (black with red dots). In Figure 33a boxplot for the monthly average discharge values for the station Vjosa Dorez within the period 1958 – 1990 is depicted. Furthermore in Figure 34the values are sorted by discharge height, also showing the range where measurements within this project were performed (black dotted box).

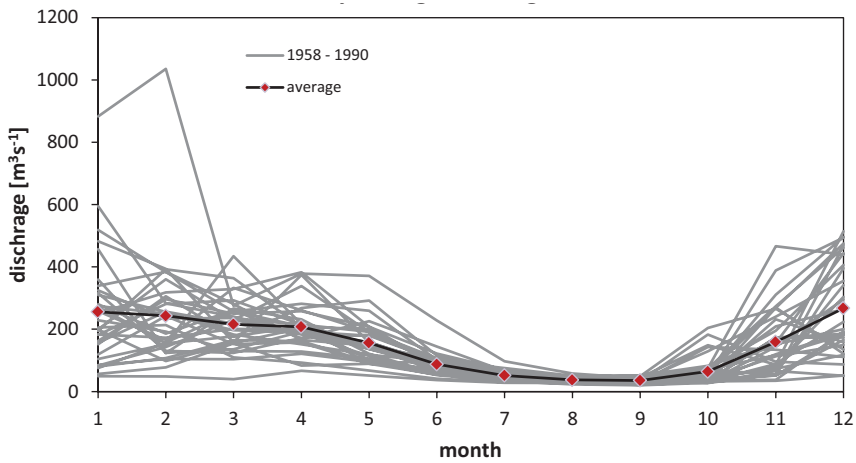

Figure 32: Monthly average discharge Vjosa Dorez 1958 -1990.

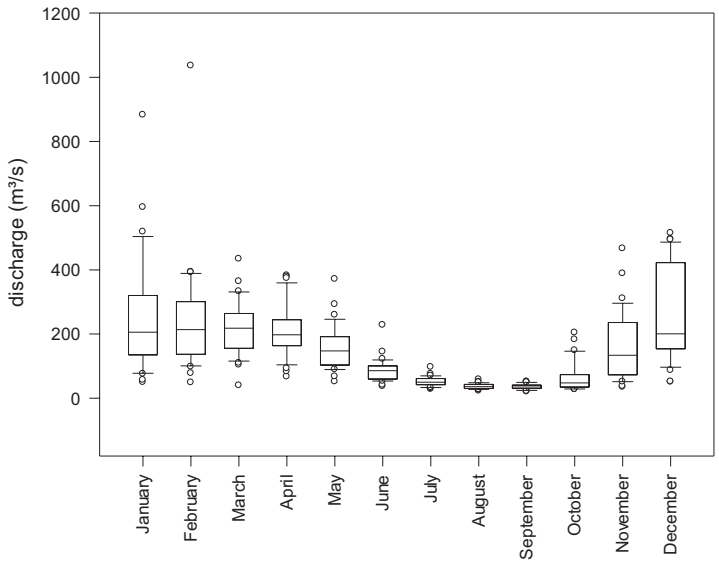

Figure 33: Box plot monthly average discharge Vjosa Dorez 1958 – 1990.

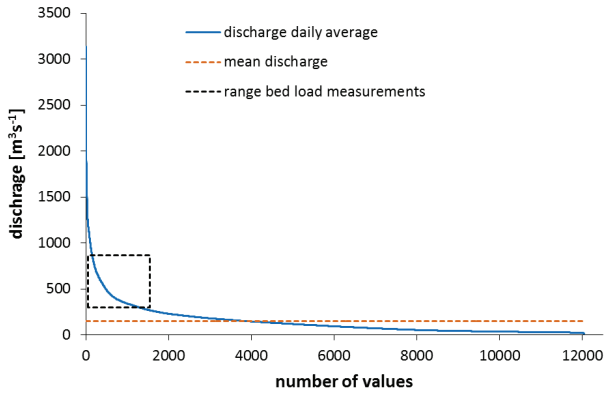

Figure 34: Daily average discharge - sorted 1958 – 1990.

05.03 Bed load measurements

The graphical results of the bedload measurements consist of 3 parts. The lower part shows the elevation of the cross section profile with the location of the bridge piers, the water level and the discharge stage during the performed measurement. Also the measured vertical lots with their distance from the right river bank are visible. The middle part of the graphic shows the bed load transport (yellow) and the measured flow velocity distribution (black line). The scaling factor for the bed load transport was chosen variable due to a better visibility of the results and needs to be considered when interpreting the graphs. In the upper part of the figure the grain size distribution is depicted.

Figure 35 shows the results of the bed load measurement from 15.03.2018 at a discharge level of 350 m3s-1 with a measured bedload transport of 0.97 ks-1 (left) and the bed load measurement from 16.03.2018 at a discharge level of 302 m3s-1 with a measured bedload transport of 1.00 ks-1 (right). Considerable sediment transport was only recognised in the deepest part of the profile near the right river bank between station 52.7 (Figure 35; left) up to the first bridge pier (Figure 35; right).

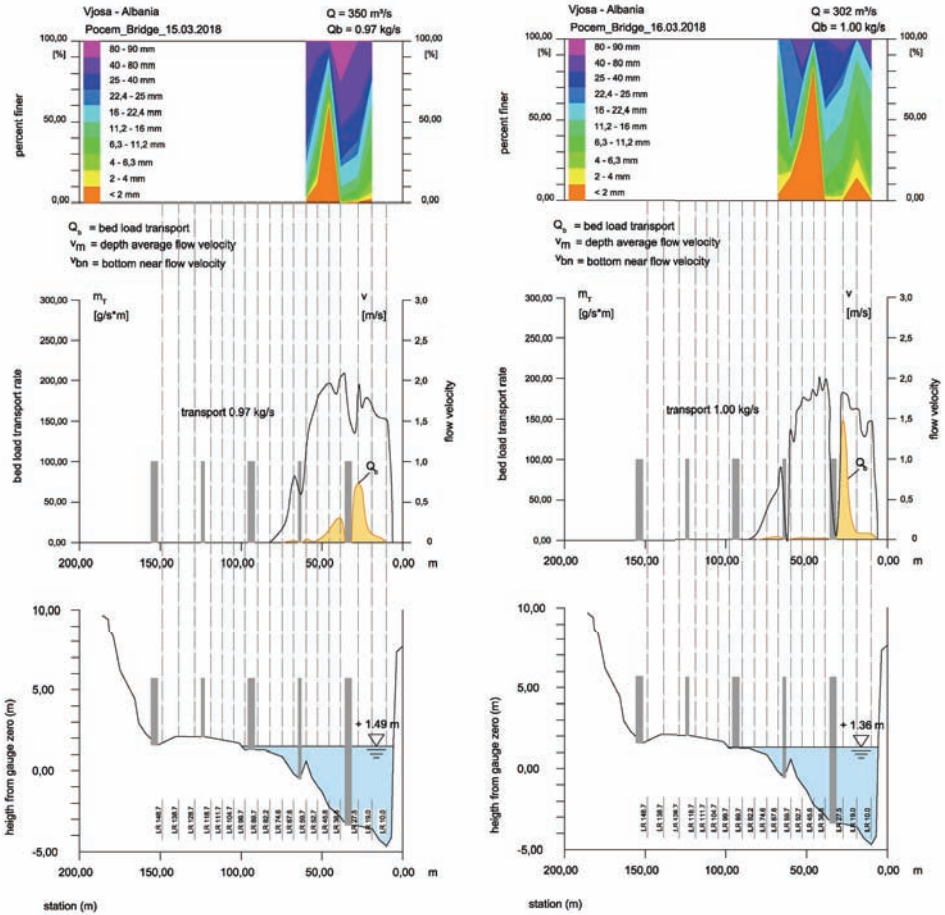

Figure 35: Result graphs of the performed bed load measurements; (left) 15.03.2018 at 350 m3s-1 (right) 16.03.2018 at 302 m3s-1.

Figure 36 shows the results of the bed load measurement from 27.03.2018 at a discharge level of 870 m3s-1 with a measured bedload transport of 28.68 ks-1 (left) and the bed load measurement from 28.03.2018 at a discharge level of 627 m3s-1 with a measured bedload transport of 24.77 ks-1 (right). At both discharges, considerable sediment transport was recognised at an equal level from the right river bank up to station 89.7 (Figure 36; left) respectively 82.2 (Figure 36; right).

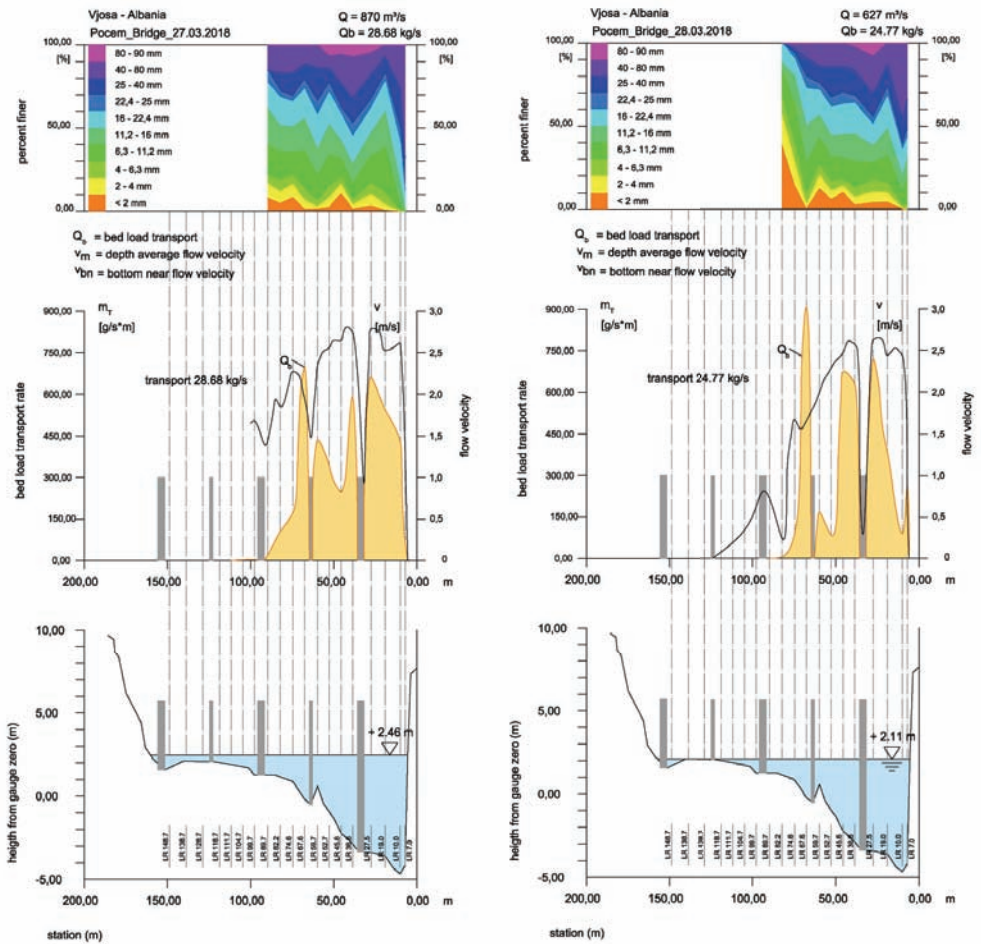

Figure 36: Result graphs of the performed bed load measurements; (left) 27.03.2018 at 870 m3s-1 and (right) 28.03.2018 at 627 m3s-1.

The dried samples have been sieved and analysed afterwards. The derived grain size distributions of the four bed load measurements are depicted in Figure 37.

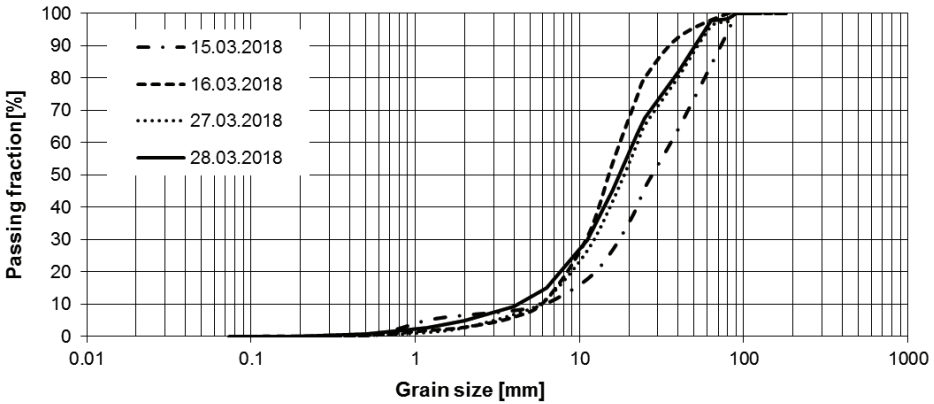

Figure 37: Bed load measurements - grain size distribution.

Table 9 shows the characteristic grain sizes for bedload samples at the bridge profile in Pocem. Besides the values for the individual samples also the composite grain size distribution was characterized. Furthermore, the values for the composite grain size distribution without fractions below 4 mm are shown to enable a comparability with the pebble counts along a transect also performed within the project.

Table 9: Characteristic grain sizes for bedload samples at the bridge profile in Pocem.

	d_m (mm)	U	Cc	d_{10} (mm)	d_{20} (mm)	d_{30} (mm)	d_{40} (mm)	d_{50} (mm)	d_{60} (mm)	d_{70} (mm)	d_{80} (mm)	d_{90} (mm)	d_{16} (mm)	d_{84} (mm)
Q350	34.9	6.0	1.4	6.0	12.2	17.3	22.4	27.7	35.9	45.7	57.6	72.5	9.8	63.1
Q297	19.0	3.2	1.2	5.6	8.1	10.9	12.9	15.0	17.7	20.9	25.0	36.3	7.2	29.0
Q870	24.7	4.2	1.2	5.4	8.7	12.1	15.3	18.7	22.6	28.9	39.6	53.1	7.4	44.5
Q626	23.1	5.1	1.4	4.2	7.6	11.2	14.1	17.6	21.4	27.0	37.6	50.5	6.5	42.5
Composite bedload	26.0	4.6	1.3	4.8	8.3	11.8	14.8	18.3	22.2	28.3	39.0	59.7	7.1	46.0
Composite bedload gravel (>4mm)	29.4	2.8	1.0	8.8	11.9	14.5	17.5	20.8	24.6	32.1	43.3	63.2	10.8	50.4

For a better visualisation the d_{50} and d_{90} grain sizes are plotted related to the discharge of the measurement in Figure 38 showing no clear correlation between discharge and grain size, probably due to the small number of samples.

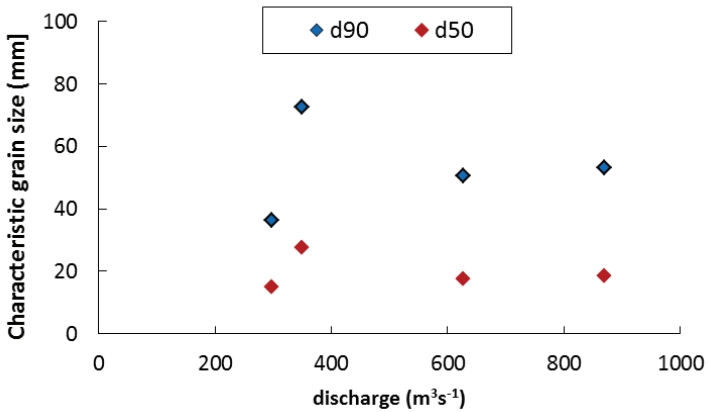

Figure 38: Bed load measurements characteristic grain sizes related to discharge.

For the calculation of sediment loads in a further step rating curves between discharge and bed load transport were created. In Figure 39 (left) the rating curves are depicted for the discharge range of the performed measurements. For further calculations a linear function (dashed line) and power function (continuous line) were chosen. As the provided hydrograph of the Vjosa at the gauging station Dorez 1958 – 1990 covers discharge values from 15 m3 s-1 to a maximum of 3.140 m3 s-1, the functions were extrapolated to the maximum discharge as shown in Figure 39 (right). At this point it has to be stated, that due to the lack of data at high discharge levels uncertainties are given for the calculation of sediment loads.

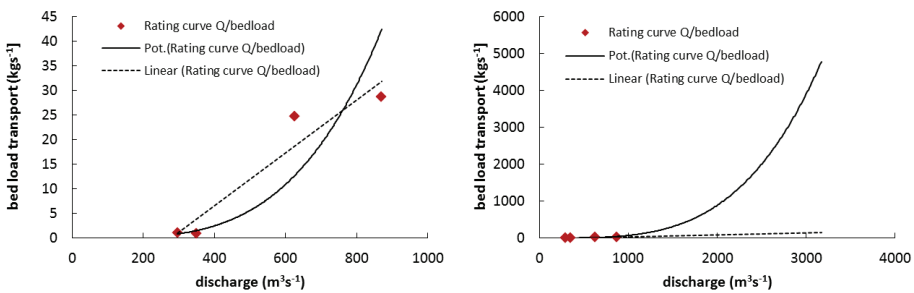

Figure 39: Rating curves discharge/ bed load transport – linear (dashed line) and power function (continuous line) – measured range (left) and extrapolated (right).

By multiplying the derived discharge/bed load transport rating curves with the discharge values of the provided hydrograph the daily bed load transport for the period 1958 – 1990 was calculated. The result is plotted in Figure 40. The graph shows that bed load transport seems to be highly sensitive to flood events, as the highest calculates daily transport reaches 13.300 t/d for the linear function (red) and almost 400.000 t/d for the power function (blue).

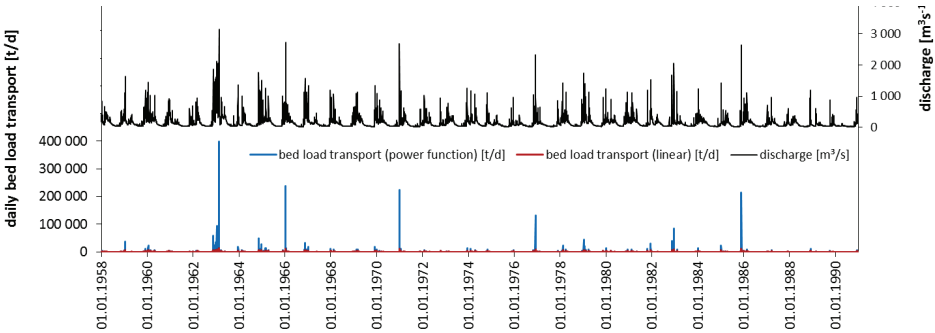

Figure 40: Daily bed load transport - 1958 – 1990 – linear function (red) and power function (blue).

In Figure 41 the daily bed load transport is integrated over time to achieve an accumulated bed load transport for the whole period 1958 – 1990. For the linear function (red) an accumulated transport of around 1.6 Mio. tons of bed load transport for the linear function was calculated (red), whereas for the power function over 4.0 Mio. tons of bed load transport were estimated (blue).

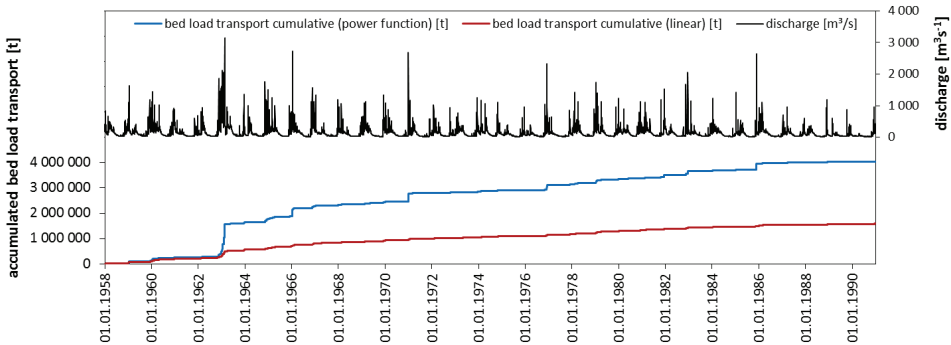

Figure 41: Accumulated bed load transport; 1958 – 1900 – linear function (red) and power function (blue).

In Figure 42 the annual bed load transport for the period 1958 – 1990 is depicted. The graph shows high temporal variability and sensitivity to flood dominated years both for the linear function (red) and even more for the power function (blue). For years with low sediment transport the variety between the two functions is lower than for years with high sediment transport. In 1963 the calculation with the derived functions leads to a calculated bed load transport of 256.000 t (linear function) and 1.16 Mio. tons by using the power function respectively.

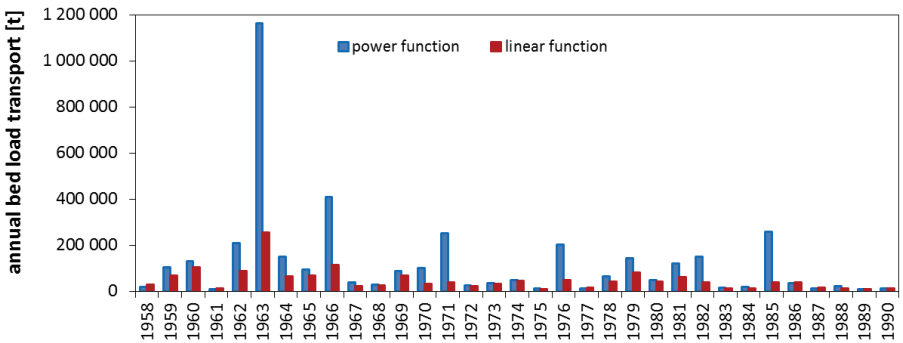

Figure 42: Annual bed load transport; 1958 – 1900 – linear function (red) and power function (blue).

For both derived functions the annual average bed load transport was calculated and depicted inFigure 43. By applying the linear function, the calculated annual average bed load transport would be around 48.000 t/a (red), for the power function the value is 2.5 times higher with a value around 123.000 t/a.

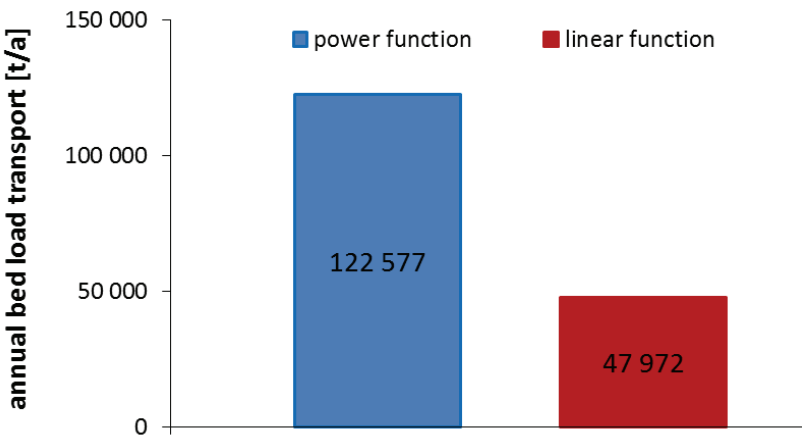

Figure 43: Annual average bed load transport; 1958 – 1900 – linear function (red) and power function (blue).

05.04 Suspended load

Due to time restrictions of the intensive monitoring program,in the current project, the depth integration method was chosen and applied for the suspended sediment measurements. Besides taking depth integrated samples, during each measurement one vertical lot was sampled with the multi-point method. The comparison of the sediment concentration in the different depth with the integrated samples showed a good correlation. This can be explained by the high turbulences leading to a constant good spatial distribution of sediments in the measurement profile. This fact approves the chosen method.

As for the bed load, also for the calculation of suspended sediment loads rating curves between discharge and fine sediment transport were created. In Figure 44 (left) the rating curves are depicted for the discharge range of the performed measurements. For further calculations a linear function (dashed line) and power function (continuous line) were chosen. Figure 44 (right) shows the extrapolated functions used to cover the discharge range for the whole period 1958 - 1990.

Just like for the rating curves of the bed load transport, also for the suspended load it has to be stated, that due to the lack of data at high discharge levels uncertainties are given for the calculation of sediment loads.

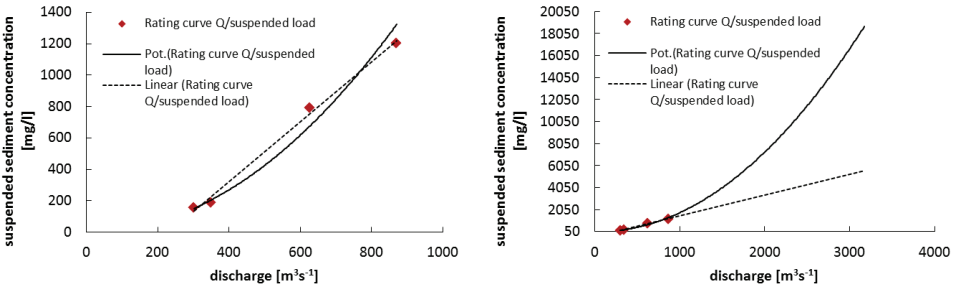

Figure 44: Rating curves discharge/suspended sediment concentration – linear (dotted line) and power function (continuous line) – measured range (left) and extrapolated (right).

By multiplying the derived discharge/suspended load transport rating curves with the discharge values of the provided hydrograph the daily bed load transport for the period 1958 – 1990 was calculated. The result is plotted inFigure 45. Similar to the bed load transport also the suspended load transport seems to be highly sensitive to flood events, as the highest calculates daily transport reaches 0.43 Mio. t/d for the linear function (red) and 4.97 Mio. t/d for the power function (blue).

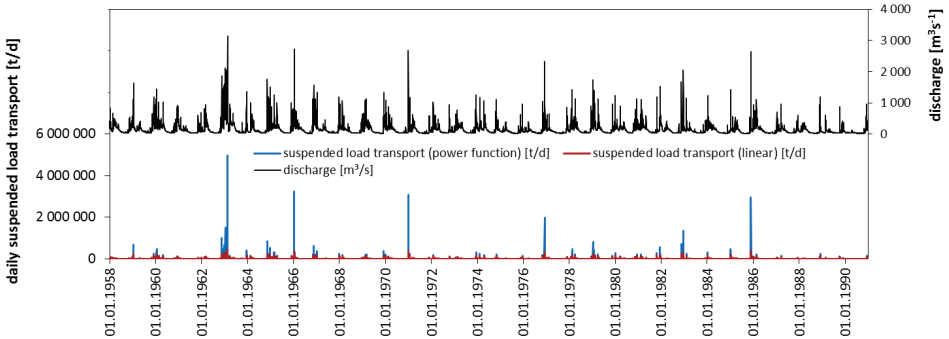

Figure 45: Daily suspended load transport; 1958 – 1990 – linear function (red) and power function (blue).

In Figure 46 the accumulated suspended load transport for the whole period 1958 – 1990 is depicted. For the linear function (red) an accumulated transport of around 47 Mio. tons of suspended load transport for the linear function was calculated (red), whereas for the power function 85 Mio. tons of bed load transport were estimated (blue).

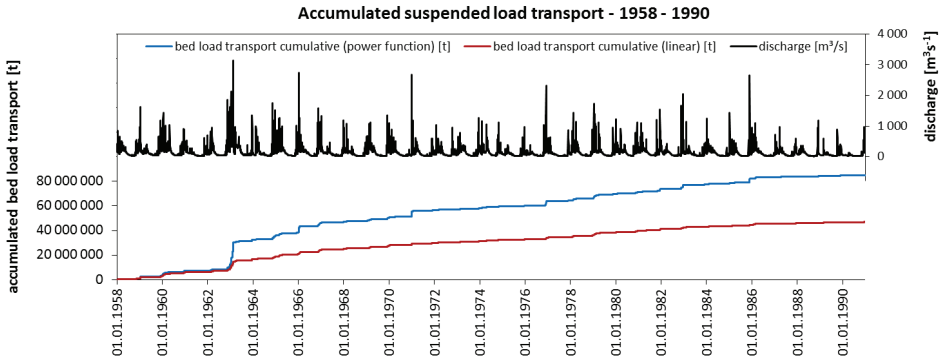

Figure 46: Accumulated suspended load transport; 1958 – 1900 – linear function (red) and power function (blue).

In Figure 47 the annual suspended load transport for the period 1958 – 1990 is depicted. The graph shows high temporal variability and sensitivity to flood dominated years both for the linear function (red) and even more for the power function (blue). For years with low sediment transport the variety between the two functions is lower than for years with high sediment transport. As for the bedload 1963 is the year with the highest fine sediment transport. The derived functions lead to a calculated suspended load transport of 7.8 Mio. tons (linear function) and 20.4 Mio. tons by using the power function respectively.

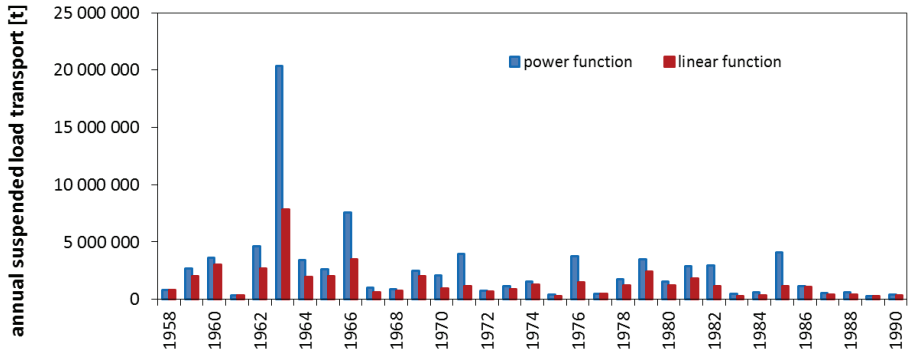

Figure 47: Annual suspended load transport; 1958 – 1900 –linear function (red) and power function (blue).

For both derived functions the annual average bed load transport was calculated and depicted inFigure 48. By applying the linear function, the calculated annual average suspended load transport would be around 1.4 Mio. t/a (red), for the power function the value is 1.8 times higher with a value around 2.6 Mio. t/a.

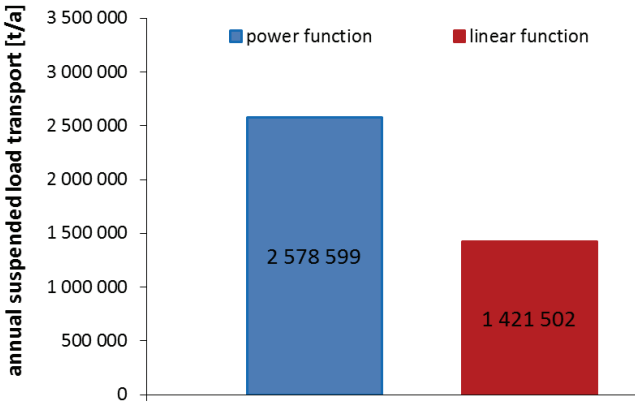

Figure 48: Annual average suspended load transport; 1958 – 1900–linear function (red) and power function (blue).

Taking both bedload and suspended transport results into account it can be stated that base on the derived power functions an average annual transport of about 3 million tons/a occur. However, due to the lack of data for discharge > 1000 m3s-1, which obviously transport the highes rates, number up to 4 million tons / a are reasonable, but have to be validated in 2019 / 2020 or at the next flooding overtopping the 1000 m3s-1.

06 Hydromorphological Assessment

River channel patters as a consequence of dynamics and physical characteristics was revealed by Schumm (1985). Nanson and Knighton (1996) describe anabranching river systems for all environmental settings reaching from alpine gravel-bed streams to lowland muddy and organic deltas. Based on (i)specific stream power (Wm-2), (ii) bed material size, (iii) bank material size, (iv) lateral migration rate, (v) vertical accretion rate, (vi) channel sinuosity and (vii) ratio island length / channel width five different anabranching types can be distinguished (Nanson & Knigthon, 1996).

06.01 Methods

Terrestrial survey of three cross sections of the Vjosa has been conducted by using a Leica TC805 theodolite. The first measurement of the Vjosa bathymetry in history has been applied for both (i) the active channel and (ii) the active floodplain in April 2017 and in July 2018. High resolution point sampling has been applied using height-dependent criteria (□h > 15 cm) for selecting terrain points for describing cross sectional variability. In a post-processing procedure, the cross sectional data (n = 3) have been used for hydrodynamic-numerical (HN) modelling.

For analysing hydromorphological parameters of the Vjosa, needed for the Nanson & Knighton (1996) classification (e.g. specific stream power), one-dimensional hydrodynamic-numerical models have been applied. One-dimensional interpretation of governing equations has found a widespread application in hydraulic and environmental engineering (Bhallamudi & Chaudhury, 1991; Correia et al., 1992; Niekerk et al., 1992). The modelling package HEC-RAS® uses the 1D St. Venant equation to calculate open channel flow, based on a four-point implicit finite difference scheme allowing modelling larger time steps than explicit numerical schemes (Ligget & Cunge, 1975). For the applied one-dimensional approach phenomena such as the Coriolis force have been neglected. For hydrodynamic-numerical modelling of each investigated reach, the one-dimensional unsteady flow model HEC-RAS® was used. The model was chosen because of its capabilities for sub-/supercritical modelling (USACE, 2002) and multifunctional parameter analysis for overbank- and main channel flow.

06.02 Results

The Vjosa shows diverse morphological patterns from the sources downstream to the mouth. The areas in the floodplains of Pocem and Kalivac are classified as `wandering gravel bed rivers´ (Church, 1983), or in terms of anabranching classified as laterally active gravel-bed river (Type 5 according to Nanson & Knighton, 1996). The hydrodynamic-numerical modelling revealed Qbf of approx. 1000 m3s-1 for all three sampled transects (9). For bankfull flow specific stream

power was calculated within the range of 22.8 W m-2 – 39.8 Wm-2. Moreover, pebble counting on the gravel bars of the Vjosa exhibited a variability of d50 = 19.7mm up to d50 = 38.3 mm (compare to Table 5) in the active channel, - and gravel, sand and mud sediment deposits along the banks. Vertical aggradation rate, however, could not be calculated due to lack of comparable datasets, similar lateral migration rate. Nevertheless, channel sinuosity as well as the ratio of island length / channel width supported the classification of a laterally active gravel bed river (compare to Schiemer et al., 2018). Multichannel sytems, supporting the Nanson & Knighton (1996) classifications are presented in Figure 49b. In this specific part of the Vjosa, three to four channels are inundated during low flow conditions. Cross sections 1 and 3 contain only one dominating, partially stable active channel (transect 3), or a second branch which is morphodynamic active (transect 1) (Figure 49 a and c).

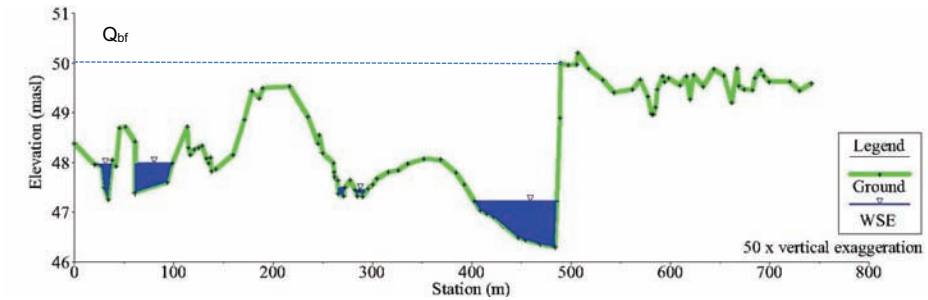

(a)

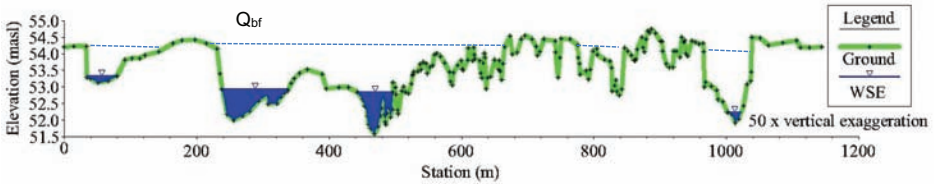

(b)

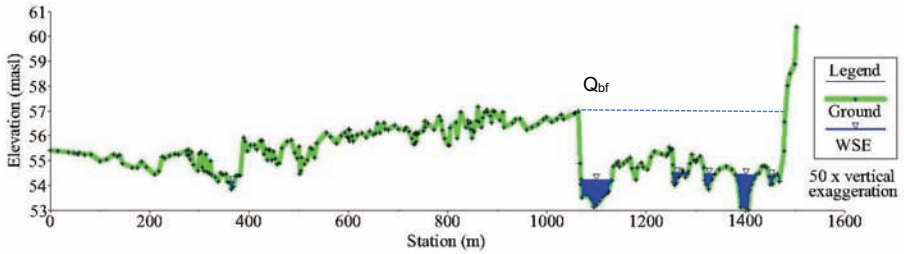

(c)

Figure 49: Bathymetry of the Vjosa in the floodplains of Pocem at (a) Transect 1, (b) Transect 2 and (c) Transect 3; Qbf = bankfull discharge.

Gravel-dominated laterally active anabranching river systems are frequently found in cold climate regions with snowmelt and glacier runoff dominated (e.g. Church, 1983; Deslodges & Church, 1989; Kellerhals, 1972; Brierley & Hickin, 1992; Nordseth 1973). The Vjosa, however, is dominated by a Mediterean and Mid-European and towards higher altitudes areas it resembles alpine conditions without any glaciation in the catchment (Seferlis et al., 2008). The hydrological regime is classified as pluvio-nival regime with peak flows in spring (Rößler, 2017), and occasional high flows in terms of heavy precipitation. However, referred to the work on Nanson & Knighton (1996) the Vjosa, contain comparable low unit stream power values for a laterally-active anabranching gravel bed river. The modelled range of stream power 22.8 W m-2 – 39.8 W m-2 are at the lower boundary for a type 5 anabranching type. They are more transitory to a so-called type 2, sand dominated anabranching river. Nevertheless, gravel-dominated laterally active channels are described as transitional between meandering and braided channels (Deslodges & Church, 1989). A classification fully proofed at the Vjosa study site. Moreover, the catchment of the Vjosa river is reflecting high sediment yields (bed load and suspended load) up to 20 – 40 tha-1year-1 underlining the fundamental principle for braided and anabranching rivers that bed load supply has to be higher than actual channel transport capacity. Reduction in bed-load supply for those gravel-dominated laterally active rivers would lead to a more stable, single, sinuous but migrating channel (Carson, 1984; Church, 1983).

Another criterion of the laterally active anabranching gravel bed type are specific forms of avulsion in term of extraordinary high flow rates. The avulsion of those river types incises into existing floodplains (Nanson & Knighton, 1996). This has been as well proven for the Vjosa, as the active channel is incised up to 3 m into the active floodplain of this type 5 anabranching river where basal unit of gravel is overtopped by overbank sands and silt (Brierley & Hickin, 1992).

In July the bathymetric survey of the three cross sections have been repeated, to assess the morphodynamics of the Vjosa related to the flooding in December 2017. In Figure 50 the results of this comparative analysis is showing the impact of this 10-years flooding on the selected cross sections. Intrestingly, all three investigated cross sections behave differently Transcet 1 showed massive side erosion (>20 m), with formation of a huge gravel bar on the inner band of the curved sections. Transect 2, was reworked in large parts but the anabranching characteristic was found similar to 2017. In Transect 3, the morphodynamics turn-overs occurred only in the active channel of 2017, with no additional side erosion in this part of the Vjos with elevated floodplain stages (> 3 m).

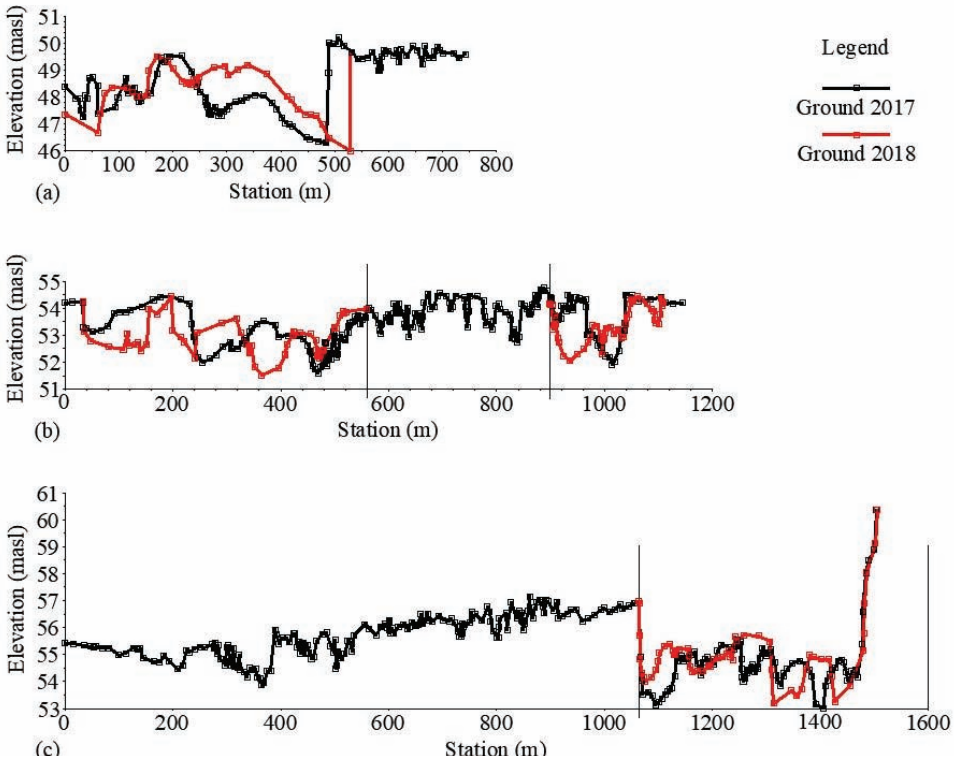

Figure 50: Comparison of the bathymetry changes of the Vjosa in the floodplains of Pocem at (a) Transect 1, (b) Transect 2 and (c) Transect 3; arrows are indicating those sites which have not been resampled in 2018.

07 Hydrodynamic-numerical modelling

07.01 Methods

In this study, two-dimensional (2D) depth-averaged hydrodynamic-numerical (HN) modeling was applied to highlight (a) the actual condition of the Vjosa River and (b) the condition after construction of a projected storage power plant from a hydromorphological point of view. The depth-averaged twodimensional model developed by Nujic (1998) (Hydro_AS-2d) calculates hydraulic parameters on a linear grid (three node triangles and four node quadrilaterals) by applying the finite volume approach. As pre- and postprocessing tool the HN model uses the software SMS (Surfacewater Modelling System 12.3.2).

Concerning the actual condition, a river reach which is located 6km upstream of the planned Kalivac dam was chosen in order to reveal the complex pattern of hydraulic variables within the Vjosa. Flow velocity and water depth reflect an interaction between the morphological and hydrological situation on site. Both parameters frame the physical habitat and therefore affect physical environment significantly (Maddock, 1999; 2010, Gostner et al., 2013). On the other hand, it is known that there is a strong correlation between physical habitat variability and biodiversity (Gorman and Karr 1978, Schlosser, 1982). Hence, a high-resolution digital terrain model (DTMs) of the investigated river reach was required.

Therefore, in July 2018 terrestrial survey data of cross-section shape (n=35) of the low-flow channel were collected via a total station (Leica TCR407). At the same time, bathymetry data above the low-flow water level was measured by using UAV photogrammetry (see chapter 2). On the basis of both, data from cross sectional bathymetry sampling and UAV photogrammetry, a finite element mesh, consisting of triangular and quadrilateral elements, was generated via the software SMS 12.3.2 (Figure 51). The total mesh area adds up to 1.220.776 m^2. Due to the fact that the low-flow channel at the study site comprises of two branches, the total inflow was divided into two dynamic (unsteady) hydrographs (Figure 51) as upstream boundary condition whereas as downstream boundary condition the gradient of the energy line (Ie = 0.002) was applied.

Out of the modelled unsteady flow hydrograph, 4 different discharge values were chosen for further analyses (Table 10). Besides, a uniform Manning's value of 0.4348 was assumed for the entire mesh.

Table 10:Analysed discharge values and associated time of exceeding in days.

Q (m^3s^{-1})	t_e (d)
50	251
150	118
250	52
400	22

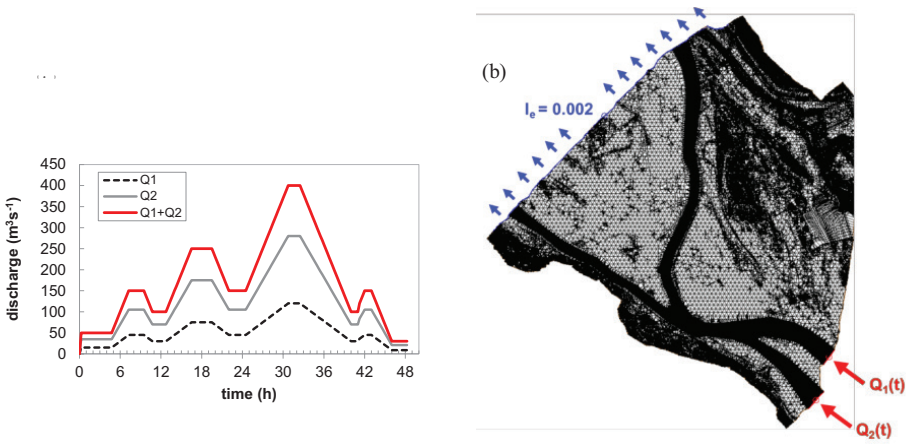

Figure 51: (a) Modelled flow hydrographs at reach Kalivac; (b) finite element mesh and boundary conditions of the HN model.

Moreover, in order to quantify hydromorphological heterogeneity of the modeled reach, calculated results were used to derive the Hydromorphological Index of Diversity (HMID) (Gostner et al., 2013) as a function of discharge. The HMID is based on a linkage between the coefficient of variation (CV) of flow velocity (v) and the CV of water depth (d). Standard deviation (s) and mean (μ) of each parameter were calculated from its modeled areal distribution.

HMID= 〖(1+σ_v/μ_v)〗 ^2* 〖(1+σ_d/μ_d)〗 ^2

In case of modelling the potential condition after construction of a storage power plant, digital terrain data used for HN modelling origins from the European Union's Earth Observation Program (Copernicus Land Monitoring Service) which provides a digital elevation model of reference (ETRS89-LAEA) in a contiguous dataset for the entire European region (EU-DEM) featuring a spatial resolution of 25 meters. A cutout (area = 2,668x107 m^2) used for this project is shown in Figure 52.

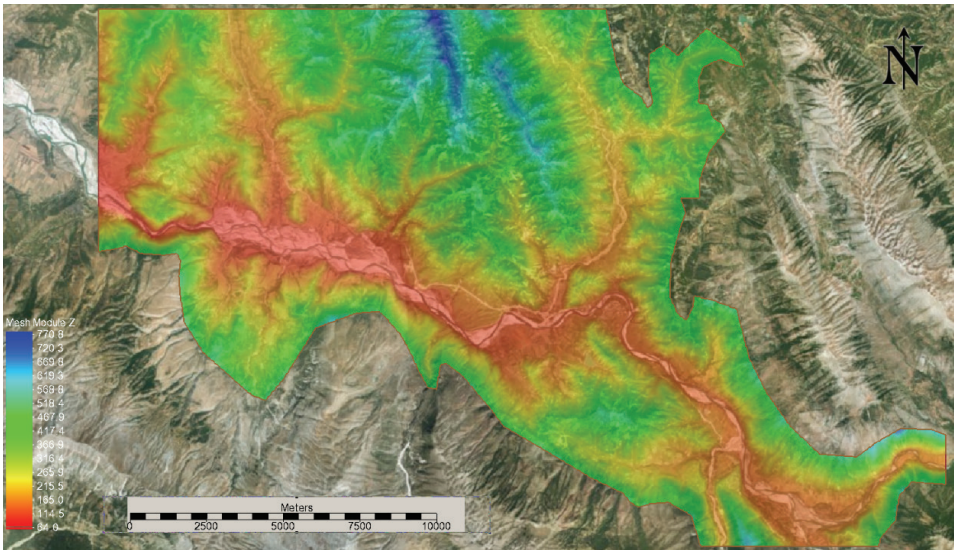

Figure 52: DEM raw data used for hydrodynamic-numerical modelling of the projected storage power plant at Kalivac.

Based on this data, it was possible to model the hydraulic conditions after the potential construction of the storage power plant on a larger scale by integrating the projected dam virtual within the finite element mesh (Figure 53). The projected dam crest of the planned hydropower plant (HPP) in Kalivac will be placed at the elevation of 116 m a. s. l. Assuming a dry freeboard of 7 meters between the dam crest and the spillway, the dam elevation within the finite element mesh was set to 109 m a. s. l. aiming to represent the hydraulic conditions in case of flooding (i.e. dam elevation within mesh equals elevation of spillway in nature). A constant inflow of Q = 1000 m3s-1 was selected as upstream boundary condition in the HN model. According to the time series analysis of Chapter 4 (long term hydrological analysis) this value equals a time of exceeding of approximately 3 days. The second boundary condition was set downstream of the dam in terms of the gradient of the energy line (Ie = 0.002) to simulate overflowing of the spillway. Here again, a uniform Manning's value of 0.4348 was assumed for the entire mesh.

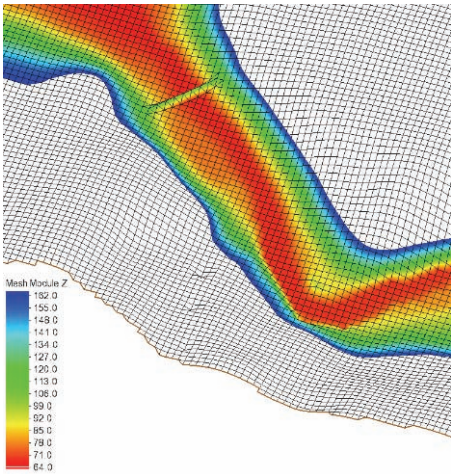

Figure 53: 3D view of the finite element mesh (25 x 25 m) with integrated dam (flow direction and location of the dam is indicated by the white arrow).

07.02 Results

07.02.01 Actual condition of Vjosa River

Distribution (boxplots) of modeled depth-averaged flow velocity and water depth are presented in Figure 54. Boxplots show, that the median flow velocity within the study reach is roughly stable over all analyzed flows. Modelled median values range from 0.52 m s-1 (Q=50 m3s-1) to 0.66 m s-1 (Q=150 m3s-1). However, upper whiskers (= 97.5th Percentile) of boxplots rise linear with flow. A similar pattern can be seen in terms of modelled water depth, where modelled median water depths range from 0.51 to 0.71 m and upper whiskers likewise rise linear with flow. The reason why the lowest median values are found at 50 m3s-1and the highest values at 150 m3s-1is related to the fact that there is a strong increase in overbank flow when discharge is higher than 150 m3s-1(Figure 55). Thus, large inundated areas are created featuring low values in flow velocity and water depth. In addition, Figure 54shows that the linear increase of top values (in terms of both analyzed variables), exclusively takes place within the permanently wetted low-flow channel.

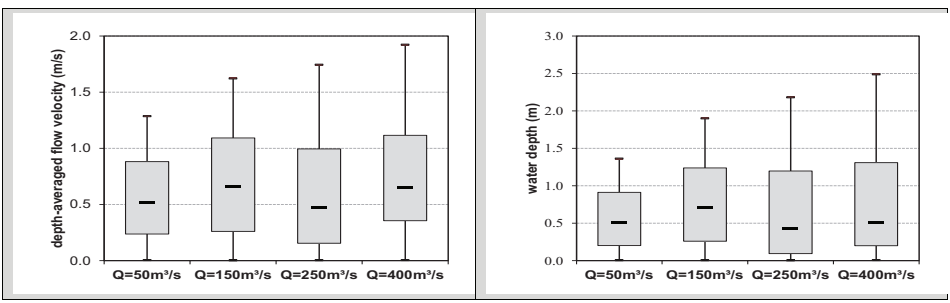

Figure 54: Left side: boxplots of modelled depth-averaged flow velocities at site Kalivac; right side: boxplots of modelled water depth (m) at site Kalivac.

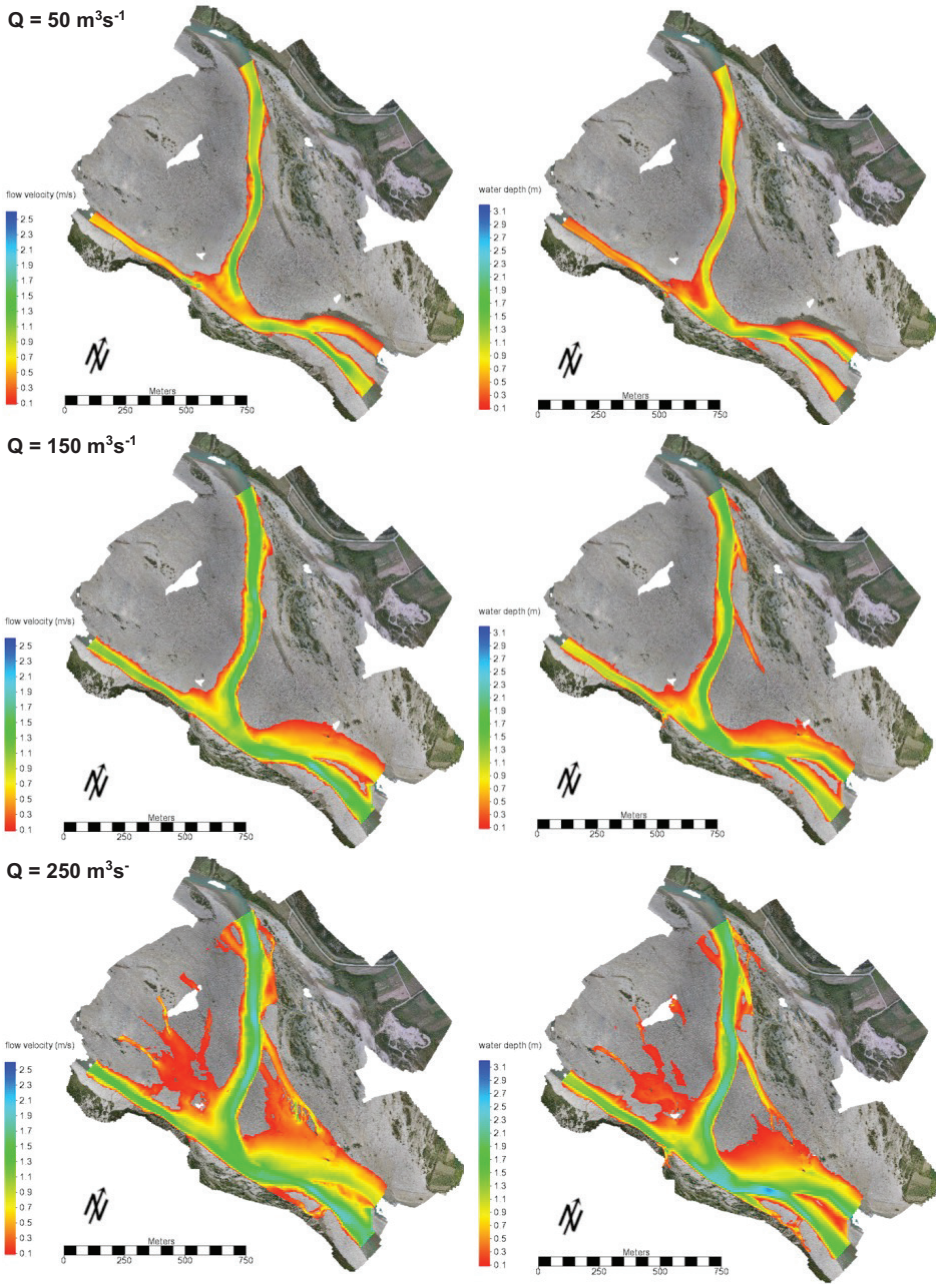

Figure 55: Left side: modelled depth–averaged flow velocity (m/s), right side: modelled water depth (m) at site Kalivac.

By calculating the HMID from the areal distribution of modelled depth-averaged flow velocity and water depth, it can be seen that within the modelled range of flow the investigated reach shows the highest HMID at a discharge of 250 m3s-1. Here again, the highest observed value (HMID=13.2) is linked to the highest increase in wetted area (Figure 56). The lowest HMID with 8.1 was observed at low-flow conditions when no overbank flow occurs. Generally, it can be stated that the investigated reach of the Vjosa River shows a complex pattern of hydraulic variables over a wide range of flow. By comparison, Gostner et al. (2013) classified the HMID in "low" (HMID < 5, channelized), "medium" (5 < HMID < 9, less modified) and "high" (HMID > 9, pristine). In his work, he suggested that streams showing a high HMID should be taken as a guiding measure for geomorphic restoration of pre-alpine gravel-bed rivers.

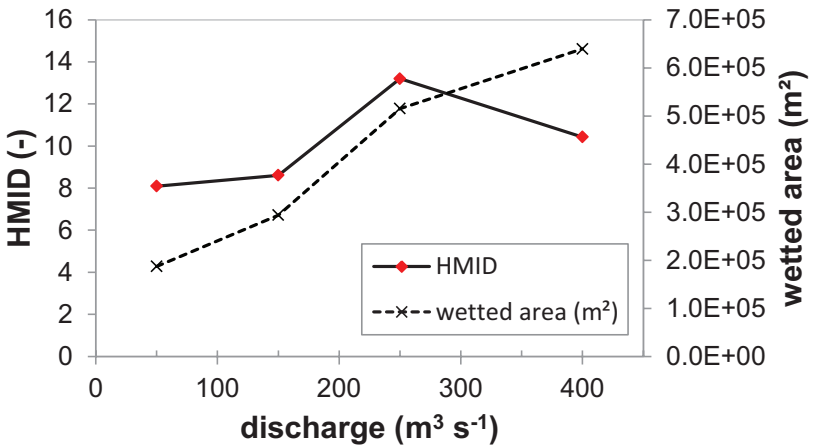

Figure 56: Hydromorphological Index of Diversity (HMID) and wetted Area as a function of discharge.

07.02.02 Condition after construction of a storage power plant

According to the results of the 2D depth-averaged HN modeling, the construction of the projected dam in Kalivac would create an impounded area of 1.83 mil. m² featuring a length of 14.5 km (linear distance). The head of the reservoir would be about 800 m downstream the bridge of Memaliaj. A total storage volume of 309 mil. m³ was calculated. The highest modelled depth-averaged flow velocity within the impoundment showed up at a narrow 3.4 km far from the head if the reservoir and featured 0.47 m s-1 (Figure 57). Within the 2.9 km long section upstream of the dam, showing a narrow valley shape, modelled velocities range up to a value of 0.2 m s-1. Nevertheless, most of the impounded area shows depth-averaged flow velocities close to zero. In the

Figures 57 – 59 the hydrodynamics (flow velocities) within the Kalivac reservoir are presented for various discharges ranges (1000 m3s-1 – 3000 m3s-1).

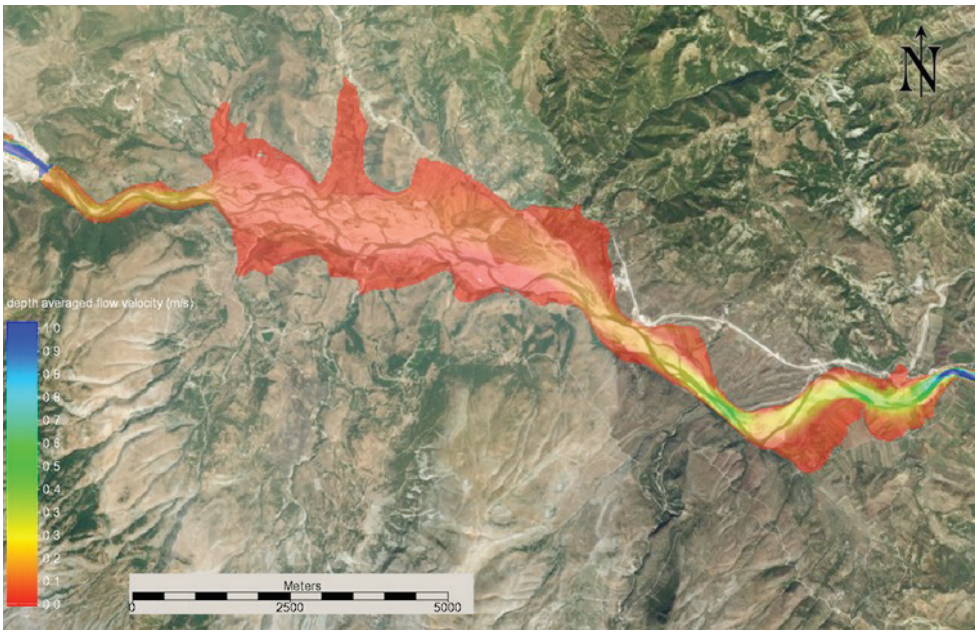

Figure 57: Modelled depth-averaged flow velocities within the impoundment of HPP Kalivac at a discharge of Q = 1000 m3s-1.

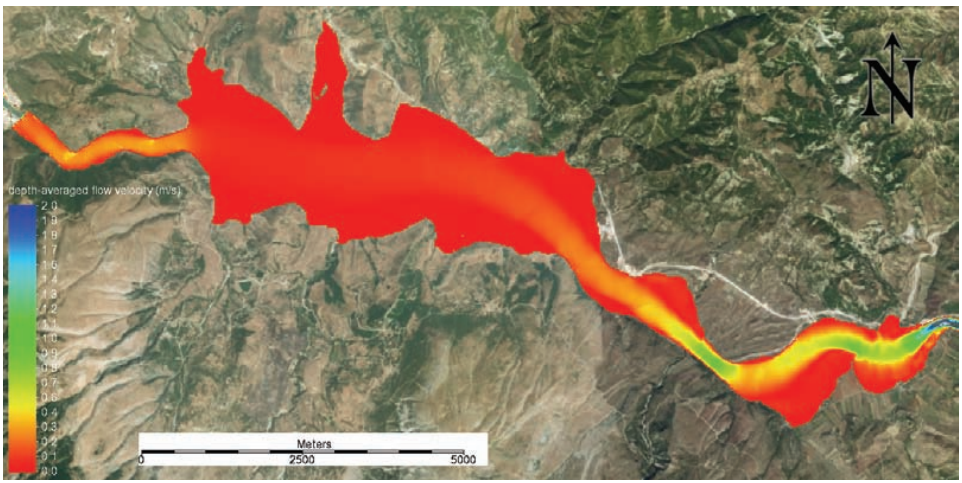

Figure 58: Modelled depth-averaged flow velocities within the impoundment of HPP Kalivac at a discharge of Q = 2000 m3s-1.

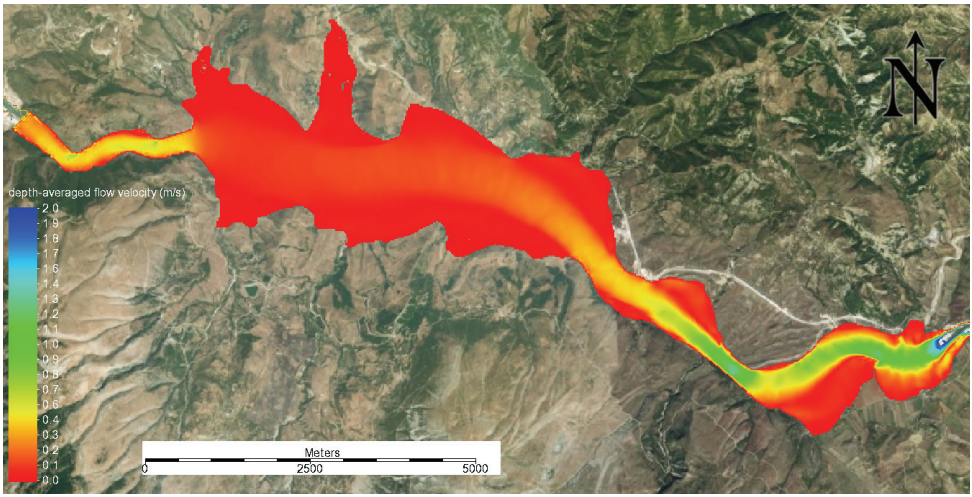

Figure 59: Modelled depth-averaged flow velocities within the impoundment of HPP Kalivac at a discharge of Q = 3000 m3s-1.

In Figure 60vector fields within the impoundment are visualized by means of flow trace animation. The figure shows a moment within the animation, where particles of zero mass are moved through the storage as a function of modelled vector fields. In the middle of the storage flow traces show a straight, linear course in the direction of the dam, whereas sideways bays feature areas with counter currents.

Figure 60: Flow trace visualisation within the impoundment upstream of HPP Kalivac at a discharge of Q = 1000 m3s-1.

08 Discussion of results for the planned dams at the Vjosa

08.01 General aspects

Some of the main economic, technical and ecological challenges in future, are the deposition, the treatments, and the disturbed dynamics of sediments in river catchments, which substenially reduce the future market potential of hydropower. Summarizing studies on these issues are yet to be conducted. Exemplarily, Basson (2009) summarized and predicted the loss in reservoir capacity for the different continentsin his work. He predicted that on average 80% of the reservoirs' capacity will be filled up withsediments in (i) Africa by 2100, (ii) Asia by 2035, (iii) Europe and Russiy by 2080, (iv) Central East by and (v) North America also by 2060. Due to a lack of awareness about these sedimentological challenges (e.g. lack of process understanding), various large economical, technical and ecological problems are emerging with an increasing relevance for the hydropower industry, water management authorities and the society in future. For instance, previous studies estimated the annual sediment replacement costs inthe US to be aroundsix billion US $ (Fan & Springer, 1990).

The major technical challenges related to sediments in reservoirs are **decrease of storage volume, loss of energy production** (Annandale, 2006) and technical issues such as clogging of bottom outlets or water intakes. Moreover, coping with the abrasion of turbines (e.g. Francis or Pelton runners) or the construction of sediment bypass systems are key challenges of hydropower use in river systems with high suspended loads. In addition, sediment depositions in backwaters of run-of-river hydropower systems may **cause problems concerning flood protection** (e.g. due to the reduction in the hydraulic effective width). Due to the remobilization of finesediments out of the reservoirs duringfloodings, other technical problems occur, increasing the potential damage downstream (e.g. overbank deposition harms theagriculture industry). Furthermore, as more and more sediments are blocked behind dam walls, river bed incision will be an increasing problem. In future, global warming will also exacerbate the challenges, as glacier melting and changes in run-off regimes (Ashmore & Church, 2001) increase the sediment production, filling up the reservoir even quicker. **Ecological problems in regards** to hydropower use are a result ofmid- to long term shortcomings in sediment management, the interruption of the sediment continuum (sediment deficit) and the subsequent impacts in downstream river sections (Figure 61).

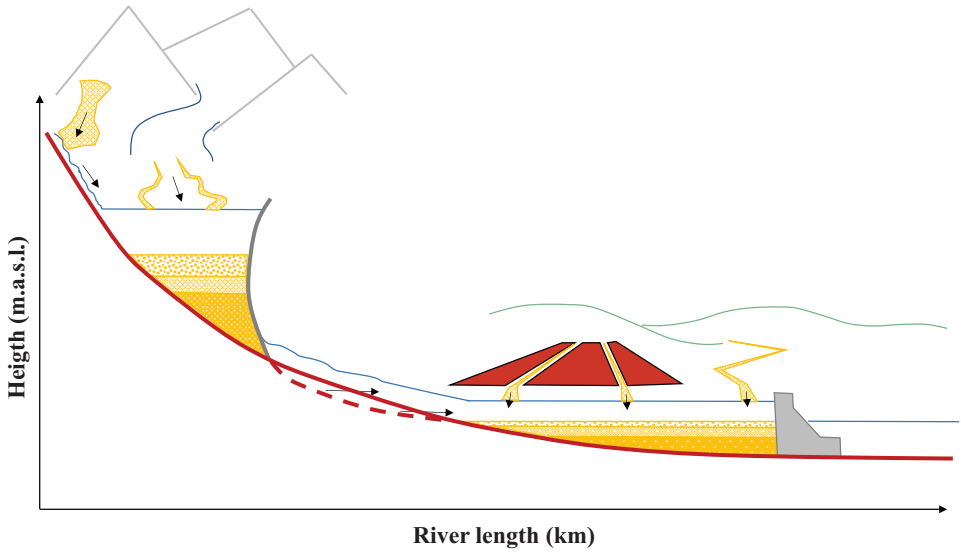

Figure 61: Schematic overview of sedimentation in hydropower reservoirs, including high-head storage power plant (sediment sources from torrents, unregulated tributaries and glaciers) and low-head run-of-river hydropower plants (sediment sources from industrialized landscape); dashed red line = continuous river bed incision due to lack of sediment supply from upstream reaches (Hauer et al., 2018).

Moreover, river sediment accumulation poses a number of challenge: **increased flood risksdue** to reduces channel discharge capacity for run-of-the river power plants as well as in the delta forming areas of reservoirs, **instream biological impacts** (e.g. degradation of fish spawning areas / rearing habitats and biodiversity) and **ineffectivenessof various implemented river restoration means (e.g. spawning gravel etc.).** Furthermore, accumulation of sediments upstream of dams reduces downstream fertilization (e.g. aquatic organisms and irrigation) due to lack of sediments and nutrients, and poses a downstream risk of pollution or even of release of anoxic water (black water), if flushed. Flushing causes severe ecological damages and in the eventof flushing (surplus of fines), local fishing companies and non-governmental ecological organizations may claim compensation foradditional costs (e.g. required stocking of fish due to impacts of flushing on instream population, as in the case of. Inn river Austria / Tyrolian fishing association) or try to stop the (technically required) reservoir flushing by law. Recently, a discussion has started whether to implement objectively investigated (laboratory or field studies) thresholds for federal institutions provided by the scientific community (e.g. for harmful turbidity rates). Moreover, as hydrological regulation has a dampening effect on natural flood dynamics it is important to understand the level of residual (flood) flows that are needed in order to flush and clean sediments (reduce embeddedness). In this regard, the interaction of instream hydraulics,

sediment transport, river morphology and ecology are not adequately understood from a process perspective, and thus implementation of sustainable sediment mitigation measures in river management plans are missing. Furthermore, there is a lack in standardized evaluation methods for detecting disturbances in the sediment regime.

08.02 Types of Depositions in reservoirs (USSD, 2015)

When a river enters a reservoir, flow velocity decreases and the sediment load begins to deposit. The bed load and coarse fraction of the suspended load are deposited first to form delta deposits, while fine sediments with lower settling velocities are transported deeper into the reservoir by either stratified or non-stratified flow. Depositional patterns vary with differences in hydrologic conditions, sediment grain size, and reservoir geometry. In reservoirs with fluctuating water levels, previously deposited sediments may be extensively eroded and reworked by streamflow, failure of exposed slopes, and wave action. Most sediments are transported within reservoirs to points of deposition by three processes: (1) transport of coarse sediment as bed load along the delta surface or topset, (2) transport of fine sediment in turbid density currents, and (3) transport of fine sediment as non-stratified flow (Morris and Fan, 1998). Of these three processes, most sediment computational models were designed to model the reservoir delta. Annandale (1996) explores both empirical and numerical techniques to predict distribution of both fine- and coarse-grained sediment deposits in a reservoir.

Sediment deposition in a reservoir and the longitudinal deposition areas are commonly divided into three main zones as shown in Figure 62. Topset beds correspond to delta deposits of rapidly settling sediment. The downstream limit of the topset bed corresponds to the break in slope between the topset and foreset beds, which is also the downstream limit of bed material transport in the reservoir. Foreset deposits represent the steep face of the delta advancing into the reservoir and are differentiated from topset beds by an increase in slope and decrease in grain size. Bottomset beds consist of fine sediments which are deposited beyond the delta by turbidity currents or non-stratified flow. They may also include organic material produced by algae or aquatic plants within the reservoir. Whereas delta deposits may contain both coarse and fine material, the bottomset beds are characteristically fine-grained. However, tributary inflows, reservoir drawdown, slope failures, and extreme floods can all deliver coarser material into zones where finer-grained material normally predominates, resulting in layering of deposits or localized variations in grain size (Morris and Fan, 1998,).

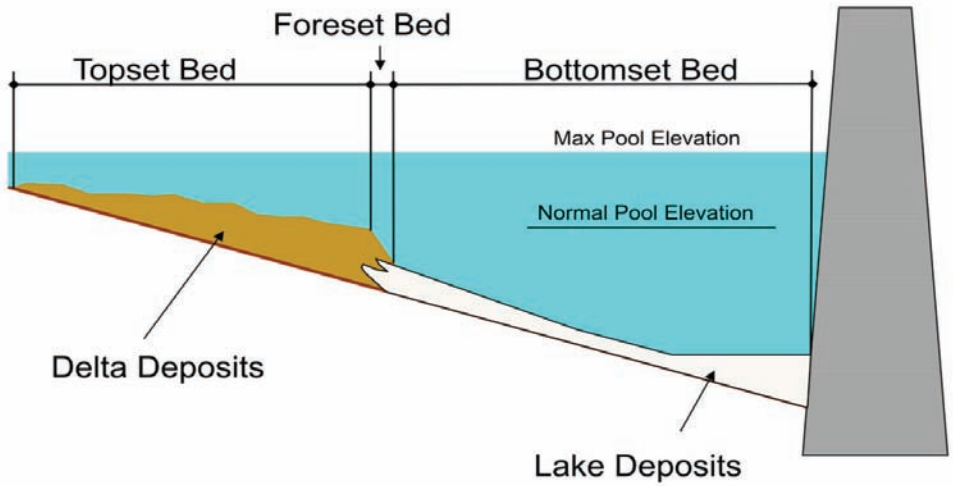

Figure 62: Conceptual View of Reservoir Deposition Zones (USSD, 2015).

Delta deposits may constitute the majority of the sediment accumulation at hydrologically small reservoirs with low sediment trap efficiencies where coarse-grained material predominates. However, for hydrologically large reservoirs with high sediment trap efficiencies, the delta more commonly accounts for only a portion of the total sediment accumulation. Since delta deposition is focused in the shallow upstream reaches of reservoirs where the width tends to be the narrowest and storage volume is small, even small reservoir deltas can be problematic from the standpoint of upstream aggradation. Delta deposits are also the most visible component of sedimentation and can extend upstream beyond the reservoir pool. In deep reservoirs which have been operated at different levels, distinct deltas may be formed at different water levels.

08.03 Sedimentation at the Vjosa Dams

For the planed dams at the Vjosa it can be stated that the loss in reservoir volumes will be above the world-wide averaged. ICOLD (2010) published 0.89% as average annual loss in reservoir volume in a global perspective. This means that without any maintenance work, reservoirs will be filled up to 80% within a period of about 90 years. For the planed dams at the Vjosa these number are not valid. Due to the high erosion rates as a result of both natural (e.g. geology) as well as anthropogenic boundary changes (e.g. clearcutting of forest) in the Vjosa catchment those deposition rates are much higher.

According to Mamede (2008), the density of deposited material in terms of dry mass per unit volume is used to convert total sediment inflow to a reservoir from a mass to a volume. Conversely, the volume of surveyed sediments in an

existing reservoir must be converted into mass to estimate sediment yield from the catchment (Morris and Fan, 1998). What is important in terms of reservoir sedimentation is the unit weight of deposits which is mainly determined by (i) initial unit weight, (ii) the operational mode of the reservoir and (iii) the consolidation rate of the deposits. Here, Lara and Pemberton (1963) derived an empirical formula to calculate the initial unit weight of a sediment mixture (W0). The empirical formula is based on 1300 sediment samples of reservoir deposits in the United States.

$$W_0 = W_c \cdot P_c + W_{si} \cdot P_{si} + W_{sa} \cdot P_{sa} \quad (7)$$

where Pc, Psi and Psa are the ratios of clay, silt and sand in the mixture, respectively; and Wc, Wsi and Wsa is the initial weights for clay, silt and sand (Table 11).

Table 11: Values of initial weight according to grain size and operation conditions (Lara & Pemberton, 1963).

Operation Conditions	Initial Weight (kg m^{-3})		
	Clay	Silt	Sand
Continuously submerged	461	1121	1554
Periodic drawdown	561	1137	1554
Normally empty reservoir	641	1153	1554
Riverbed sediment	961	1169	1554

Devoll Case study

To underline the problems of sedimentation in Albanian reservoirs, the Devoll case study can be mentioned. The Devoll river is one of the biggest rivers in Albania,characterized by large stream flows with high sediment loads (Ardichoglu et al., 2013). The Devoll river has in fact been referred to as the most turbid river draining into the Mediterian Sea. For the gauging station Kozare (N40°49´33´´ / E 19°54´26´´), which was used for measuringthe hydrological characteristics of the reservoirs Banja, an average suspended load of 2.8 million tons per year wasmeasured (time period: 1974 – 1983) (Ardichoglu et al., 2013). The catchment area of the Devoll river at the gaugingstation is 3122 km^2, which is significantly lower than the study sites at the Vjosa (approx. 5500 km^2). The observed suspended load patterns at the Devoll river were rapidly increasing and decreasing loads (similar to the Vjosa). Due to the hydrological regime the highest loads occurred in autumn and winter (similar to the Vjosa).

The data from Devoll river were used to support the presented Vjosa study for (i) grain size distribution of suspended sediments (Figure 63) and (ii) extrapolated suspended sediment concentrations for high-flows in form of total annual loads (Table 12).

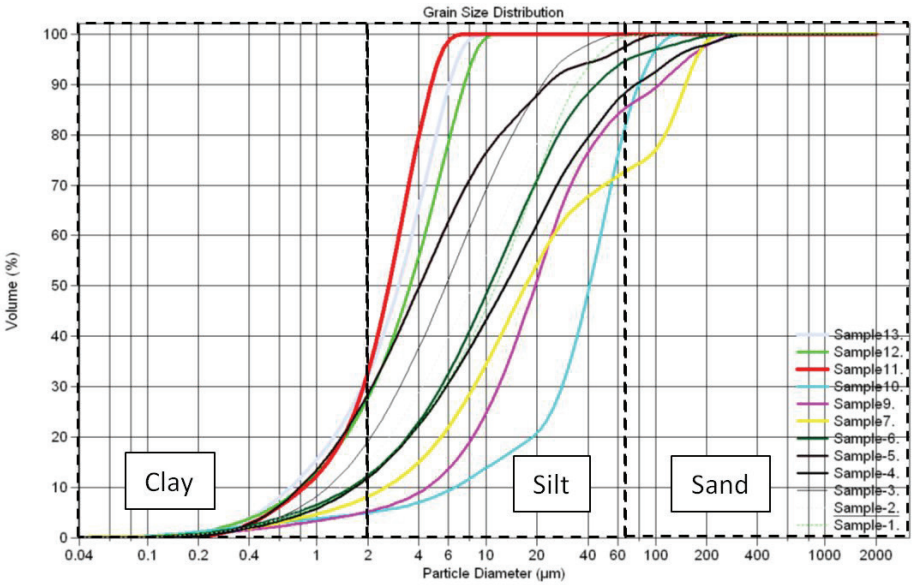

Figure 63: Grain size analyses of suspended sediments of Devoll river sampled in 2009 (modified after Ardichoglu et al., 2013).

Table 12: Average annual loads and average annual specific loads for Devoll (Ardichoglu et al., 2013).

Period:	**1974-1983**	
Load:	**Average load (tons/yr)**	**Average area specific load (tons/km² and yr)**
Shequeras	90 344	210
Gjinkas	415 421	307
Kokel	1 450 239	770
Kozare	2 851 464	913

The grain size analyses of suspended sediments of the Devoll river sampled in 2009 (Figure 63) were used to derive relative rates of clay, silt and sand for the calculation of suspended sediment deposition in different scenarios. To cover the whole range of occurring grain size compositions the finest and coarsest grain size distribution was chosen (Table 13).

Table 13: Fine sediment fractions of the Devoll river sampled in 2009 (modified after Ardichoglu et al., 2013).

	Fine sediment fraction (%)		
	Clay	**Silt**	**Sand**
Devoll - coarse	0.06	0.70	0.24
Devoll - fine	0.32	0.68	0.00

Applying the two determined fine sediment fraction scenarios to the formula of Mamede (2008) and taking into account the initial weight for fine sediment depositions published by Lara and Pemberton (1963) (continuously submerged; periodic drawdown; normally empty reservoir),six different initial weights for the calculation of deposition volumes were derived (Table 14):

Table 14: Values of initial weights.

	Initial Weight (kg m^{-3})		
	Continuously submerged	**Periodic drawdown**	**Normally empty reservoir**
Devoll coarse	1185	1203	1219
Devoll fine	910	953	989

Deposition volumes were calculated by multiplying the derived initial weights with the determined annual sediment transport of 2.7 Mio tons. Taking into account the storage volume of the projected hydro power plants in Kalivac and

Pocem, the fill up time for the six scenarios were determined for a sedimentation rate of 80 % of the storage volume as plotted in Figure 64. For Kalivac with an assumed operation level of around 109 m a. s. l., the fill up time based on this data would range from 85 to 110 years. In Pocem a sedimentation of 80 % of the reservoir volume would occur after 55 to 70 years assuming an operational level of 65 m a. s. l.

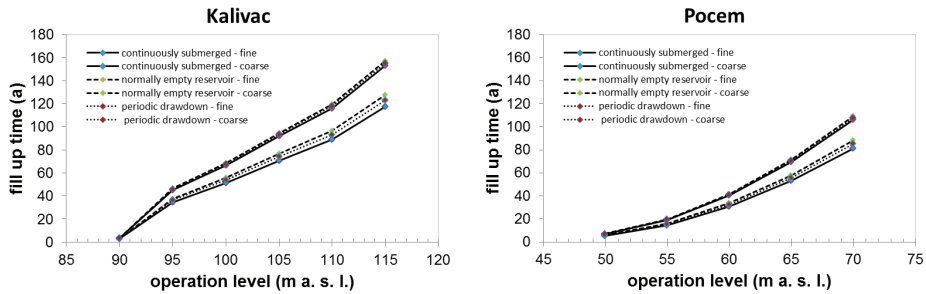

Figure 64:Fill up time for 80% reservoir loss in relation to the construction heigth for the planned hydropower Kalivac (left) and Pocem (right) using sediment measurement data at the Pocem bridge.

However, due to the lack of recorded data at high flows (> 1000 m3s-1), which are responsible for transporting the highest loads, we used the catchment data from Devoll river. Referring to the average annual specific loads of 913 t km-2a-1 for the Devoll river (Ardichoglu et al., 2013) and the catchment size of 5.500 km2, an average annual sediment load of more than 5.0 million. tons can be expected (still smaller than Fouache et al., 2001). Based on this dataset, the 80% fill up time for Kalivac would range from **45 to 60 years.** In Pocem a sedimentation of 80% of the reservoir volume would occur after **30 to 40 years** (Figure 65).

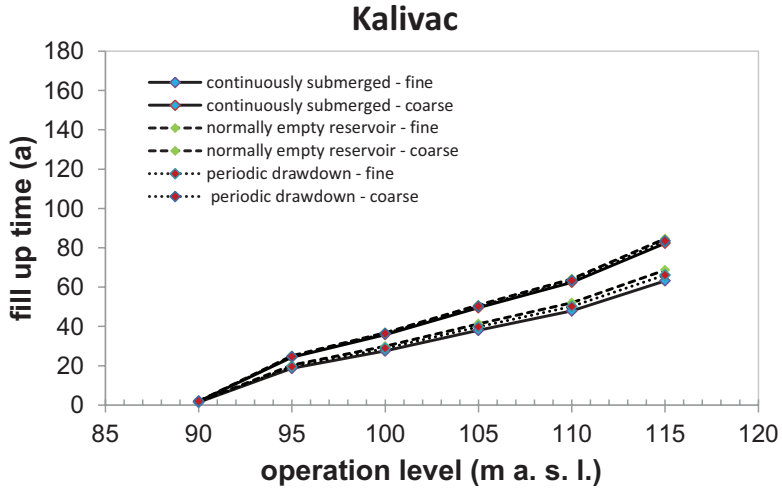

(a)

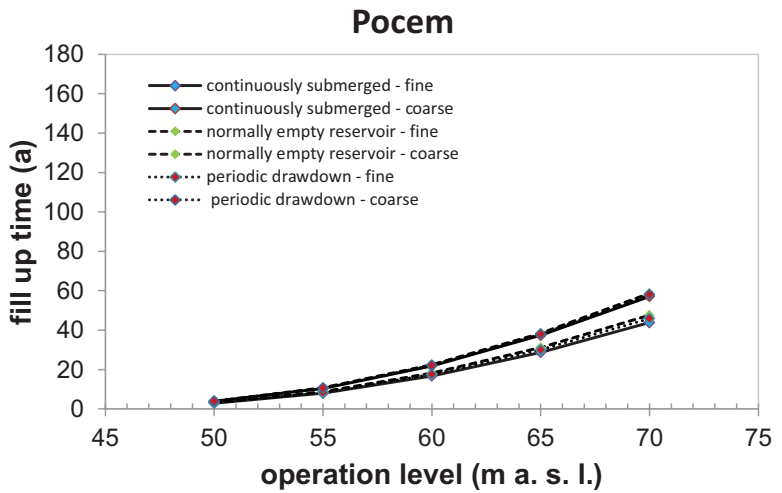

Figure 65: Fill up time for 80% reservoir loss in relation to the construction heigth for the planned hydro power plants Kalivac (a) and Pocem (b) using annual specific loads of the Devoll River.

Comparing our findings to thenatural erosion rates documented for Albania (20 – 40 t/ha/year), the **fill up of the Kalivac and Pocem** reservoirswill reach a level of 80% even earlier, i.e. within <25 years. Moreover, the studies of Pano et al. (2005) resulted in aloss of 80% in storage volume within**< 30years; - similar to the study of Fouache et al. (2001). Thus, our presented values are conservatively calculated and fill-up and capacity losses up to 80% maybe reached earlier than our calculations suggest.**

The second important finding of the presented study is related to the hydrodynamics which have been simulated for the implementation of the Kalivac dam. It turned out that during floodings (starting from annual recurrence intervals to larger events), the reservoir of Kalivac is not able to capture the entire water masses and that currents in the reservoir will occur due to the overspill of flood discharges over the dam. As a direct consequence, suspended sediments are transported by the river through the tail of the reservoir, wide into the reservoir and deposit at various sites within the reservoir where the settling velocity dominates. This results in depositions of sediments not only in area of entrance but also in the centre of the reservoir. In addition to its negative impacts on morphodynamics and river ecology, deposited sediments are also affecting the available reservoir capacity:, sedimentation-especially in the centre and the areas near the dam-are considered to have negative consequences for electricity generation (e.g. obstructon of outlet structures, abrasion of turbines and other technical equipment). Moreover,depending on the magnitude of the flood event, transport downstream and deposition at the dam will occur.

The derived findings clearly shows that the concept of building large dams in rivers with large catchment areas (in this case 5500 km2), isproblematic; - especially when the rivers are transporing high loads of sediments. Reservoirs – usually built in headwater sections of rivers – aredesigned in principle to capture all the amount of run-off from the upstream catchment on a (i) daily, (ii) weekly and (iii) yearly basis. Transfering this concept from the headwaters to downstream river sites (Figure 67) leads to frequent overspilling of the dam via flood spillways (examples Figure 66) in the event of flooding. This is caused by the huge volume of typical annual floodings which can´t be stored by the reservoir under regular operation.

(a) (b)

Figure 66:Operating flood spillways at (a) Glenmaggie Dam / Australia and (b) Three-Gorges Dam / China.

This results in deposition patterns of transported suspended sediments (bottomset bed),which are not concentrated at the tail of the reservoir. In Figure 68, the long-term hydrology of the Vjosa is presented. Since the magnitude in discharge of the planed turbine runners is unclear at this point, a maximum threshold for operational discharge of 200 m3s-1 was assumed. Considering the fact, that a certain amount of flood discharge is able to be handled due to hydropower operations in the reservoir (pre-lowering of reservoir volume), the threshold for flood overspill was set to 500 m3s-1. Figure 68 clearly shows, how often this 500 m3s-1 threshold is exceeded. Such eventsinduce flow and sediment transport in and through the reservoir, with sediment deposits all over the reservoir area, even in the area close to the dam.

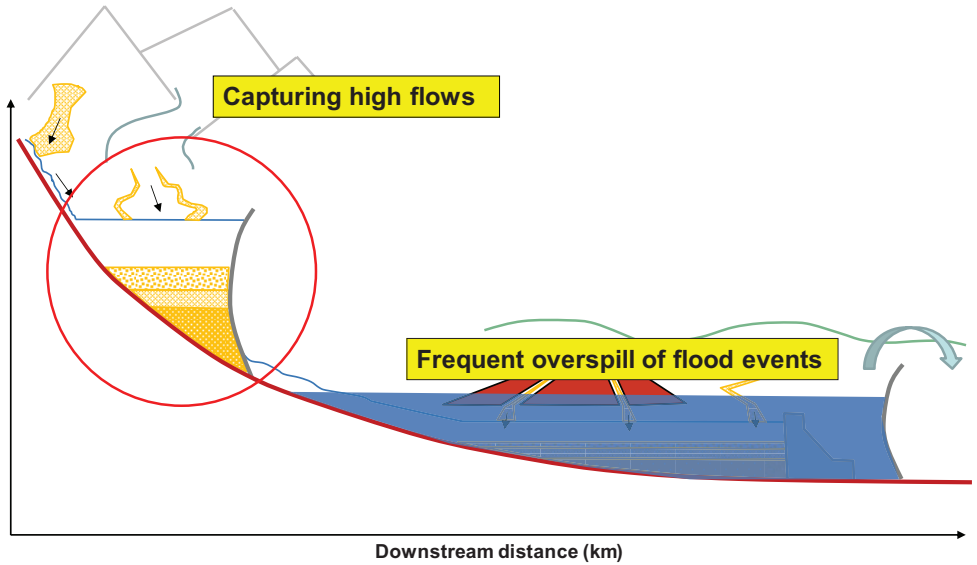

Figure 67: Schematic overview of sedimentation in hydropower reservoirs and what is the concept of setting large dams in rivers with huge catchments like the Vjosa (data based on Hauer et al., 2018); grey arrow = flow over flood spillways.

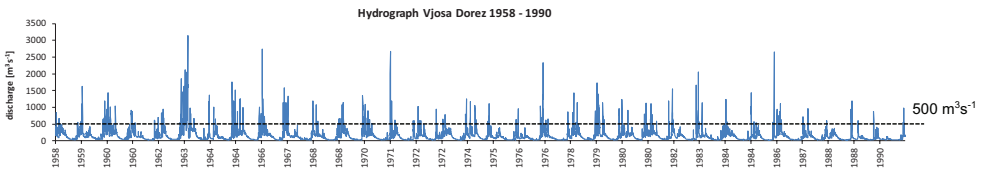

Figure 68:Long-term hydrograph of the Vjosa for the gaging station Dorez, operation from 1958 – 1990.

It is important to state at this point, that this **currentinduced sediment transport and sediment deposition caused by floodingswill be very cost intensive for hydropower companies planning to build dams on the Vjosa.** This is related to the fact that, depending on the hydrological variability, the clogging of the bottom outlet as well as the sensitive inlet to the turbines are at high risk of deposition or intake of fine sediments (suspended load) respectively. Bottom outlets are depicted in Figure 69 for (a) an emptied reservoir as well (b) during operation. To ensure dam security,operation must be stopped if these bottom outlets are clogged and must befreeed from deposits,(e.g. Haregeweynet al., 2012).

(a) (b)

Figure 69: Bottom outlets at reservoirs for (a) an emptied reservoir, - picture taken from upstream side and (b) during operation, picture taken from the downstream side of the reservoir.

In case of the Vjosa, there is a very high risk that these depositions will occure at a very early stage of project implementation. Especially in the phase of dam building, sediment will deposit close to the dam, which poses a riskright from day one of dam operation. Sucha deposition hazard, as predicted for the Vjosa dam,is quite well known in various parts of the world. Figure 70 shows an example from Switzerland, however there is a huge number of other examples found in areas with high sediment production rates (India, Nepal, Egypt.) (e.g. El-Moattassem et al., 2001).

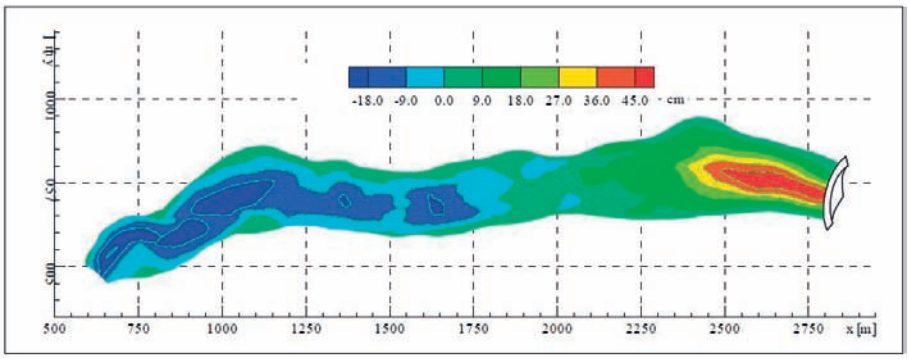

Figure 70:Deposition of sediments at the bottom outlet of a reservois (Althaus et al., 2009).

Additional costs will arise from necessary **dredging activities** and abrasion at turbine runners. In central Europe, cost for dredging are currently 10 – 20 €/m3. **In Albania,** depending on whether the material needs to be transported to deposition areas by trucks or released downstream to the river, **costs of 5 – 10** €/**m3** are expected. Considering the volume which needs to be dredged (multi 10.000 m3), costs can be estimated at several100.000 €- with cost for maintenance from year one of operation. Moreover, the turbine runners are at high risk of abrasion and if this risk exists, the turbine manufactors will **not ensureguarantee** for the achieved time of operations. Thus, cost in the range of millions of € are expected for the sensitive turbines, if abrasion occur (compare to Padhy, M. K., & Saini, 2009 (Pelton-runners); Thapa et al., 2015 (Francis-runners); Rai & Kumar, 2016 – Kaplan runners).

09 River bed incision downstream of dams

There is a common agreement in science that the impact of sediment deficits is responsible for river bed incision and related habitat degradation (Habersack & Piégay, 2008). Human-induced reductions in the sediment load due to hydropower use or torrent controls may have two different consequences, sometimes occurring simultaneously in one and the same river. First, depending on the frequency of floods, the coarsening of substrate due to selective transport leads to fluvial armor or pavement layers (Sutherland, 1987; Parker & Sutherland, 1999). Second, in alluvial basins such as those of the Vjosa, severe impacts due to continuous river bed incision occur. An extreme form of river bed incision – the so-called "river bed breakthrough" (Habersack & Klösch, 2012) – occurs in some specific alpine river basins where incision reaches the fine material deposits below the quaternary gravel layer of the river bed. Such river bed breakthrough can be produced by a single flood event (e.g. the Salzach River in 2002; Hopf, 2006) (Figure 71).

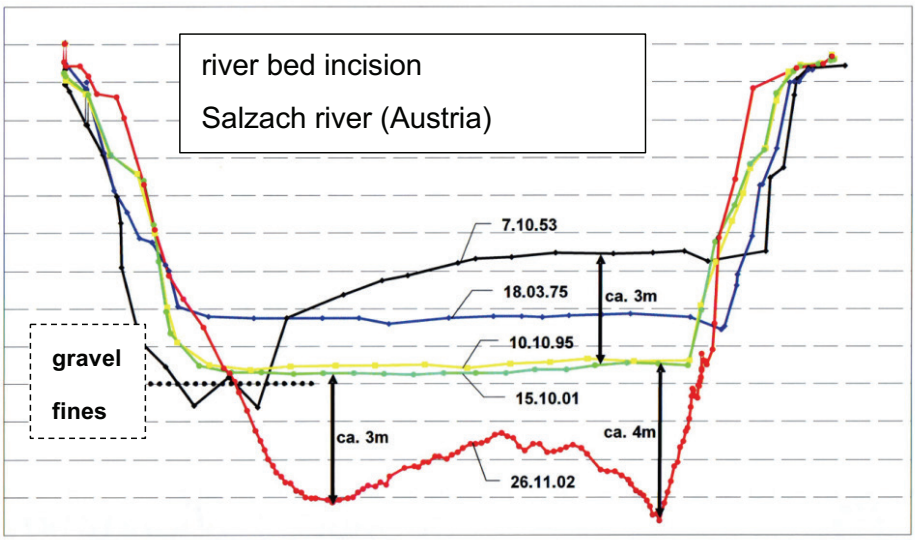

Figure 71: River bed incision at the Salzach river showing continuous river bed degradation of 3 m for the period 1953 until 2001 and the so called "river bed breakthrough" by the floodings of 2002 causing erosion rates of 3 – 4 m.

Consequences of sediment deficits and impacts on the river are: (i) decrease in habitat diversity (Kondolf, 1997), (ii) risk of river bank erosion (Rinaldi & Casagli, 1999), (iii) risk of damage to infrastructure, e.g. scouring bridge piers (Klinga &

Alipour, 2015), (iv) lack of spawning habitats for salmonid fish species (Hauer et al., 2013) and underdevelopment ofmacroinvertebrate fauna (Graf et al., 2016), (v) decrease in sediment turnover rates and river-type-specific sediment quality (Kondolf, 1997), (vi) risk of channel avulsion during extreme events (Brizga & Finlayson, 1990).

Channel avulsion refers to abrupt changes of the river course leading to a new active channel in the former floodplain (Slingerland & Smith, 2004). It is expected that all these negative aspects of river bed incision will occur at the Vjosa, if the sediment continuum downstream of Kalivac / Pocemis interrupted due tothe implementation of the planned dams(Figure 72). The lack of sediment supply in the range of 3 – 5million / tons per year, as it is held back by the dam wall, will cause constant river bed incision (degradation). In combination with extraordinary high-flows (which cannot be contained bythe reservoirs), this poses ahigh risk of uncontrolled river bank (land) erosion as a result of the unbalanced sediment regime, in addition to predicted coastal erosion.

Figure 72:Aerial picture of the Vjosa downstream of Pocem, which will face river bed incision if the sediment continuum is interrupted by the large dams of Pocem and Kalivac (data source: Google-Earth).

Another increasingly frequent problem connected withsediment retention is the flushing of reservoirs. During flushing, large amounts of the retained suspended load are released in a short period of time, mostly in conjunction with flood events. This leads to a surplus of sediments in downstream river sections. Consequently, high loads of mostly fine sediments cause high concentrations of turbidity, which tiypically results in losses and mass mortality of aquatic organisms (e.g. Espa et al., 2015).

10 Coastal erosion

The last critical point in this report is dedicated to coastal erosion. Although no direct field studies on coastal erosion were conducted for this study, the importance of this topic is underlined by some calculations and reviews of existing reports. Figure 73 depictsthe mouth of the Vjosa into the Adriatic Sea. On this aerial picture both (i) the highly sensitive wetlands as well as (ii) the suspended sediment transport of the river and the distribution into the Sea is visible. If the projected dams are built, this sediment transport will be interrupted, resulting in thedegradation of the highly sensitive wetlands as well as of the lagoon it self. This is caused by the unbalance situation of erosion via wave-energy due to the sea and the lack of (fine) sediment supply by the river (approximately 3 - 5 million tons / year).

Figure 73:Mouth of the Vjosa river (www.view.stern.de); red arrow = indicating suspended sediment transport into the sea.

The energy of the sea is also reflected in terms of coastal erosion. Figure 74 presents the findings of the study of de Leo et al. (2017). comparative the different couloured lines in thet aerial pictures show the changes in the coastline from 2007 – 2017 (Figure 74a) and 1985 – 2015 (Figure 74b) for Lalzit Bay, Albania (N41°29´02´´/E 19°30´43´´). The changes are the consequence of lack in sediments due to impounded river systems. The 30 years-study presented in Figure 74b shows a reduction in coastline of 211 m on average (approx. 7 m / year). This leads to the erosion of beaches and buildings and has huge economic impacts on infrastructure and tourism.The Danube Delta, exemplarily, is

eroded by 24 m annually by the Black Sea driven by the lack of sediment supply due to the high number of sediment traps / reservoirs (Stanica et al., 2007).

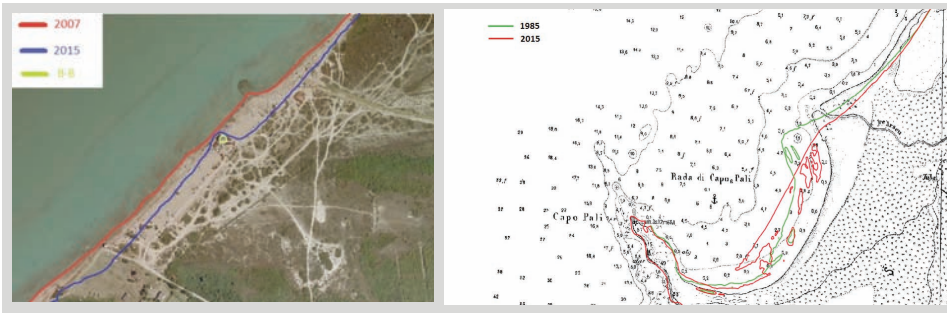

(a) (b)

Figure 74:Coastal erosion for LALZIT BAY, ALBANIA for(a) 2007 – 2015 and for(b) 1985 – 2015 (de Leo et al., 2016).

10.01 Coastal erosion / climate change

Many research activities were carried out in the past to examine the impact of climate change, especially on the coastline in the North of the Adriatic Sea. Exemplarily, Torresan et al. (2012) showed that a sea level rise resulted in changes in storms and wave climate. Therefore, global climate change is expected to increase the size and magnitude of flooded and eroding coastal areas, having profound impacts on coastal communities and ecosystems. River deltas, beaches, estuaries and lagoons are considered to be particularly vulnerable to the adverse effects of climate change, however, this needs to be studied at the regional/local scale. Thus, countries along the Adriatic Sea must identify and prioritize vulnerable areas to different climate-related impacts as well assuitable areas for human settlements, infrastructures and economic activities, and, on that basis, develop coastal zoning and land use plan (Torresan et al., 2012).

Errors in sediment management of rivers are responsible for increased coastal erosion on a global scale, with severe socio-economic damages especially in the event of maritime storms. The Mississippi River Delta and coastal Louisiana are disappearing at an astonishing rate (Figure 75): “a football field of wetlands vanishes into open water every 100 minutes”. Since the 1930s, Louisiana has lost over 2,000 square miles of land, an area roughly the size of Delaware (http://mississippiriverdelta.org/our-coastal-crisis/land-loss/). Many factors have contributed to this collapse, but one of the main causes is the damming of the Mississippi River (e.g. Meade & Moody, 2010; Mossa, 1996). Without these lagoon and island buffer, storm impacts (e.g. hurricanes) are increasing, as has been evident in New Orleans in 2005 (Hurricane Katrina) oralong the Florida Coast in 2017 (Hurricane Irma).

These devastating events show the importance of providing a dynamic buffer against coastal erosion, especially in view of ever-increasing climate change impacts. Only the natural delivering, transporting and depositing of sediments by the rivers can guarantee such buffer along the coastline of Albania. The building of new dams on Albanian rivers will counteract sediment buffers against coastal erosion. Mismanagement in this regard will have severe socioeconomic costs (tourism, infrastructure) of millions of €.

Figure 75:Coastal and lagoon erosion in the Mississippi – Delta (www.mississippiriverdelta.org).

11 Summary and conclusions

(1) "The filling up of Vjosa reservoirs with sediments is calculated within 30 – 40 years for Pocem and 45 – 60 years for Kalivac". Due to the high sediment transport rates of the Vjosa, an annual reservoir loss of about 2% in the case of Kalivac and > 2% in the case of Pocem is forecasted. These numbers are more than twice as high as the global average of annual storages losses (0.87% per year). Due to the lack of sediment transport data for discharges above 1000 m3s-1, there are some uncertainties concerning these predictions. However, it is expected that additional data for very high discharges will increase the forecasted annual deposition rates.

(2) "High economic cost are expected for sediment management and treatment". The numerical modelling of the planed reservoir in Kalivac clearly showed that frequent (annual) flood events in the range of >1000 m3s-1 create currents in the reservoir, which will transport the suspended load through the reservoir with various stages of deposition in the impounded sections. Those currents, induced by frequent floodings, will (with a high certainty) cause severe problems (i) at the bottom outlet and (ii) intakes to the turbines due to depositions. To overcome these issues, dredging will be necessary with high costs, from the first year of operation.

(3) "River bed incision will be the consequence" if the transported sediments of the Vjosa are trapped in hydropower reservoirs. This incision results in (i) changes in downstream groundwater levels (problems for agricultural land use and floodplain vegetation), (ii) risk of uncontrolled channel avulsion in the event of floods (loss in agricultural land and ecological degradation in the long-term perspective).

(4) "Coastal (Lagoon) erosion will increase due to lack of sediment transport". The interruption of the sediment continuum will have severe consequences for the coastline in this part of Albania. As previous studies have already shown, the erosion of the coastline is already in progress and will accelerate drastically if dams hold back the sediments in the Vjosa. This erosion is of high socio-economic relevance to the Albanian state and poses high risk for infrastructure in the event of Adriatic storms (compare to Hurricane – coastline experiences from the US).

(5) "Degradation of ecology, loss of European sea-side tourism as well as of eco-tourism in the Vjosa catchment must be expected". This has not been directly assessed in the preseted study, however the expected severe degration in the Vjosa catchment as a result of all four points mentioned above will inevitably lead to socio-economic consequences related to tourism for the coastal part of Albania as well as to a loss of potential for eco-tourism along

the Vjosa. Infrastructure projects along the coast line will be at risk and marine resources related to the lagoon will disappear.

Based on (1) and (2) it can be concluded that the construction of dams (reservoirs) in this specific river and particularly in this section of the river system (huge catchment area and high sediment loads) is a problematic concept in terms of energy generation and profitability. Dams (reservoirs) are created to capture the rainfall and run-off on a daily, weekly or annual basis. In addition to high annual losses in the storage volume, the frequent overspill of floodings will cause severe operational problems. Since the interaction of instream hydraulics, sediment transport, river morphology and ecology are not adequately understood (from a process perspective) implementation of sustainable sediment mitigation measures in river management plans are missing. Furthermore, there is a lack in standardized evaluation methods for detecting disturbances in the sediment regime. In summary, there is the risk of a **"lose-lose-lose situation"**:

Lose 1: High economic costs due to sediment related problems in the reservoir.

Lose 2: Ecological degradation of a large unique river system in Europe.

Lose 3:Long-term negative impacts on the coastline and tourism in this part of Albania.

12 List

12.01 List of figures

12.02 List of tables

12.03 References

Annandale, G.W. (2006). Reservoir sedimentation: John Wiley & Sons, Ltd.
Annandale, G.W. (1996). "Spatial Distribution of Deposited Sediments in Reservoirs,"Proceedings of the International Conference on Reservoir Sedimentation, Volume 1,Albertson, M.L., Molinas, A., and R. Hotchkiss, ed., Colorado State University, FortCollins, CO.

Ardiclioglu, M., Kocileri, G., & Kuriqi, A. (2013). Assessment of Sediment Transport in the Devolli River. International Balkans Conference on Challenges of Civil Engineering.

Ashmore P, Church M. (2001). The impact of climate change on rivers and river processes in Canada. Geological Survey of Canada. 555:55.

ASTM D4822-88 (2014). Standard Guide for Selection of Methods of Particle Size Analysis of Fluvial Sediments (Manual Methods), ASTM International, West Conshohocken, PA.

Basson, G.R. (2009). Management of siltation in existing and new reservoirs. 23rd Congress of the International Commission on Large Dams. Brasilia.

Bhallamudi, S. M., Chaudhury, M. H. (1991). Numerical modelling of aggradation and degradation in alluvial channels. ASCE Journal of Hydraulic Engineering 119: 1145–1164, DOI/10.1061/(ASCE)0733-9429.

BMLFUW (2017). Schwebstoffe im Fließgewässer – Leitfaden zur Erfassung des Schwebstofftransportes. Bundesministerium für Land- und Forstwirtschaft, Umwelt und Wasserwirtschaft, Wien.

Bognar, A., Faivre, S., Buzjak, N., Pahernik, M., & Bočić, N. (2012). Recent landform evolution in the Dinaric and Pannonian Regions of Croatia. In Recent Landform Evolution (pp. 313-344). Springer, Dordrecht.

Brierley, G.J., Hickin, E.J. (1991). Channel planform as non-controlling factor in fluvial sedimentology: the case of the Squamish River, British Columbia, Geomorphology 4, 381 – 391.

Brizga, S. O., & Finlayson, B. L. (1990). Channel avulsion and river metamorphosis: the case of the Thomson River, Victoria, Australia. Earth Surface Processes and Landforms, 15(5), 391-404.

Bunte, K., Abt, S.R. (2001). "Sampling Surface and Subsurface Particle-Size Distributions in Wadable Gravel-and Cobble-Bed Streams for Analyses in Sediment Transport, Hydraulics, and Streambed Monitoring." Gen. Tech. Rep. RMRS-GTR-74. Fort Collins, CO: US Department of Agriculture, Forest Service, Rocky Mountain Research Station. 428 P. 74.

Carson, M.A. (1984). Observations on the meandering-braided river transition. Canterbury Plains, New Zealand: Part 2 – New Zealand Geographer, 40, 89 – 99.

Church, M. (1983). Pattern of instability in a wandering gravel bed channel. in Collinson, J. D. and Lewin, J. (Eds.) Modern and Ancient Alluvial Systems, International Association of Sedimentologists Special Publication 6, 169 – 180.

Colomina, I., Blázquez, M., Molina, P., Parés, M. E., Wis, M. (2008). Towards A New Paradigm for High-Resolution Low-Cost Photogrammetryand Remote Sensing, In: International Archives of the Photogrammetry, Remote Sensing and Spatial Information Sciences, ISPRS Congress, Beijing, China, XXXVII. Part B1, 1201-1206.

Correia, L. R. P., Krishnappan, G., Graf, W. H. (1992). Fully coupled unsteady mobile boundary flow model. ASCE Journal of Hydraulic Engineering 118: 476–494, DOI/10.1061/(ASCE)0733-9429.

De Leo, F., Besio, G., Zolezzi, G., Bezzi, M., Floqi, T., & Lami, I. (2017). Coastal erosion triggered by political and socio-economical abrupt changes: The case of Lalzit Bay, Albania. Coastal Engineering Proceedings, 1(35), 13.

Deslodges, J. R., Church, M.A. (1989). Wandering gravel bed rivers. Canadian Geographer, 33, 360 – 364.

DIN 38 409 Teil 2 (1987): Deutsche Einheitsverfahren zur Wasser-, Abwasser- und Schlammuntersuchung, Summarische Wirkungs- und Stoffkenngrößen (Gruppe H), Bestimmung der abfiltrierbaren Stoffe und des Glührückstandes (H2), Normungsausschuß Wasserwesen (NAW) im DIN Deutsches Institut für Normung e.V.

Dröge, B., Nicodemus, U., Schemmer, H. (1992). Instruction for bed load and suspended material sampling. Koblenz: Federal Institute of Hydrology.

urović, P., Petrović, A. (2007). Large canyons in Dinaric and Prokletije mountains region of Montenegro. Geographica Pannonica, (11), 14-18.

DVWK (1986). Schwebstoffmessungen, Regeln zur Wasserwirtschaft Nr. 125/1986; Kommissionsvertrieb Verlag Paul Parey, Hamburg und Berlin.

Edwards, T., Glysson, G. (1999). Field Methods for Measurement of Fluvial Sediment, Techniques of Water-Resourses Investigations of the U.S. Geological Survey, Book 3, Applications of Hydraulics, Chapter C2.

El-Moattassem, M., Abdel-Aziz, T.M., EL-Sersawy, M. (2001). Modleling of sedimentation process in Aswan High Dam Reservoir.

Eisenbeiß, H. (2009). UAV photogrammetry, Doctoral dissertation, ETH Zurich.

Espa, P., Crosa, G., Gentili, G., Quadroni, S., & Petts, G. (2015). Downstream ecological impacts of controlled sediment flushing in an Alpine valley river: a case study. River Research and Applications, 31(8), 931-942.

EuroNatur & Riverwatch (2018). Eco-Masterplan for Balkan Rivers. Drawing

a line in the sand. Radolfzell, Vienna.

Everaerts, J. (2008). The Use of Unmanned Aerial Vehicles (UAVS) for Remote Sensing and Mapping, In: The International Archives of the Photogrammetry, Remote Sensing and Spatial Information Sciences, ISPRS Congress, Beijing, China, XXXVII. Part B1, 1187-1192.

Fan, S., Springer, F. (1990). Major sedimentation issues and ongoing investigations at the Federal Energy Regulatory Commission. ASCE; p. 1015–20.

Fehr, R. (1987). "Geschiebeanalysen in Gebirgsflüssen (Grain Size Analyses in Torrents)." Mitteilung Nr. 92.
Versuchsanstalt Für Wasserbau, Hydrologie Und Glaziologie (VAW), ETH Zürich, Zürich.

FISP – Federal Interagency Sedimentation Project (2007). Operator's manual for the US p-61-A1point integrated suspended – sediment sampler, http://fisp.wes.army.mil/Instructions US P-61-A1030115.pdf (26.01.2007).

Fouache, E., Gruda, G., Mucaj, S., & Nikolli, P. (2001). Recent geomorphological evolution of the deltas of the rivers Seman and Vjosa, Albania. Earth Surface Processes and Landforms: The Journal of the British Geomorphological Research Group, 26(7), 793-802.

Frasheri & Pano (1995). The climate change in Albania, its impact on hydrographic system and Adriatic coastline.

Gorman, O. T., Karr. J.R. (1978). Habitat structure and stream fish communities. Ecology 59:507–515.

Gostner, W., Alp, M., Schleiss, A. J., & Robinson, C. T. (2013). The hydromorphological index of diversity: a tool for describing habitat heterogeneity in river engineering projects. Hydrobiologia, 712(1), 43-60.

Graf, W., Leitner, P., Hanetseder, I., Ittner, L.D., Dossi, F. & Hauer C. (2016). Ecological degradation of a meandering river by local channelization effects: A case study in an Austrian lowland river. Hydrobiologia. 772(1): 145-160.

Habersack, H. (1997). Raum-zeitliche Variabilitäten im Geschiebehaushalt und dessen Beeinflussung am Beispiel der Drau. Univ. für Bodenkultur, Inst. für Wasserwirtschaft, Hydrologie u. Konstruktiven Wasserbau.

Habersack, H., Klösch, M. (2012). Monitoring und Modellierung von eigendynamischen Aufweitungen an Drau, Mur und Donau. Österreichische Wasser- und Abfallwirtschaft, 64, 411-422.

Habersack H., Piégay H. (2008). River restoration in the Alps and their surroundings: past experience and future challenges. In: Gravel-Bed Rivers VI: From Process Understanding to River Restoration H. Habersack, H. Piegay, M. Rinaldi, (eds), Elsevier.

Haregeweyn, N., Melesse, B., Tsunekawa, A., Tsubo, M., Meshesha, D., & Balana, B. B. (2012). Reservoir sedimentation and its mitigating strategies: a case study of Angereb reservoir (NW Ethiopia). Journal of soils and sediments, 12(2), 291-305.

Hauer, C., Unfer, G., Habersack, H., Pulg, U., Schnell, J. (2013). Bedeutung von Flussmorphologie und Sedimenttransport in Bezug auf die Qualität und Nachhaltigkeit von Kieslaichplätzen. KW–Korrespondenz Wasserwirtschaft, 4/13, 189-197.

Hauer, C., Wagner, B., Aigner, J., Holzapfel, P., Flödl, P., Liedermann, M., ... & Haimann, M. (2018). State of the art, shortcomings and future challenges for a sustainable sediment management in hydropower: A review. Renewable and Sustainable Energy Reviews, 98, 40-55.

Hopf, G. (2006). Die Sanierung der unteren Salzach. – LWF Wissen, 55, 62-66, 8 Abb., Freising (Bayerische Landesanstalt für Wald und Forstwirtschaft).

Hubbell, D. W. (1964). Apparatus and techniques for measuring bedload (No. 1748). US Govt. Print.

Hughes, P. D., Woodward, J. C., Van Calsteren, P. C., Thomas, L. E. (2011). The glacial history of the Dinaric Alps, Montenegro. Quaternary Science Reviews, 30(23-24), 3393-3412.

Kellerhals, R. Neill, C.R., Bray, I.D. (1972). Hydraulic and geomorphic characteristics of rivers in Alberta, Research Council of Alberta, River Engineering and Surface Hydrology Report 72-1.

Kerle, N., Heuel, S., Pfeifer, N. (2008). Real-time data collection and information generation using airborne sensors, In: Geospatil information Technology for Emergency Response, Ed.: Zlatanova S and Li, J., Taylor & Francis, London, UK, 43-74.
Klinga, J. V., & Alipour, A. (2015). Assessment of structural integrity of bridges under extreme scour conditions. Engineering Structures, 82, 55-71.

Kondolf, G. M. (1997). PROFILE: hungry water: effects of dams and gravel mining on river channels. Environmental management, 21(4), 533-551.

Lara, J.M. and Pemberton, E.L. (1963). Initial unit weight of deposited sediments. Proc. of Federa
Interagency Sedimentation Conference, Denver.

Liedermann, M., Gmeiner, P., Niederreiter, R., Tritthart, M., Habersack, H. (2012). Innovative Methoden zum Geschiebemonitoring am Beispiel der Donau. Österreichische Wasser-und Abfallwirtschaft, 64(11-12), 527-534.

Liedermann, M., Gmeiner, P., Kreisler, A., Tritthart, M., Habersack, H. (2018). Insights into bedload transport processes of a large regulated gravel□bed river. Earth Surface Processes and Landforms, 43(2), 514-523.

Liggett, J. A., Cunge, J. A. (1975). Numerical methods of solution of the unsteady flow equations. In Mahmood K., Yevjevich V., (eds) Unsteady Flow in Open Channels, Vol. I, Water Resources: Fort Collins, Colorado; 89–179.

Maddock, I. (1999). The importance of physical habitat assessment for evaluating river health. Freshwater Biology 41: 373–391.

Mamede, G.L. (2008). Reservoir Sedimentation in Dryland Catchments: Modelling and Management. Dissertation. Mathematisch-Naturwissenschaftlichen Fakultät der Universität Potsdam. 120 pp.

Meade, R. H., & Moody, J. A. (2010). Causes for the decline of suspended sediment discharge in the Mississippi River system, 1940–2007. Hydrological Processes: An International Journal, 24(1), 35-49.

Morris and Fan (1998). Reservoir Sedimentation Handbook, McGraw-Hill, New York,
NY. (available online http://reservoirsedimentation.com/).

Mossa, J. (1996). Sediment dynamics in the lowermost Mississippi River. Engineering Geology, 45(1-4), 457-479.

Mueller, D. S., Wagner, C. R., Rehmel, M. S., Oberg, K. A., Rainville, F. (2009). Measuring discharge with acoustic Doppler current profilers from a moving boat (p. 72). Reston, Virginia (EUA): US Department of the Interior, US Geological Survey.

Nanson, G. C., & Knighton, A. D. (1996). Anabranching rivers: their cause, character and classification. Earth surface processes and landforms, 21(3), 217-239.

Niekerk, A., Van Vogel, K. R., Slingerland, R. L., Bridge, J. S. (1992). Routing of Heterogeneous Size-Density Sediments Over a Movable Stream Bed: Model Development. ASCE Journal of Hydraulic Engineering 118: 246–263.

Nordseth, K. (1973). Fluvial processes and adjustments on a braided river. The islands of Kopangsoyene on the River Glomma, Norsk Geografiska Tidsskrift, 27, 77-108.

Nujic, M., 1998. Praktischer Einsatz eines hochgenauen Verfahrens für die Berechnung von tiefengemittelten Strömungen. Univ. der Bundeswehr München, Institut für Wasserwesen, Neubiberg (Deutschland, Bundesrepublik) 148 pp.
Padhy, M. K., & Saini, R. P. (2009). Effect of size and concentration of silt particles on erosion of Pelton turbine buckets. Energy, 34(10), 1477-1483.

Pano, N., Lazaridou, M., & Frasheri, A. (2005). Coastal management of the ecosystem Vlora Bay-Narta Lagoon-Vjosa River Mouth. Albanian J. Nat. Techn. Sci., 11, 141-157.

Parker, G., Sutherland, A.J. (1987). Fluvial amor. Journal of Hydraulic Re-

search, 28, 529-544.

Rai, A. K., & Kumar, A. (2016). Analyzing hydro abrasive erosion in Kaplan turbine: A case study from India. Journal of Hydrodynamics, Ser. B, 28(5), 863-872.

Rinaldi, M., & Casagli, N. (1999). Stability of streambanks formed in partially saturated soils and effects of negative pore water pressures: the Sieve River (Italy). Geomorphology, 26(4), 253-277.

Rinaldi, M., Wy□ga, B., & Surian, N. (2005). Sediment mining in alluvial channels: physical effects and management perspectives. River Research and Applications, 21(7), 805-828.

Rößler, N. (2017). The riparian vegetation of the Vjosa (Albania) – one of the Europes last wild rivers. Exams thesis, KIT- Karlsruhe Institute of Technology. 135 pp.

Schiemer, F., Drescher, A., Hauer, C., Schwarz, U. (2018). The Vjosa River corridor: a riverine ecosystem of European significance. In: Acta ZooBot Austria, The Vjosa in Albania – a riverine ecosystem of European significance 155, 1, 1-40.

Schleiss A, Boes R. (2011). Dams and reservoirs under changing challenges. In: Proceedings of international symposium on dams and reservoirs under changing challenges, 79 Annual Meeting of ICOLD. Lucerne, Switzerland: Swiss Committee on Dams.

Schlosser, I. J. (1982). Fish community structure and function along two habitat gradients in a headwater stream. Ecological Monographs 52:395–414.

Schumm, S. A. (1969). River metamorphosis. Journal of the Hydraulics division, 95(1), 255-274.

Schumm, S. A. (1985). Patterns of alluvial rivers. Annual Review of Earth and Planetary Sciences, 13(1), 5-27.

Seferlis, M.T., Laco, T., Papadimos, D. (2008). Identification of human pressures and impacts on the surface waters of Aoos/Vjosa watershed. The Goulandris Natural Museum – Greek Biotope / Wetland Centre. Thermi, Greece. 70 pp.

Slingerland, R., & Smith, N. D. (2004). River avulsions and their deposits. Annu. Rev. Earth Planet. Sci., 32, 257-285.

Stanica, A., Dan, S., & Ungureanu, V. G. (2007). Coastal changes at the Sulina mouth of the Danube River as a result of human activities. Marine Pollution Bulletin, 55(10-12), 555-563.

Sutherland, A.J. (1987). Static armour layers by selective erosion, Sediment Transport in Gravel-Bed Rivers CR Thorne, JC Bathurst, RD Hey, 243-260.

Thapa, B. S., Dahlhaug, O. G., & Thapa, B. (2015). Sediment erosion in hydro turbines and its effect on the flow around guide vanes of Francis turbine. Renew-

able and Sustainable Energy Reviews, 49, 1100-1113.

Torresan, S., Critto, A., Rizzi, J., & Marcomini, A. (2012). Assessment of coastal vulnerability to climate change hazards at the regional scale: the case study of the North Adriatic Sea. Natural Hazards and Earth System Sciences, 12(7), 2347-2368.

USSD (2015). Modeling Sediment Movement in Reservoirs. U.S. Society on Dams. 26 pp.

USACE (2002). HEC – RAS User manual 3.1.1. U.S. Corps of Engineers.

Van Blyenburgh, P. (1999). UAVs: and Overview, In: Air & Space Europe, I, 5/6, 43-47.

van Rijn, L. C. (1986). Applications of sediment pick-up function. Journal of Hydraulic Engineering, 112(9), 867-874.
-
Wass, P. D., Leeks, G. J. (1999). Suspended sediment fluxes in the Humber catchment, UK. Hydrological Processes, 13(7), 935-953.

Whipple, K. X., Tucker, G. E. (1999). Dynamics of the stream□power river incision model: Implications for height limits of mountain ranges, landscape response timescales, and research needs. Journal of Geophysical Research: Solid Earth, 104(B8), 17661-17674.

Measuring of sediment transport and morphodynamics at the Vjosa river / Albania